UNIVERSITY OF BERGEN

Geophysical Institute

MASTERS THESIS

Understanding the dynamics of recent Norwegian extreme weather events and their influence on energy production

Author: Martin Pečnjak

Supervisor: Nour-Eddine Omrani

Co-supervisors: Tarjei Breiteig, Noel Keenlyside

August 4, 2021

Abstract

The growing frequency and severity of extreme weather events in the Northern Hemisphere has prompted a lot of research being done on their origin and physical mechanisms. Both simplified and complex approaches have been introduced in defining and understanding these events, where they look into high-amplitude quasi-stationary Rossby waves and their quasi-resonant amplification. However, different approaches exist to investigating extreme events and these were just a motivation for this thesis. Since the resonance method is suitable mostly for summer events and the events discussed in this thesis have happened in all seasons, a different approach was needed. The events in question were a winter drought, two summer and autumn floods, a winter snowfall and a spring/summer heatwave in the areas of south and southwestern Norway. In order to detect certain features which would help solve this issue, we look into anomalies of different meteorological variables such as geopotential height, surface temperature, precipitation and snowfall rate and zonal and meridional winds. Deep and thorough statistical and dynamical analyses are applied to define the outcomes and the physical origins which would help us obtain a clear picture on the whole case. The finite-amplitude local wave activity (LWA) diagnostic, as a measure of the meandering of the jet stream, has helped to give a clear picture along with the large-scale circulation. This method can be used as a proxy for the strength of the eddy-driven jet and the storm track. It has proven to be the key factor in defining what has exactly caused the events in question. The results and findings have shown that the LWA is a conclusive tool in determining whether an extreme event was related to a blocking pattern or not, while the LWA budget equation components have shed light on the so far poorly understood dynamical aspects which led to the events. The zonal LWA flux has proven to be a good predictor of blocking with its onset in the early stages of the events, similar to the traffic jam concept introduced by (Nakamura and Huang, 2018). The jet stream has a capacity for the LWA flux similar to how a highway has a capacity for the number of vehicles on it. If the capacity is exceeded, blocking occurs, and this is readily shown in the results and findings of this work. As for the budget equation components, the zonal LWA flux convergence has proven to be the key in maintaining the increase of the LWA as well as also having an early onset in each blocking event in agreement with the LWA flux. On the other hand, the residual in the LWA budget, which represents the non-conservative small-scale processes (diabatic sources and sinks of LWA), dampens the LWA. The LWA method has also proven to be useful in all seasons. The motivation for the thesis also came from the influence of the events on the meteorological variables related to the Norwegian energy production. The results show us clues into possible ways of improving forecasting of such events and minimizing their harmful impacts. They also show possibilities in improving energy management, infrastructure, allocation of resources and preparedness of the society for damages and hazards caused by the events. This was not fully investigated in this thesis and is the next step in the research of this topic.

Acknowledgment

First of all, I would like to thank my main supervisor, Nour-Eddine Omrani, for his devoted and constant contribution to this thesis with his knowledge and expertise on the various topics dealt with during the work on this thesis as well as a lot of advice and support on how to improve my working habits, problem-solving and research skills. I also want to thank my co-supervisors, Tarjei Breiteig from Agder Energi and Noel Keenlyside, for their significant input and guidance on all steps of the work and great cooperation with Nour-Eddine.

Secondly, I thank all of my dear colleagues at the Geophysical Institute of the University of Bergen, as well as my friends and family, for being so supportive and caring throughout all the issues I have encountered during writing and working on this thesis in this challenging time of the Covid-19 pandemic.

Thirdly, I would like to also thank Clare S. Y. Huang from the University of Chicago, USA, on the cooperation regarding setting up and adjusting the Python local wave activity scripts for usage in this thesis, which have provided some crucial results and findings.

Finally, I acknowledge the institutions which have provided the data for this thesis with the following: (Hersbach et al., 2018a,b) was downloaded from the Copernicus Climate Change Service (C3S) Climate Data Store. The results contain modified Copernicus Climate Change Service information 2020. Neither the European Commission nor ECMWF is responsible for any use that may be made of the Copernicus information or data it contains.

M.P.

Contents

List of Figures

Chapter 1

Introduction

The observed increasing frequency of extreme weather events in the Northern Hemisphere in the last two decades (Coumou et al., 2014) has led to extensive research being done on the physical mechanisms behind them and their societal impacts. Certain studies point to anomalous jet stream circulation patterns with connection to persistent high-amplitude quasi-stationary Rossby waves, which are assumed to have had a large contribution to these events (Coumou et al., 2014; Petoukhov et al., 2013; Mann et al., 2017; Kornhuber et al., 2017). Some suggested mechanisms for their occurrence are the weakening of the zonal mean jets and resonance of free and forced waves in mid-latitude regions, which amplify the aforementioned Rossby waves, mostly occurring in the summer season. The goal of this thesis is to investigate a series of extreme weather events that have occurred in different regions of Norway in different seasons using the newly developed finite-amplitude LWA approach, which can be used for all seasons, to pinpoint the specific dynamical mechanisms leading to them. Furthermore, the influence of these on European power parameters (wind, temperature, precipitation) will give more insight on how to improve energy production, protection of the infrastructure and human preparedness for these events.

1.1 Background

1.1.1 Introduction to extreme events

Many studies (Branstator, 2002; Schubert et al., 2011; Tachibana et al., 2010; Trenberth and Fasullo, 2012; Lau and Kim, 2012) have linked changes in the large-scale circulation to different extreme weather events. One of the most relevant changes discussed in current research are the persistent quasi-stationary high-amplitude Rossby waves, which have been linked to different anomalous jet stream circulation patterns. These formations can occur in two main ways (Coumou et al., 2014):

- Weakening of the zonal mean jets
- Amplification by resonance between free and forced waves in mid-latitude wave guides

The persistent patterns in summer can result from the amplification of quasi-stationary waves with zonal wave numbers 6-8 (Coumou et al., 2014) with the influence of the weakening of the zonal mean jet in the summer. There are other mechanisms that can be involved and the authors didn't study all different extreme weather events. (Coumou et al., 2015; Lehmann and Coumou, 2015) have shown a trend of the weakening of the storm tracks and the zonal mean flow. (Horton et al., 2015) have further shown the trend of the increase in the persistence and frequency of blocking anticyclones over the mid-latitudes. The features mentioned in the previous sentences also lead to surface weather extremes, such as heavy precipitation events and heat waves (Coumou et al., 2014). Another prominent feature that contributes to resonant flow regimes is the double jet formation in the summer in the extra-tropics, with some evidence linking it to rapid warming in the Arctic that has influenced the changes in the zonal mean zonal wind profile (Francis and Vavrus, 2012).

Some arguments claim that one contribution to the higher frequency of extreme events comes from basic thermodynamics and global warming. Higher temperatures lead to more heat waves, while also increasing the moisture content in the atmosphere through more evaporation from warmer sea surfaces (Westra et al., 2013; Zhang et al., 2013; Coumou et al., 2013; Coumou and Robinson, 2013; Huntingford et al., 2013). For example, in (Lehmann et al., 2015; Min et al., 2011; Zhang et al., 2013), it has been shown that heavy precipitation increases with up to 7% by 1°C of warming according to the Clausius-Clapeyron relation. These have resulted in an increase of the intensity and frequency of heavy rainfall extremes in different regions around the world (Westra et al., 2013; Lehmann et al., 2015; Groisman et al., 2004; Seneviratne et al., 2012). It is also important to note that specifically for precipitation extremes there's a considerable influence from non-linear, complex and dynamical changes (Trenberth et al., 2015; Coumou and Rahmstorf, 2012). For example, locally, rainfall intensity can be increased beyond the Clausius-Clapeyron relation by changes in convective regimes coming from higher temperatures (Lenderink and Meijgaard, 2008, 2009; Berg et al., 2013; Meredith et al., 2015).

Another slew of studies relate the reduction in Arctic sea ice concentration with changes in the atmospheric circulation, which could be crucial in enforcing patterns causing these types of events. (Petoukhov and Semenov, 2009) have shown that a decrease in winter sea ice in the Barents and Kara seas can lead to extreme cold events. It is clarified that heating in the lower troposphere can reduce meridional temperature gradients in the subpolar latitudes, which can possibly weaken the zonal winds in the mid-latitudes. (Francis and Vavrus, 2012) have found that the Arctic amplification (pronounced warming in higher latitudes) has contributed to weaker zonal winds and increased wave amplitudes. They have also found that these changes are mostly seen in autumn and winter, consistent with the sea ice loss. The slower progression of the upper-level waves would cause persistent events such as floods, droughts etc. It is suggested that the enhanced warming in the summer would release more energy into the atmosphere, therefore making changes in its circulation patterns. (Liu et al., 2012) have demonstrated that a decreased autumnal sea ice cover influences the winter circulation over the Northern Hemisphere by causing more persistent and blocking patterns. Also, the increase in the water vapor content in late autumn may lead to stronger snowfall in the upcoming winter. (Francis et al., 2009) suggest that the winter polar jet stream could be under the influence of the summer and autumn ice concentrations, which have a significant impact on poleward thickness gradients, cloud variability and the stability of the lower troposphere. (Jaiser et al., 2012) have pinpointed that the lower sea ice concentration in August and September causes an earlier onset of baroclinic instability, which has a profound impact on the large-scale atmospheric circulation in winter. The decrease in sea ice also causes different pressure patterns at the surface and in the mid-troposphere. However, some studies (Ogawa et al., 2018) suggest the influence of the sea ice loss is limited to the high-latitude lower troposphere in winter.

1.1.2 Quasi-resonant Rossby wave amplification

To get to the bottom of the zonal wind jet weakening in the summer, we first look into the weakened poleward thermal gradient that influences the eastward propagation of Rossby waves (Francis and Vavrus, 2012). From the linearized, barotropic, non-divergent vorticity equation without orographic and thermodynamic forcing, the phase speed relation of the waves can be derived from (Pedlosky, 2013):

$$c = U - \frac{\beta}{k^2 + l^2} \tag{1.1}$$

From this relation, it is obvious that the propagation of the waves changes linearly with the magnitude of the zonal mean zonal wind. In this relation, c is the phase speed of the waves relative to the surface, U is the zonal mean zonal wind and k and l are the zonal and meridional wave number, respectively. β is the Rossby parameter.

Looking at the large-scale mid-latitude circulation we can decompose it into two components (Kornhuber et al., 2017):

- Free synoptic-scale Rossby waves travelling in the eastward direction with higher wave numbers (6-8)
- Quasi-stationary planetary-scale Rossby waves with very low phase speeds (or close to zero) as well as low frequencies, with various zonal wave numbers related to the circulation's response to spatially inhomogenous diabatic sources and sinks and orography

These types of motions can be described with a non-stationary, non-divergent barotropic vorticity equation on a sphere at the equivalent barotropic level (EBL) written in a quasi-geostrophic approximation (Pedlosky, 2013):

$$\begin{gathered}\left(\frac{\partial}{\partial t}+\alpha\frac{\partial}{\partial\lambda}\right)\nabla\Psi'+\left(2\Omega-\frac{\Delta\overline{u}}{a\cos\phi}\right)\frac{\partial\Psi'}{\partial\lambda}=\\ \frac{2\Omega\alpha a^2}{\tilde{T}}\sin\phi\frac{\partial T'}{\partial\lambda}-\frac{2\Omega\sin\phi\alpha_{or}a^2}{H}\frac{\partial h_{or}}{\partial\lambda}-\left(k_h\frac{\nabla\Psi'}{a^2}+k_z\frac{\nabla\Psi'}{H^2}\right)\end{gathered} \tag{1.2}$$

In the equation, Ψ' represents the stream function at the EBL, ϕ, λ and t are the latitude, longitude and time, a is the radius of the Earth, while Ω is its angular velocity. $\alpha = \overline{u}/\cos\phi$ presents the index of atmospheric circulation, h_{or} is the large-scale orography height, $\alpha_{or} = \overline{u}_{or}/\cos\phi$, where u_{or} is the zonal wind at the zonally averaged orography height (Held, 2001; Charney and Eliassen, 1949). Further, $\overline{u}$ is the zonally averaged zonal wind at the EBL. It is assumed the EBL is at a height of 500-300 hPa (Charney and Eliassen, 1949; Hoskins and Karoly, 1981). $\tilde{T}$ is an assumed constant reference temperature, while T' is a mid-tropospheric azonal temperature representing thermal forcing and the natural variability of temperature. k_h and k_z are horizontal and vertical coefficients of eddy viscosity, while H is the atmospheric density scale height (Petoukhov et al., 2013). The atmosphere is generally baroclinic, but this barotropic equation is used since the meridional wind fields at different pressure levels show a significant level of barotropity (Petoukhov et al., 2013). The waves consisting the circulation need to be held within the troposphere so there is no energy dissipation to the stratosphere and this condition is fulfilled for waves with wave numbers 6-8 (Charney and Drazin, 1961).

When we talk about the trapping of the free synoptic waves within mid-latitude wave guides with the aforementioned zonal wave numbers 6-8, we note that usually the quasi-stationary dynamical response to the climatological mean thermal and orographic forcing is weak, since their energy is dispersed to the equator and pole (Hoskins et al., 1977; Hoskins and Karoly, 1981). Through double-peak jet formations the mid-latitude wave guides can experience a much higher response to the mentioned forcing (Coumou et al., 2014). If the wave numbers of the trapped free and the forced wave are similar, the resonance between them can significantly increase the amplitude of the Rossby waves (Coumou et al., 2014).

1.1.3 Finite-amplitude local wave activity

Another way of investigating this problematic is to look into the novel finite-amplitude local wave activity (LWA) diagnostic. The LWA is a dynamic field that determines the interaction of the Rossby wave packets with the westerly wind on smaller, regional scales (Nakamura and Huang, 2018). It can be seen as a diagnostic of the jet stream meandering (Huang and Nakamura, 2015, 2017). If there is pronounced (reduced) jet stream meandering, stronger (weaker) LWA occurs when the jet stream is weaker (stronger). It was developed within the quasi-geostrophy assumptions and conditions, where the potential vorticity, through its property of conservation and its relations to the temperature and the zonal and meridional winds, dictates the motion of air parcels (Vallis, 2006; Pedlosky, 2013; Hoskins et al., 2007). The finite-amplitude LWA differs to the regular wave activity in the sense that it can be used not only for waves with small amplitudes, but also for all waves with finite amplitudes. For the purposes of calculating LWA, the quasi-geostrophic PV is calculated as follows:

$$q(\lambda, \phi, z, t) \equiv \frac{1}{acos\phi}\left[\frac{\partial v}{\partial \lambda} - \frac{\partial(u\cos\phi)}{\partial\phi}\right] + f\left(1 + e^{z/H}\frac{\partial}{\partial z}\left[\frac{e^{-z/H}(\theta - \tilde{\theta})}{\partial\tilde{\theta}/\partial z}\right]\right) \tag{1.3}$$

Here, λ, ϕ, z and t are the longitude, latitude, height and time, respectively. u, v and θ are the zonal wind, meridional wind and the potential temperature. f, H and $\tilde{\theta}$ are the Coriolis parameter, reference scale height and the global area mean of the potential temperature, respectively. The PV generally increases going north, but at any time there is significant waviness of the contours and they show deviations from the mean state (Nakamura and Huang, 2018). These changes in the contours are what forms the Rossby waves. The changes can occur due to thermal and orographic forcing or the transient properties of growing and decaying weather systems (Held and Hoskins, 1985). The LWA is then calculated from the displacement of the PV from its reference state in the following way (Huang and Nakamura, 2015; Lubis et al., 2018):

$$A(\lambda, \phi, z, t) \equiv -\frac{a}{\cos\phi}\int_0^{\Delta\phi(\lambda,\phi,z,t)} q_e(\lambda, \phi+\phi', z, t)\cos(\phi+\phi')\, d\phi' \tag{1.4}$$

Here, q_e is the aforementioned displacement of the PV from its reference state, while ϕ' is the latitudinal displacement. The deviation of the PV is calculated as follows:

$$q_e(\lambda, \phi+\phi', z, t) = q(\lambda, \phi+\phi', z, t) - q_{\text{REF}}(\phi, z, t) \tag{1.5}$$

In this equation, q_{REF} is the reference state of the PV that is supposed to be wave-free without meandering. High values of LWA are at longitudes where the displacement of q is the highest or even overturned (Huang and Nakamura, 2015). It tells us about both the amplitude and the phase of Rossby waves. Column and weak time averaging are performed to exclude the phase dependence. To separate the LWA into different drivers related to different fluxes and non-conservative forcing (diabatic sources and sinks of LWA), a budget equation for the column averaged LWA is used (Nakamura and Huang, 2018):

$$\begin{aligned}&\frac{\partial}{\partial t}\langle A\rangle\cos\phi\\ &= \underbrace{-\frac{1}{a\cos\phi}\frac{\partial\langle F_\lambda\rangle}{\partial\lambda}}_{\text{I}} + \underbrace{\frac{1}{a\cos\phi}\frac{\partial}{\partial\phi'}\langle u_\mathrm{e} v_\mathrm{e}\cos^2(\phi+\phi')\rangle}_{\text{II}} + \underbrace{\frac{f\cos\phi}{H}\left(\frac{v_\mathrm{e}\theta_\mathrm{e}}{\partial\tilde{\theta}/\partial z}\right)_{z=0}}_{\text{III}} + \underbrace{\langle\dot{A}\rangle\cos\phi}_{\text{IV}}\end{aligned} \tag{1.6}$$

The quantities in $\langle\rangle$ are column-averaged. F_λ represents the zonal LWA flux, $\dot{A}$ is the derivation of LWA in time and v_e and θ_e are the zonal wind and potential temperature deviations from their respective reference states. The marked terms in the equation are the following:

- I - Zonal advective LWA flux convergence
- II - Eddy meridional momentum flux divergence
- III - Low-level eddy meridional heat flux
- IV - Diabatic sources and sinks of LWA

The column-averaged zonal LWA flux $\langle F_\lambda\rangle$ can be decomposed into several components as well and its relation is as follows (Nakamura and Huang, 2018):

$$F_\lambda = \underbrace{\langle u_\mathrm{REF} A\cos\phi\rangle}_{F_1} \underbrace{-a\langle\int_0^{\Delta\phi} u_e q_e\cos(\phi+\phi')\,d\phi'\rangle}_{F_2} + \underbrace{\frac{\cos\phi}{2}\langle v_e^2 - u_e^2 - \frac{R}{H}\frac{e^{-\kappa z/H}}{\partial\tilde{\theta}/\partial z}\theta_e^2\rangle}_{F_3} \tag{1.7}$$

In this equation, the F_1 and F_3 terms represent the group propagation of the Rossby waves in the reference state (Nakamura and Huang, 2018). Their sum is linearly related to the the column-averaged LWA, where the proportionality constant is the mean wave zonal group velocity (Nakamura and Huang, 2018). The F_2 term is the flux modification by the waves with larger amplitudes (Nakamura and Huang, 2018).

Each of the terms of the LWA budget equation and the zonal LWA flux equation gives valuable insight into the nature of the atmospheric circulation on smaller scales which has led to a certain weather event with persistence and blocking patterns and is therefore of great importance for this study. The advantage of this approach is that it is possible to distinguish between different eddy and non-conservative (diabatic sources and sinks) effects (Lubis et al., 2018), since it gives insight into the amount of the mean-flow modification by the eddies (Nakamura and Solomon, 2010).

Winds steer cyclones and anticyclones that cause the jet stream meandering over large areas (Nakamura and Huang, 2018). This jet stream meandering can then be described by the LWA and can propagate eastward as transient Rossby waves (Rossby, 1939; Platzman, 1968). Sometimes, the meandering becomes persistent in certain regions and blocking conditions occur (Rex, 1950; Woollings et al., 2010; Berggren et al., 1949). (Nakamura and Huang, 2018) have found that the LWA and its budget demonstrate a close analogy between blocking and a traffic congestion on a highway. The highway has a traffic capacity and in turn so does the jet stream have a capacity for the LWA flux or meandering. When this capacity is exceeded, the blocking manifests as congestion like a traffic jam. The LWA flux is explained by 1.7.

1.2 Problem Formulation

The first problem to solve is whether to approach these events through either a simplistic or more complex approach. The insight could provide valuable information for the scientific community working with this topic, as well as some parts of the economy sector like hydropower companies, which need better forecasting and managing of extreme events. A lot of research and analysis has been done to shed more light on this, but more remains to be done in order to obtain a sustainable and effective approach. One of the more important specific problems to solve is to find a clear approach of defining an extreme event and its probability of occurring and then to adjust ways of reacting and dealing with these events. Starting from the proposed concept of wave resonance, there are different ways of investigating it and each has its own advantages and disadvantages. One is to opt for a more complex definition of the resonance, where extensive analysis is done on high-amplitude quasi-stationary Rossby waves of certain wave numbers as well as upper-level winds and surface extremes such as heat and rainfall extremes (Petoukhov et al., 2013). In a more simplistic approach, the changes in the zonal mean temperature profile and changes of the strength and the position of the maxima in the mid-latitude westerly jet were investigated (Mann et al., 2017). In (Petoukhov et al., 2013; Mann et al., 2017), further investigation was performed to identify the so-called double jet structures, which are more likely to lead to resonance events. The approach for the analysis of the extreme events selected in this thesis will be based on the finite-amplitude LWA, which can analyze the role of persistent meandering of the circulation and the dynamical processes driving the meandering. In the case of blocking, the role of the zonal LWA flux in the onset development phase and its similarity to the traffic jam concept will also be investigated. Such development of the LWA flux in the early onset blocking phase could help in predicting different extreme weather events. Also, due to the differences in suggested mechanisms affecting extreme events in different seasons (weakened jet in summer and possible sea-ice cover influence in autumn and winter), a more general and conclusive approach is needed to be ready for use in all seasons and times of year. Most of the extreme events that are generally analyzed and researched occur on the Northern Hemisphere and have a strong impact of its population. The analysis in this thesis focuses on events occurring in different regions of Norway.

1.3 Related and Future Work

The source for the idea of this thesis came mostly from different articles (Mann et al., 2017; Petoukhov et al., 2013; Coumou et al., 2014; Kornhuber et al., 2017), which contain the relevant starting concepts and introductory research about the topic, as well as from case studies done by Agder Energi on different extreme weather events in Norway in the last several years. The mentioned papers and studies suggested resonance might be increasing the frequency of extremes. Most of the work done has been carried out in the way of investigating different variables quantifying the large-scale atmospheric circulation, such as the geopotential height and upper-level winds for different summer events. Research has also been done in investigating different variables related to surface extremes, such as temperature, rainfall, snowfall and sea-ice cover. The information and insight from these articles and studies is a starting point for the development of the work done on this thesis and its goals.

To further investigate and clarify the occurrence of extreme weather events related to persistent meandering and the corresponding dynamical mechanisms related to it, more analysis of various parameters needs to be done. A larger number of events throughout longer time frames in all seasons needs to be investigated. One of the main challenges is to develop an appropriate climate index for these events to define their occurrence, probability and variability as well as connecting them to LWA as a proposed proxy for blocking events. More research also needs to be done to understand the link of these patterns to internal modes of climate variability, such as the El Niño Southern Oscillation (ENSO), the North Atlantic Oscillation (NAO) and the Arctic Oscillation (AO).

1.4 Objectives

The main objectives of this Master's thesis are:

1. Set a general and conclusive way to identify Northern Hemisphere extreme weather

events regardless of the season

2. Investigate possible ways of efficient prediction of the events
3. Understand the dynamics of the events using the finite-amplitude LWA approach
4. Investigate the influence of the events on the meteorological variables relevant for the production of energy in Norway

1.5 Approach

The approach used in this thesis will be different to the approach described in the previous paragraphs from the papers referenced. A more robust approach with broader dynamical and statistical analysis of more events throughout a longer time period is required. Furthermore, comparisons to the actual events in question will help to probe deeper into how extreme an event was and how does it relate to similar previous and following events. Also, since (Mann et al., 2017; Petoukhov et al., 2013; Coumou et al., 2014; Kornhuber et al., 2017) have shown that the idea of resonance is questionable and it isn't yet clear to what extent such resonance is related to extremes in Norway, a different type of approach based on the finite-amplitude LWA will be used, as mentioned previously. Furthermore, the resonance approach is applicable mostly in summer, so a different scheme is needed to investigate all of the events in this thesis. There will also be a focus on the large-scale circulation, like in the mentioned papers, but in a different way. Instead of investigating Rossby wave wave number decomposition, more focus will be set on investigating the LWA diagnostic, which can serve as a direct proxy for showing the prominence of the persistence and blocking patterns of a certain event.

For most of the thesis, the main aspects which will be investigated and analyzed are the large-scale atmospheric motion and waves through different meteorological and thermodynamical variables. This will give insight into the causes of the various extreme weather events considered. Starting from the time periods in which the mentioned extreme events have occurred, the daily anomalies of different atmospheric variables, such as geopotential height, meridional and zonal wind, temperature, precipitation and snowfall rate are analyzed to make their time series plots and define certain extreme weather patterns. After that, a thorough statistical analysis is carried out with index creation, correlation analysis, percentile and composite analysis being made. After obtaining a broad statistical data set, the dynamics and mechanisms of these events will be analyzed using the finite-amplitude LWA approach.

1.6 Contributions

Main contributions for this work come from the input of my three supervisors Nour-Eddine Omrani, Tarjei Breiteig and Noel Keenlyside including their systematic guidance throughout the problematic of the research on this topic with different analyses and techniques used. The data used is contributed by the Copernicus Climate Data Store (CDS) and the European Centre for Medium-Range Weather Forecasting (ECMWF). A very significant contribution came from Clare S. Y. Huang from the University of Chicago, who is the author of the LWA Python library used to obtain different results in the thesis and who has also helped with honing the scripts for the specific cases investigated. Other contributions come from the different papers and sources referenced throughout the manuscript.

1.7 Limitations

Most limitations have occurred in the way of analyzing the data in order to define an extreme event. Some of the methods used, such as creating an appropriate index, are very sensitive to the usage of the region for the index, where small changes in the region can make significant changes in the final result. The broadness of the research topic has also proven to be an issue during the work and more time is needed to properly investigate the influence of different meterological variables (temperature, precipitation, snowfall) on the Norwegian energy production.

1.8 Outline

In this paragraph I give an overview of the remaining parts of the report:

- Data and Methods: Description of all relevant data and the mathematical, statistical and programming tools used.
- Results: Different plots of each of the methods used in the analysis for all events.
- Discussion: Broader description of the results with their relevance and significance to the expected outcomes and goals.
- Conclusion: Short summary of the results and achieved goals with suggestions for future work and research.
- Bibliography

Chapter 2

Data and Methods

2.1 Introduction

The analysis is based on the daily data of different atmospheric variables (geopotential height, zonal wind, meridional wind, surface temperature, precipitation rate and snowfall rate). The data are manipulated using the Python programming language (Van Rossum and Drake, 2009) in an Anaconda distribution (Anaconda Inc., 2020). The following Python packages were of great use in the project:

- CDO (Climate Data Operators) (Schulzweida, 2019)
- NCO (NetCDF Operators) (Zender, 2008)
- statsmodels (Seabold and Perktold, 2010)
- NumPy (Harris et al., 2020)
- xarray (Hoyer and Hamman, 2017)
- Matplotlib (Hunter, 2007)
- SciPy (Jones et al., 2001)
- cartopy (Met Office, 2015)

2.2 Data

The data used in this thesis comes from the ERA5 and ERA-Interim reanalysis products. The ERA5 was obtained from the CDS, while the ERA-Interim was obtained from the ECMWF.

ERA5 is actually a replacement for the ERA-Interim data set, which was stopped being produced on August 31, 2019. However, due to the incompatibility of the LWA Python package used in the analysis with the ERA5 data set, the ERA-Interim was used instead. The ERA5 and ERA-Interim data sets used came from these configurations (Hersbach et al., 2018a,b):

1. ERA5 hourly data on pressure levels from 1979 to present
    a) 500 hPa geopotential height
    b) 250 hPa zonal wind
    c) 250 hPa zonal wind
2. ERA5 hourly data on single levels from 1979 to present
    a) Mean total precipitation rate (sum of large-scale and convective precipitation)
    b) Mean snowfall rate (sum of large-scale and convective snowfall)
    c) 2m temperature (2m above the surface of land, sea or inland waters)
3. ERA-Interim
    a) Zonal wind
    b) Meridional wind
    c) Temperature

The ERA5 data sets have a regular latitude-longitude grids with a 0.25°x0.25° resolution. The time series of the sets go from January 1, 1979 to December 31, 2019. For ERA-Interim, the mentioned variables span across 37 different levels from 1000 to 1 hPa, which are essential in calculating LWA and its budget components. As mentioned previously, the ERA-Interim data sets extend from January 1, 1979 to August 31, 2019 and have a lower resolution of 1.5°x1.5°.

2.3 Anomaly fields

The extreme events are characterized in terms of daily anomalies (i.e., as deviations from the daily climatology). For each day in the year, a mean of it is calculated using values throughout the whole time series. For example, the mean of January 1st is the mean of all of the days with that date throughout the time series. This is how the daily climatology is obtained. Then, each day in the time series is subtracted from its mean to obtain the daily anomalies. They are the starting points to all other calculations and analysis done. The plots of the anomaly fields are used to determine the basics of the relevant large-scale circulation patterns and the peaks of the extreme events. The anomalies of the variables such as the geopotential height and the zonal and meridional winds tell us more about the large-scale circulation situation as well as the persistence. The anomalies of the precipitation and snowfall rate and the surface temperature tell us more about the severity and impact of the events, but again also about the persistence of the extremes. From this, the time period in which the extreme event is happening is determined and the analysis is deepened to other diagnostics. In the end, the anomalies of the barotropic LWA, zonal wind, LWA flux as well as the LWA budget equation components provide the full picture on the events in question.

2.4 Standardized index

The standardized index is a climate index made by using the daily anomalies of the 500 hPa geopotential height. First, a relevant time period along the Northern Hemisphere has to be defined according to the selected extreme event. A 29-day time period is determined for further analysis, where the central day is supposed to be the indicator for the extreme event in terms of an anomaly pattern, which is then used as an identification for the event. Following that, a 29-day time mean of the field is made and is then checked for the most appropriate pattern to use in defining the index region. It is most appropriate to encompass a region where we see a clear high-pressure and low-pressure anomaly, which are interacting and are adjacent to each other. It is crucial to use a region which contains the area in which the extreme event actually happened. Afterwards, a dot product of the time mean and the daily anomalies at each time step is calculated followed by a sum of that product over the whole region, for each time step. In this way, the prominent pattern related to the event is projected to the daily anomalies. After that, standardizing of the index is performed. In this procedure, a time standard deviation of the sum is calculated and the sum and its standard deviation are divided. Some background information from (National Center for Atmospheric Research Staff (Eds)., 2020) was used to better understand the general climate index patterns and rules. This defines a daily varying index to identify other events of similar character to the extreme used to define it. The formula for the product of the anomalies and the pattern (non-standardized index) is:

$$I(t) = \sum_{x,y} Z'(x,y,t) \cdot Z_{\text{pat}}(x,y) \tag{2.1}$$

Here, Z' are the daily anomalies, Z_{pat} is the time mean anomaly pattern around the extreme event time frame and x, y and t are the latitude, longitude and time. The formula for the standardized index then is:

$$SI(t) = \frac{I(t)}{\sigma_{I(t)}} \tag{2.2}$$

Here, σ_I is the time standard deviation of the product of the daily anomalies and the anomaly pattern (the non-standardized index). The obtained index values are then used to define extreme events and are helpful in further calculation. They are used in the percentile and composite analysis explained in the following sections.

2.5 Percentile analysis

A percentile is a statistical quantity that determines what is the range of values below a certain threshold in a data set (Merriam-Webster.com Dictionary, 2021). For example, in a data set consisting of N values, the 95th percentile would be the value below which 95% of the values in the data set are. The percentile analysis in this thesis is used on the index mentioned in the previous paragraph in order to determine the 5% of the highest and lowest index values. These are the values above the 95th and below the 5th percentile, respectively. The values were calculated with an appropriate operator from Python's NumPy package. This method is used to determine the most extreme values of the index on both sides of the distribution. The obtained values above the 95th percentile are used for making (lag) composites of the days with these values in order to test the validity of the index and later on for showing the large-scale circulation and time scale of the events related to these values. The values below the 5th percentile are used to show the linearity in the occurence of the anomaly pattern used for the index calculation. The compositing method is discussed in detail in one of the following sections.

2.6 Autocorrelation function

The autocorrelation function is used as one of the tools to determine the length and time scale of the extreme events. It measures how a lagged version of a time series is related to the same time series and quantifies the rate at which anomalies typically decay (Smith, 2021). It was calculated with Python's statsmodels package. A lag of 30 days is used to determine the autocorrelation and from the plots it is easy to see the time scales of the events. The data used for the calculation are the index values throughout the whole time period (January 1, 1979 to December 31, 2019). The 30 days were used in order to be able to see the persistence further back in time. This is a useful tool in determining the time scale of the extreme event, since it is not possible to determine it just from the anomaly fields and the index. Since the autocorrelation is symmetric, the actual life cycle of the event is double the time scale. The autocorrelation is one of the key points in the argument for the persistence of the events.

2.7 Compositing

Compositing is a procedure that starts from the index values. The idea of it is to show the time scale of the extreme events together with the large-scale circulation and compare the actual event with similar previous and following events. The index is set up in a way that extreme events occur for the days with the maximum values of the index and around them. In the maximum cases, it is expected the values of the index correspond to the days with circulation patterns similar to the pattern used for the index calculation. For the minimum cases, it is expected the pattern is opposite and symmetric. First, compositing was used to test the validity of the index, where in the case of the values of the index above the 95th percentile, the anomaly fields of those days were averaged to see if they reproduce the anomaly pattern used for the index calculation. This is the way to test the validity of the index. Then, the same procedure was used for anomaly fields on the days with index values below the 5th percentile to see if they reproduce an opposite and symmetric pattern. This is the way to see if there is linearity in the occurrence of the pattern.

Next, since 41 years of daily data were used, an assumption was made of 2 extreme events per year, corresponding to a total of 82 events. For values of the index above the 95th percentile, 82 maximum index values were selected. For each of these values, the values 15 days before and after were used in order to display the timeline of the events. A time mean of each of these individual lags is made (from 15 days before to 15 days after), so each time mean consists of 82 fields at a given lag and there is a total of 31 time means. Since the circulation in all cases is mostly meridionally distributed, a meridional mean of the time mean fields is made and then those are merged from 15 days before to 15 days after to form a whole composite. Then, from the composite it is possible to define the timeline of the events projecting onto the single event, which tells us more about the zonal propagations of the systems included as well as the large-scale circulation. It is also useful to see if the composite replicates the circulation pattern that was seen in the anomaly fields as well as in the anomaly pattern used for the index calculation. Composite analyses done in (Hocke et al., 2015; Limpasuvan et al., 2004) were used as guidance in this work.

2.8 LWA Python library

For calculating the LWA and its budget equation components, a specific Python package (Huang, 2015b) was used based on the formulations and diagnostics in (Huang and Nakamura, 2015, 2017; Nakamura and Huang, 2018). The final product gives time series of the barotropic LWA and zonal wind, the LWA budget equation components (the zonal advective

LWA flux convergence, eddy meridional momentum flux divergence and low-level meridional heat flux), the three different components of the zonal advective LWA flux, the reference states of the PV, zonal wind and pressure, the non-averaged LWA, the quasi-geostrophic PV and the interpolated zonal and meridional winds and potential temperature. The tendency of the LWA is calculated from the barotropic LWA itself, while the residual term in the budget equation is then calculated from the known tendency, zonal advective LWA flux convergence, eddy meridional momentum flux divergence and the low-level meridional heat flux in accordance with the equation 1.6. Specifically, an adjusted version of the following script (Huang, 2015a) was used in order to obtain the full set of the aforementioned parameters and then to use them further in the analysis.

Chapter 3

Results

The extreme weather events investigated in this thesis are:

- Lærdal fire and drought (January 2014)
- Odda flood (October 2014)
- Petra flood (August-September 2015)
- Finsland snowfall (January 2018)
- Mykland heatwave (May-June 2018)

Further descriptions of the event will be given in their respective sections. In the investigation of each event, different types of plots for the 500 hPa geopotential height, 250 hPa meridional and zonal wind, barotropic LWA and zonal wind, zonal LWA flux and the different components of the LWA budget equation are obtained. The 500 hPa geopotential height is used to detect prominent weather systems like troughs, ridges, cyclones and anticyclones. The winds are used to determine the dominant flow patterns and the level of 250 hPa is used because that is the usual height of the subpolar jet stream, therefore from them the jet stream state can be seen as well. The barotropic LWA and zonal wind are used to determine whether a blocking pattern has developed or not. The LWA budget equation components are used to determine which particular dynamical mechanisms have had the biggest influence on LWA in terms of increasing it or decreasing it. For each event, plots are also presented for the variable that is tightly related to it. This includes the precipitation rate for the drought and the two floods, the snowfall rate for the extreme snowfall event and the surface temperature for the heatwave. The types of plots are anomaly fields, (lag) composites, climate indices and field averaged line plots.

In the plots for the event anomaly fields, lag composites and the differences of the event anomaly fields and lag composites of the different variables we see the states in different stages of the events: 0 (central day), -7 and 7 (7 days before and after the event) and -14 and 14 (14 days before and after the event). In the event anomaly fields, (lag) composite plots and the event deviations from the lag composites, the anomalies used were the daily anomalies. The deviations from the zonal mean are only seen in one of the sets of the composite plots. Also, composites were not made for the precipitation rate, snowfall rate and the surface temperature due to excessive noisiness in the plots. For the event anomaly fields of the 500 hPa geopotential height and the 250 hPa meridional and zonal winds, an additional mean plot is added which is a mean of the anomalies of the 29 days of each event.

The regions used in making the different composite plots for the 500 hPa geopotential height and the 250 hPa zonal and meridional winds were 90°W-90°E, 55-75°N. This latitude and longitude range was used since it encompasses the region of interest of Norway. The (lag) composites are based on the values above the 95th percentile. Different regions were used for calculating the composites of the barotropic LWA and zonal wind, zonal LWA flux and the LWA budget equation components in each case, discussed further in their respective sections.

The index plots are shown with their event values together with the composites of the events projecting on the single event for comparison. In the autocorrelation plots, the significant correlations are the ones outside the shaded tail interval around the x-axis. The mean fields of the barotropic LWA and zonal wind are made from a mean of 29 days centered around the day 0 of the event in question. The line plots of the barotropic LWA and zonal wind and the LWA budget equations were made by making a field mean around the regions used for the composite calculations.

3.1 Laerdal fire event

3.1.1 General event description

On January 18, 2014, a fire broke out in Lærdal in western Norway. Prior to the fire, there was a one-month period with very low precipitation and high temperatures (Yr, 2013). The strong winds during the fire contributed to the vicious spreading of it (Ighoubah and Solheim, 2014). No people were injured or killed, but a lot of buildings were damaged or totally destroyed. This was the biggest city fire in Norway since the Second World War.

3.1.2 Basic variables anomaly fields

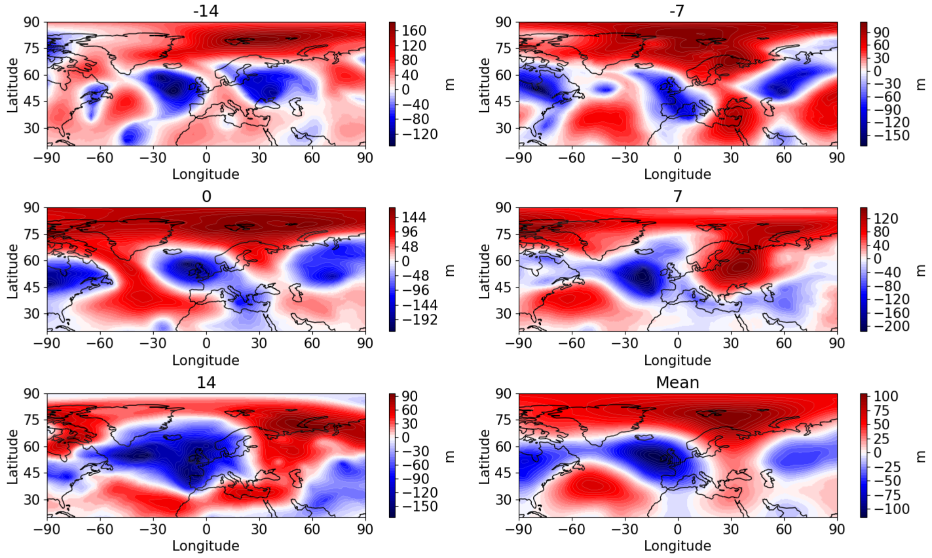

Figure 3.1: The 500 hPa geopotential height event anomaly fields for the Laerdal fire event for days -14, -7, 0, 7 and 14 and the 29-day mean

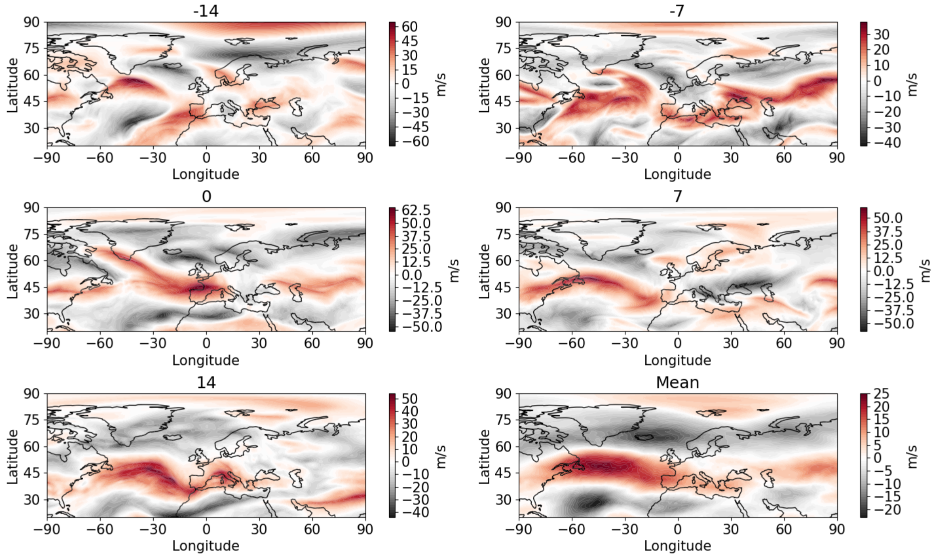

Figure 3.2: The 250 hPa zonal wind event anomaly fields for the Lærdal fire event for days -14, -7, 0, 7 and 14 and the 29-day mean

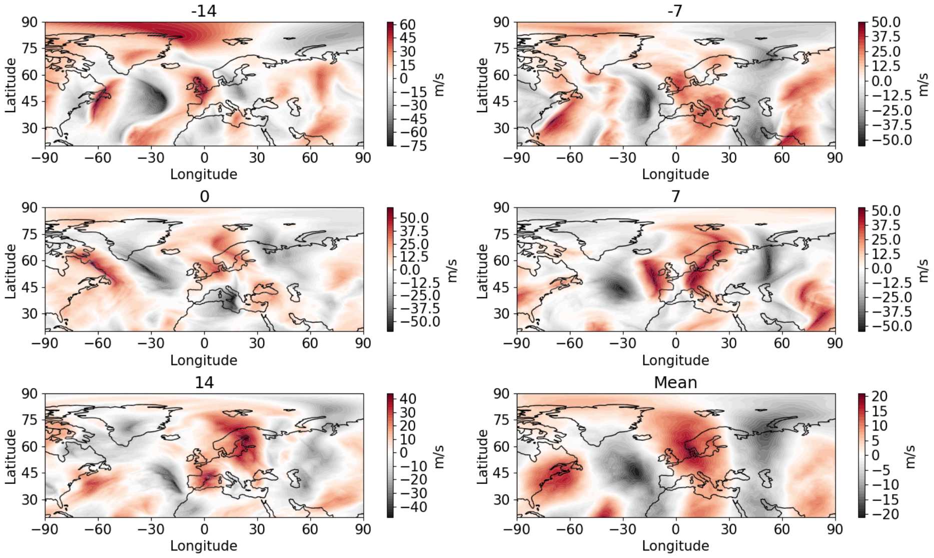

-14 -7 0 7 14 Mean

Figure 3.3: The 250 hPa meridional wind event anomaly fields for the Laerdal fire event for days -14, -7, 0, 7 and 14 and the 29-day mean

Looking at Fig. 3.1, we can see a persisting dipole with a high-pressure anomaly situated between Norway and the North Pole and a negative anomaly in the mid-latitude North Atlantic throughout lags -14, -7, 0 and 7. The pattern is clearly visible in the mean too. According to geostrophic balance, this pattern is associated with the strong weakening of the westerlies downstream of the eddy-driven jet, as seen in Fig. 3.2 and thus causes persistent, blocking-like conditions.

In Fig. 3.2, we see the weakening of the zonal wind in all of the lags with the negative anomalies around the region of interest (western Norway and its surroundings) throughout most of the phases. The mean plot gives a very clear pattern of the negative anomaly situated west of the Norwegian coast in the North Atlantic. The meridional wind plot in Fig. 3.3 shows us the wavy pattern of the negative and positive anomalies in all of the lags indicating strong meandering. The pattern is once again very prominent in the mean plot.

3.1.3 Standardized index

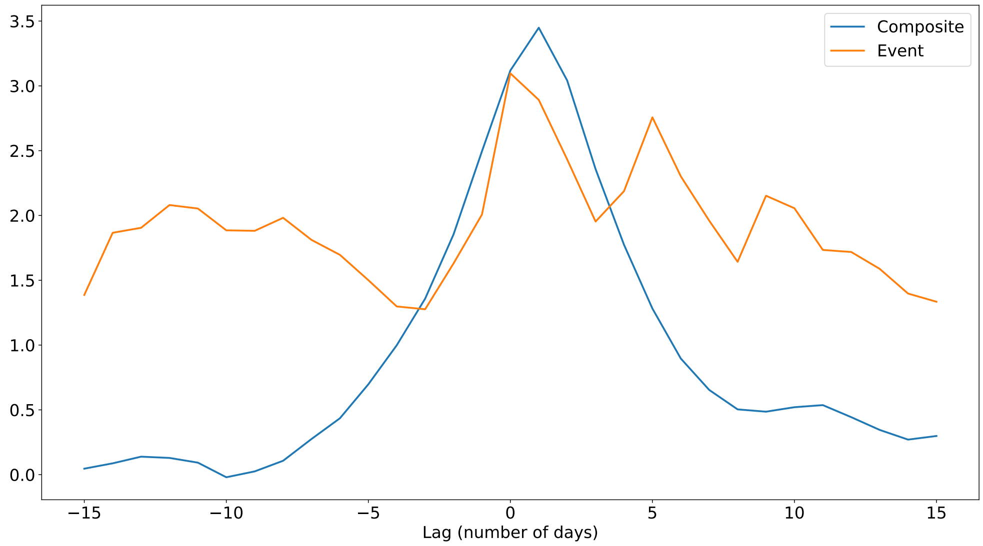

Figure 3.4: The standardized index for the Laerdal fire event and for the composite of the events projecting on it

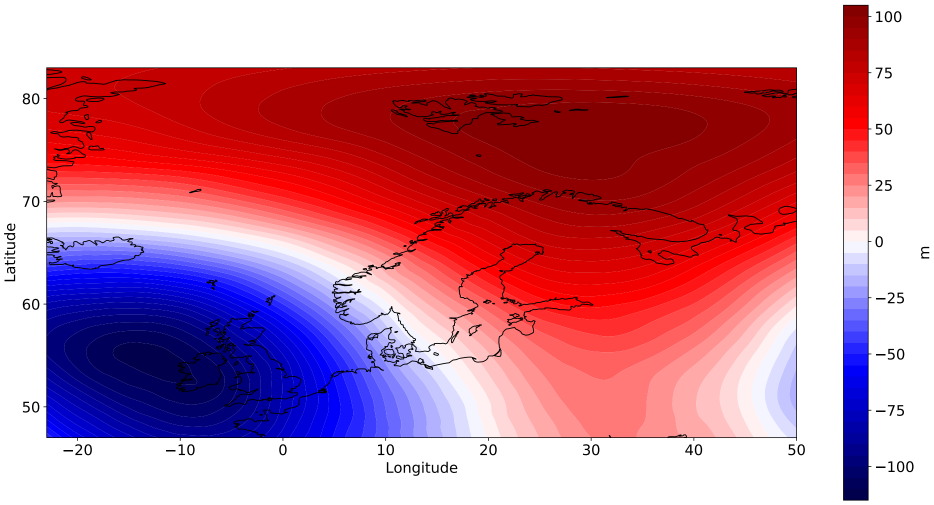

Figure 3.5: The 500 hPa geopotential height anomaly pattern for the Laerdal fire event

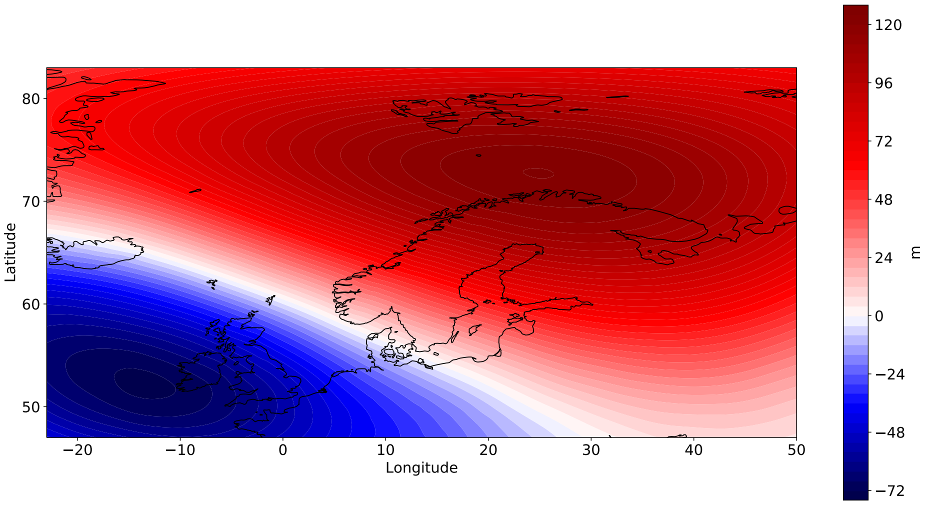

Figure 3.6: The 500 hPa geopotential height 0-day lag composite of the events projecting on the Lærdal fire event for days with index values above the 95th percentile

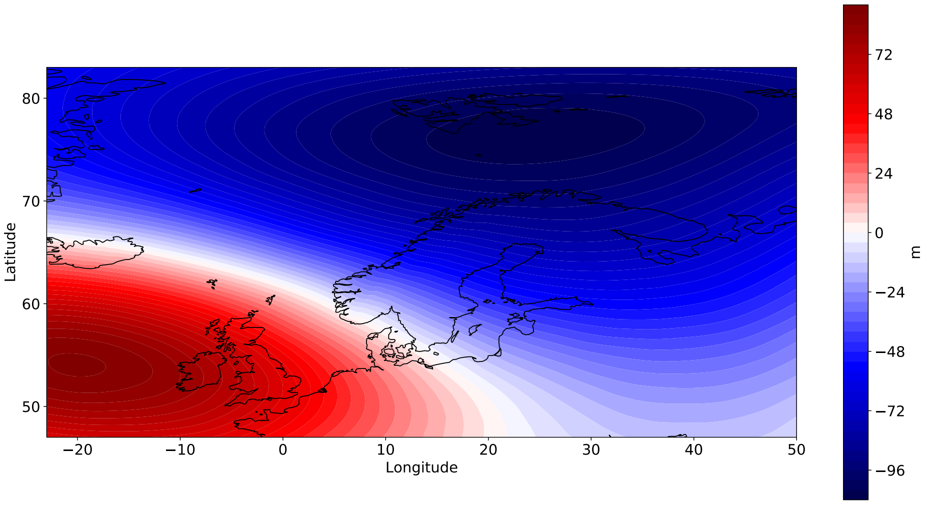

Figure 3.7: The 500 hPa geopotential height 0-day lag composite of the events projecting on the Lærdal fire event for days with index values below the 5th percentile

On the anomaly plot in Fig. 3.5, we see a clear ridge centered around northeastern Scandinavia and a trough in the Irish sea similar to the northeast-southwest meridional dipole seen in previous event geopotential height anomaly fields. This pattern is then projected to the daily anomalies for the same selected region. The index plot in Fig. 3.4 shows the standardized index for the event and for the lag composite of 82 events projecting on the single event, where the central day has an index value larger than the 95th percentile throughout the whole time series. The index can be seen as a proxy for the dipole structure seen in Fig. 3.5, with a positive index indicating an enhanced dipole similar to Fig. 3.6, and a negative index indicating an opposite pattern, seen in Fig. 3.7. The composite shows a clear pattern of rising towards the central day of the event and then falling down. The event index shows a good correlation with the composite. We can also see how the event index has much larger values than the composite at the beginning and end of the time period, indicating it was much more persistent than the composite.

On Fig. 3.6 and 3.7, we see the 0-day lag composites for all days with an index value above the 95th percentile and all days with values below the 5th percentile. The 95th percentile plot shows great agreement with the anomaly pattern used for the index calculation, indicating the validity of the index. The 5th percentile plot shows an opposite and symmetric pattern, which shows the linearity in the occurrence of the pattern.

3.1.4 Autocorrelation function

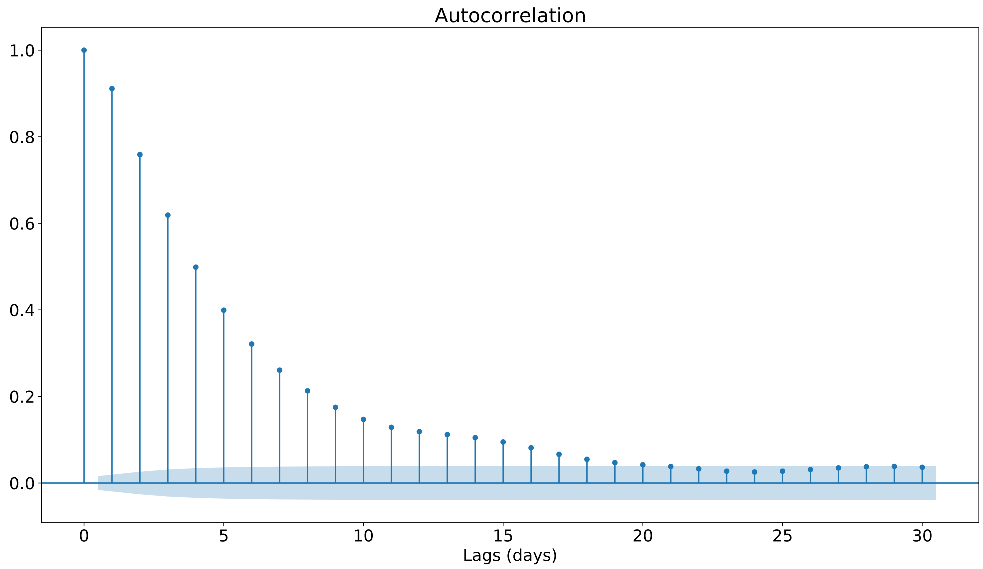

Figure 3.8: The standardized index autocorrelation function for the Laerdal fire event

The autoccorelation plot shown in Fig. 3.8 tells us more about the time scale of the event. We can see that the correlation with the previous days is lost at around 20 days, showing once again that the event had a high persistence.

3.1.5 Basic variables composite maps

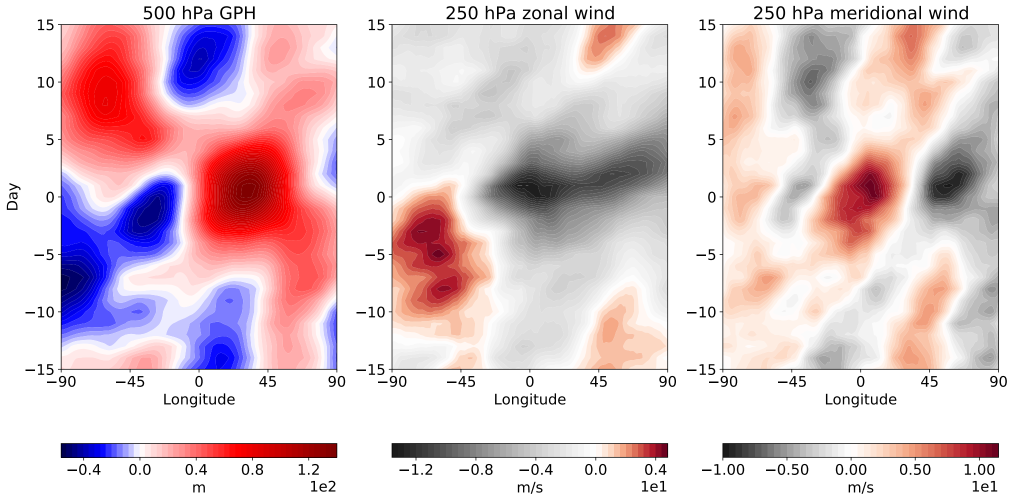

Figure 3.9: The 500 hPa geopotential height and 250 hPa zonal and meridional wind composite of the events projecting on the Laerdal fire event (daily anomalies) for 90°W-90°N and 55-75°N

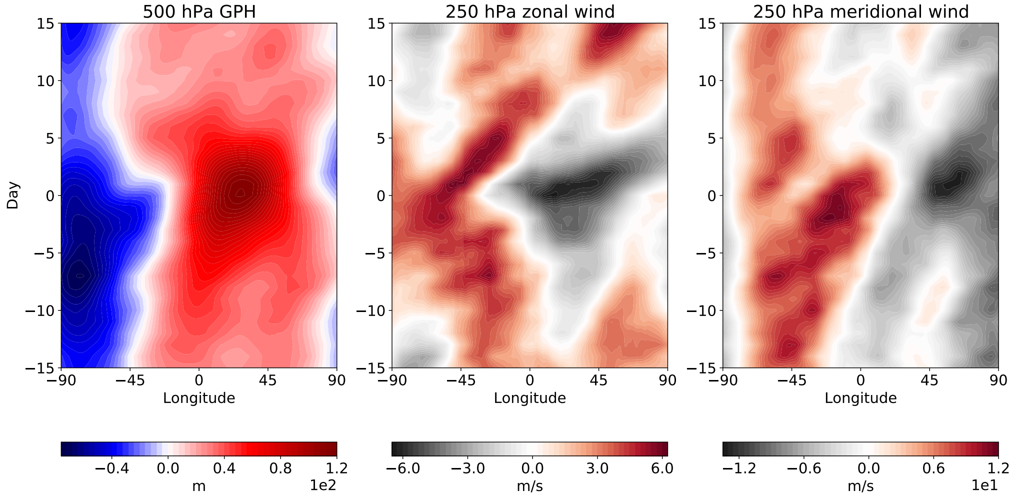

Figure 3.10: The 500 hPa geopotential height and 250 hPa zonal and meridional wind composite of the events projecting on the Laerdal fire event (deviations from the zonal mean) for 90°W-90°N and 55-75°N

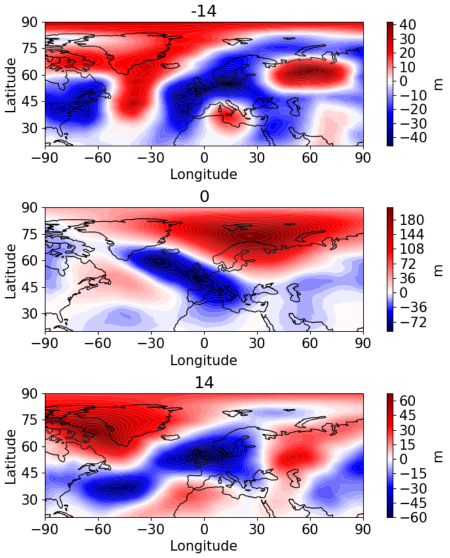

Figure 3.11: The 500 hPa geopotential height lag composites of the events projecting on the Lærdal fire event for lags -14, -7, 0, 7 and 14

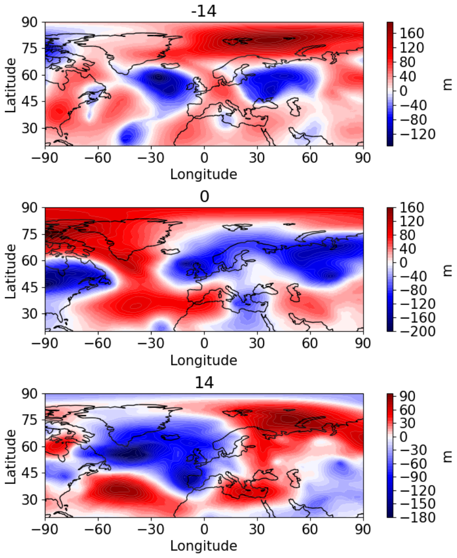

Figure 3.12: The 500 hPa geopotential height event deviations from the lag composites of the events projecting on the Lærdal fire event for lags and days -14, -7, 0, 7 and 14

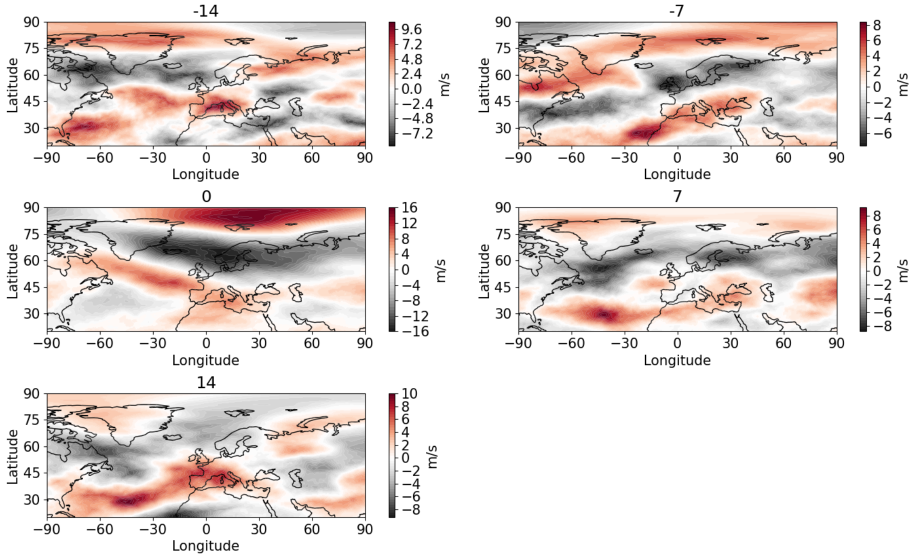

Figure 3.13: The 250 hPa zonal wind lag composites of the events projecting on the Lærdal fire event for lags -14, -7, 0, 7 and 14

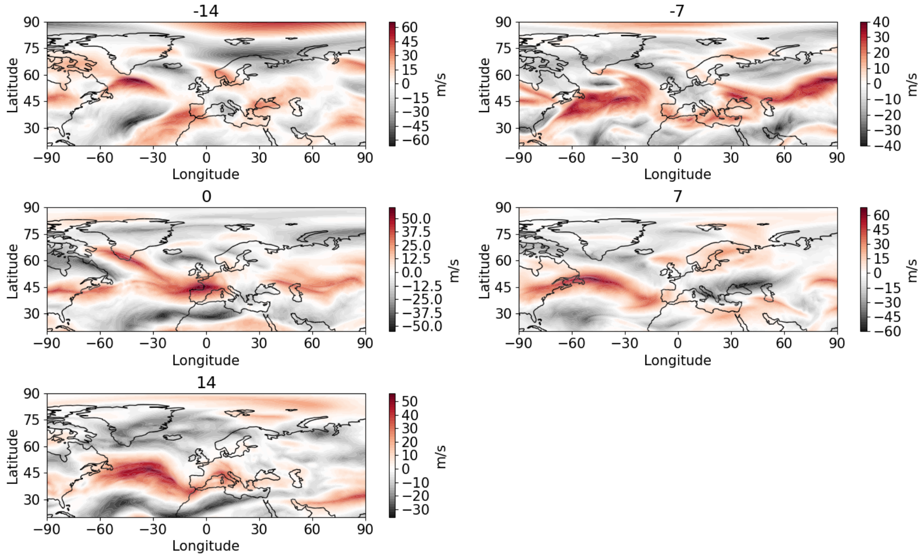

Figure 3.14: The 250 hPa zonal wind event deviations from the lag composites of the events projecting on the Lærdal fire event for lags and days -14, -7, 0, 7 and 14

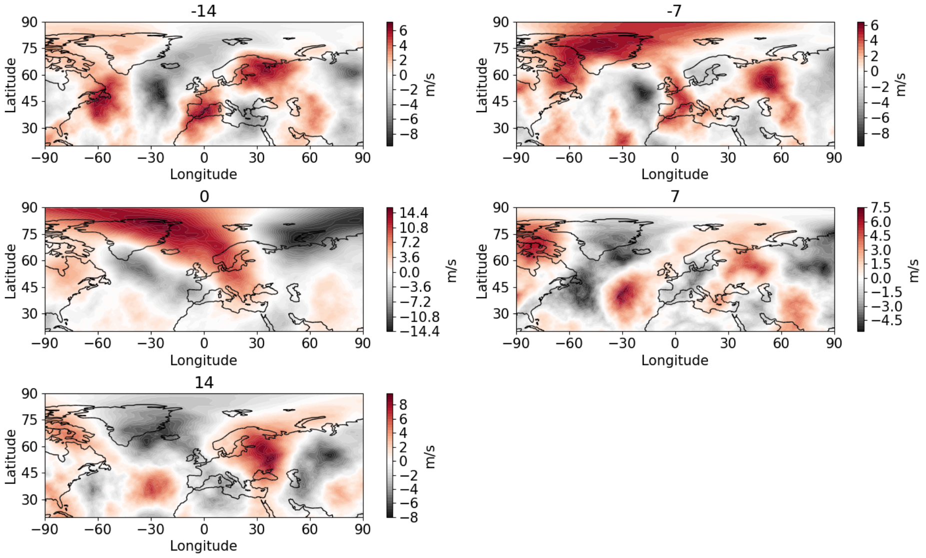

Figure 3.15: The 250 hPa meridional wind lag composites of the events projecting on the Lærdal fire event for lags -14, -7, 0, 7 and 14

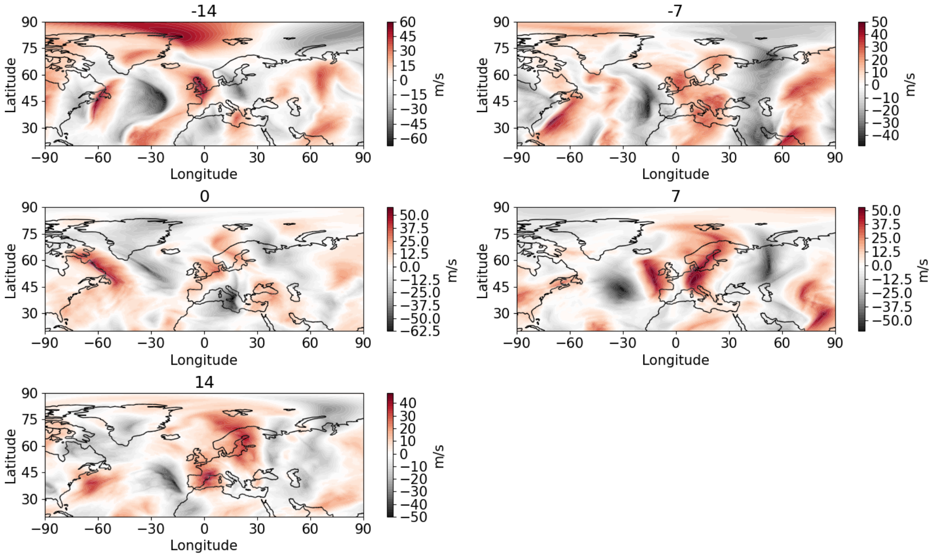

Figure 3.16: The 250 hPa meridional wind event deviations from the lag composites of the events projecting on the Lærdal fire event for lags and days -14, -7, 0, 7 and 14

The composite plots in Figs. 3.9 and 3.10 show us the prominent dipole pattern in the geopotential height, where we can see how the positive anomaly persists from lags -5 to 5. For the zonal wind, we see the negative anomaly also spread out in the same time period, as well as the positive anomaly of the meridional wind similar to the event anomaly field plots. The deviations from the zonal mean plots show even more persistence.

Looking at the geopotential height lag composites in Fig. 3.11, in lag 0 we can recognize the anomaly pattern of the index and of the event. The other lags (especially -7 and 7) show some signs of persistence in the upper latitudes. The difference plots in Fig. 3.12 show that the event was weaker than the composite mean (lag 0), which is in agreement with the index plot in Fig. 3.4.

The zonal wind lags in Fig. 3.13 show a persistent negative anomaly over the northern North Atlantic, while in the differences in Fig. 3.14, we can again see the event was weaker than the composite mean with slighlty positive values, but more persistent.

The meridional wind lags in Fig. 3.15 show some interesting patterns with a prominent dipole in lag 0, where we see the beginning of the development of the positive anomaly in lag 7. In lags -14, 7 and 14, we see wavy patterns indicating meandering. The difference plots in Fig. 3.16 show little difference to the event anomalies in Fig. 3.3.

3.1.6 Precipitation rate

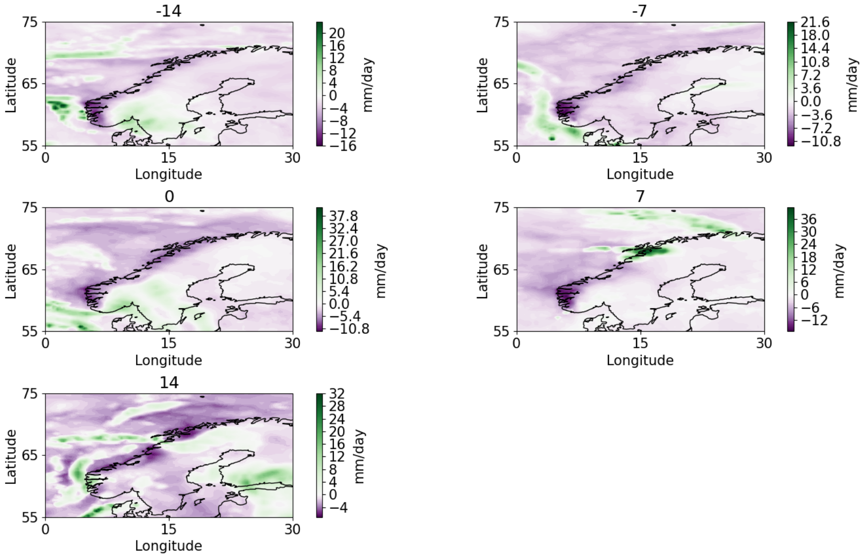

Figure 3.17: The precipitation rate event anomaly fields for the Lærdal fire event for days -14, -7, 0, 7 and 14

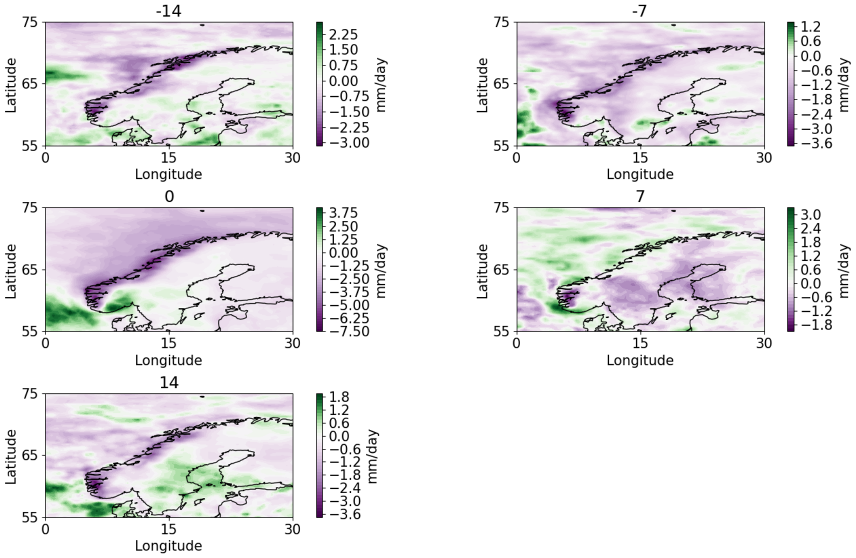

Figure 3.18: The precipitation rate lag composites of the events projecting on the Lærdal fire event for lags -14, -7, 0, 7 and 14

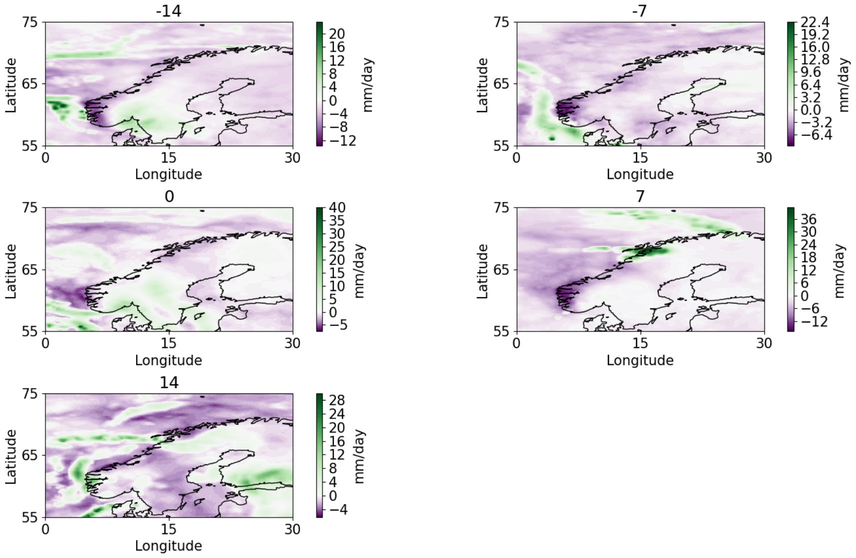

Figure 3.19: The precipitation rate event deviations from the lag composites of the events projecting on the Lærdal fire event for lags -14, -7, 0, 7 and 14

For this particular event, we look into the precipitation rate as a relevant variable, since from it we can exactly see the rate of the impact of the drought. In the event anomaly fields in Fig. 3.17, we see how the negative anomaly persists over southwestern Norway in all lags besides lag 14. This persistence of the negative anomalies over all lags was crucial for the impact of the event. The composite plots in Fig. 3.18 show the same patterns with even more persistence, and in lag 14 as well. The difference plots in Fig. 3.19 show very little difference to the event anomalies.

3.1.7 Barotropic LWA and zonal wind

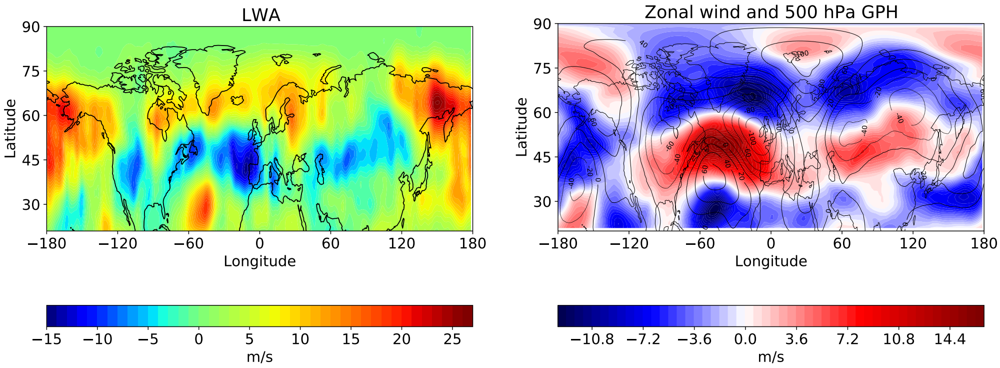

Figure 3.20: The barotropic LWA and zonal wind 29-day event anomaly means for the Lærdal fire event

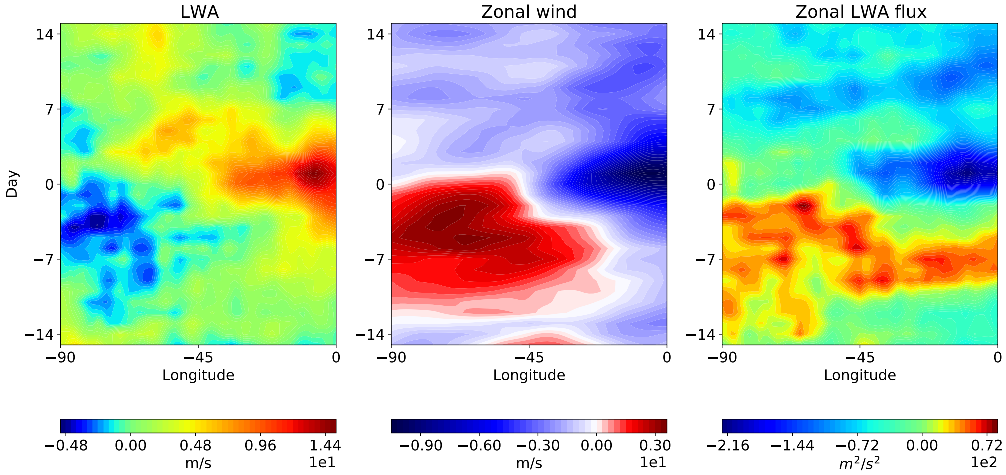

Figure 3.21: The barotropic LWA, zonal wind and zonal LWA flux composites of the events projecting on the Lærdal fire event for 90°W-0° and 60-70°N

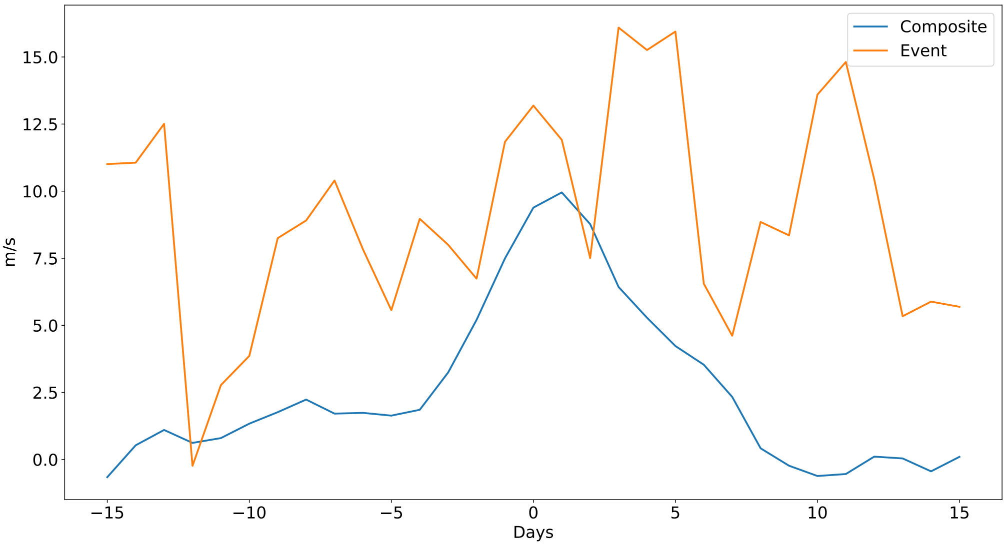

Figure 3.22: The barotropic LWA for the Lærdal fire event and the composite of the events projecting on it for 45°W-0° and 60-70°N

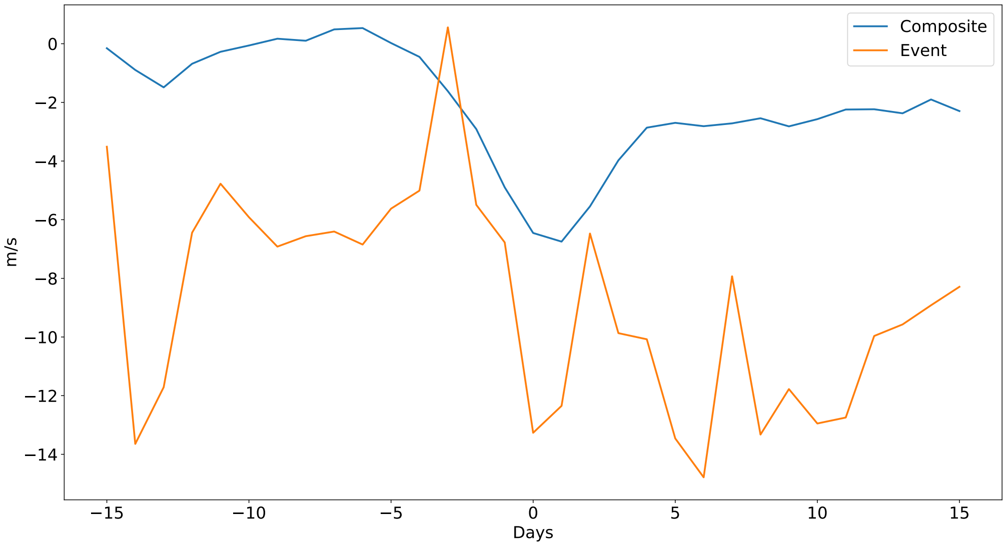

Figure 3.23: The barotropic zonal wind event for the Lærdal fire event and for the composite projecting on it for 45°W-0° and 60-70°N

In Fig. 3.20, we see that generally the LWA and the zonal wind are anticorrelated with positive LWA and negative zonal wind values in the region of interest around Norway, which is what we would expect and a good sign for showing us the blocking patterns. The enhanced LWA or meandering is associated with a weakened westerly, which favors the blocking. This is consistent with the traffic jam concept (Nakamura and Huang, 2018). The next step is to create composite plots from specific regions. For this case, the negative wind anomaly region of 90°W-0°, 60-70°N was chosen, based on Fig. 3.20.

From the composite plot in Fig. 3.21, we see a positive LWA anomaly and negative zonal wind anomaly corresponding to the mean anomaly plots seen before and to the assumed circulation conditions. Consistent with the traffic jam concept introduced by (Nakamura and Huang, 2018), in which the capacity of the LWA flux downstream of the jet behaves like traffic capacity in a highway, there is a strong increase of the LWA flux in the onset phase of the blocking development. Such increase exceeds the jet stream capacity of the LWA flux leading to a blocking situation similar to a traffic jam.

The line plot of the event and the composite of the barotropic LWA, seen in Fig. 3.22, shows us the LWA was stronger and more persistent than in the composite mean, while for the zonal wind in Fig. 3.23, we can see it had a stronger negative anomaly indicating high persistence and blocking. There was one modification made in the region used for the line plot where instead of the 90°W-0° longitude, only the 45°W-0° longitude was used corresponding to the negative zonal wind anomaly around the central days in Fig. 3.21. This region was used in order to avoid cancelling between positive and negative values to get a clearer picture of the event.

3.1.8 LWA budget equation components

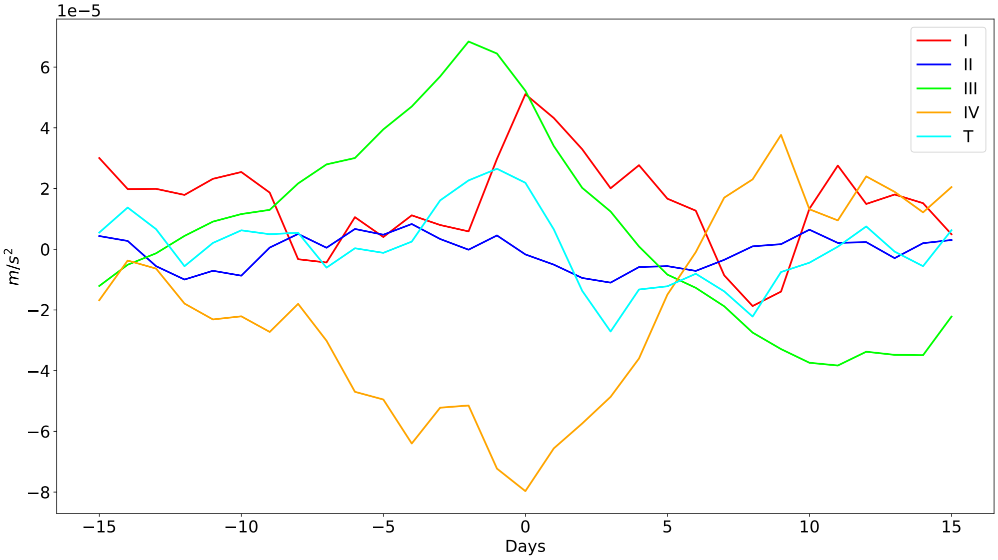

Figure 3.24: The LWA budget equation components (zonal LWA flux convergence (I), eddy meridional momentum flux divergence (II), low-level meridional heat flux (III), residual (IV) and the LWA tendency (T)) for the composite of the events projecting on the Laerdal fire event for 45°W-0° and 60-70°N

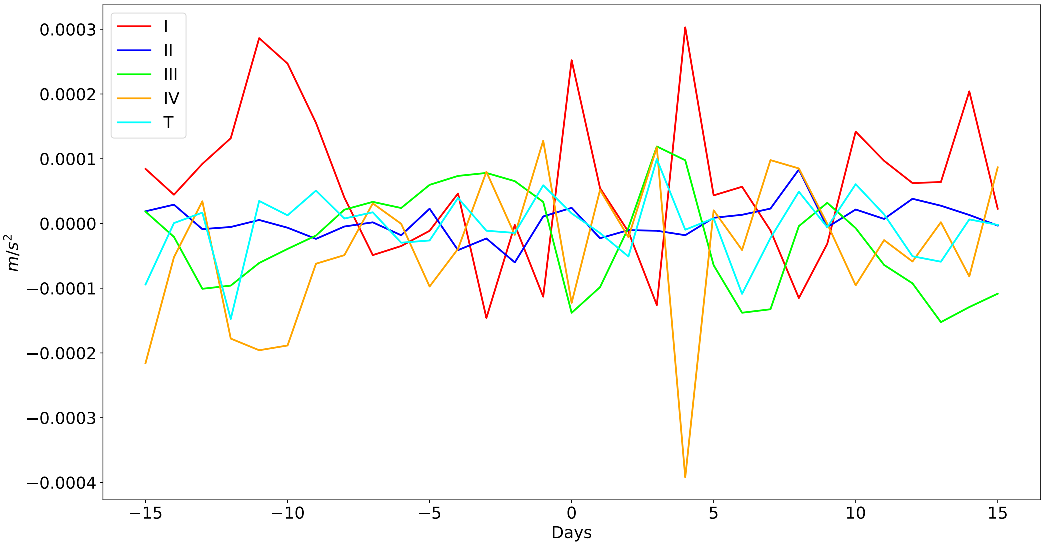

Figure 3.25: The LWA budget equation components (zonal LWA flux convergence (I), eddy meridional momentum flux divergence (II), low-level meridional heat flux (III), residual (IV) and the LWA tendency (T)) for the Laerdal fire event for 45°W-0° and 60-70°N

The line plot of the composite in Fig. 3.24 shows us the biggest influence on the tendency (T) go to the meridional heat flux (III), residual (IV) and the zonal LWA flux convergence (I). The eddy meridional momentum flux divergence (II) is mostly stable at 0, while the tendency (T) shows small oscillations around zero. The flux convergence and the heat flux help to increase the LWA, while the residual helps to dampen it.

The line plot of the event in Fig. 3.25 shows the zonal LWA flux convergence and the residual have a similar contribution as in the composite, while the meridional heat flux has a significantly lower contribution. The tendency and the eddy meridional momentum flux divergence are mostly stable around 0 as in the composite. The zonal LWA flux convergence helps to increase the LWA and its early onset is in agreement with the zonal LWA flux composite plot in 3.21. Here we can see the relation to the traffic jam analogy mentioned earlier. The residual is the one that dampens the LWA. As in the previous section, a different region of 45°W-0° was used in accordance with the negative zonal wind anomaly in Fig. 3.21.

3.2 Odda flood event

3.2.1 General event description

In October 2014, a large flooding event affected a large part of the Hordaland and Sogn og Fjordane regions of Norway. The biggest damages occurred on October 28 and 29 where Odda, Lærdal, Aurland and Voss were the most affected (Audardottir Oldeide, 2014). The flood was a result of a long period of very high precipitation accompanied by snow melting from the mountains, which also contributed to the flooding (Løset et al., 2014; Støfring Skovro, 2014). In a three-day period, there were many places which received over 200 mm of precipitation, with the wettest place being Opstveit in Kvinnherad with 332.2 mm (Rommetveit, 2014).

3.2.2 Basic variables anomaly fields

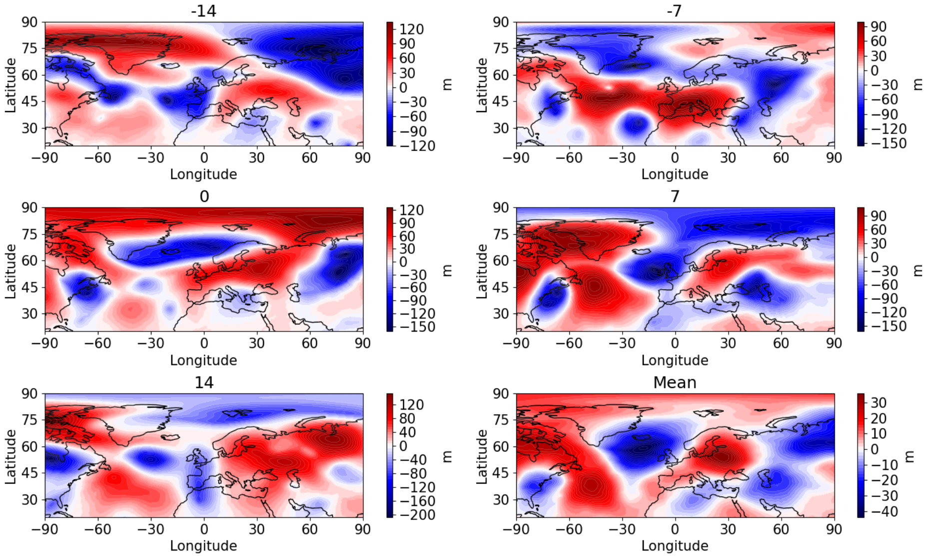

Figure 3.26: The 500 hPa geopotential height event anomaly fields for the Odda flood event for days -14, -7, 0, 7 and 14 and the 29-day mean

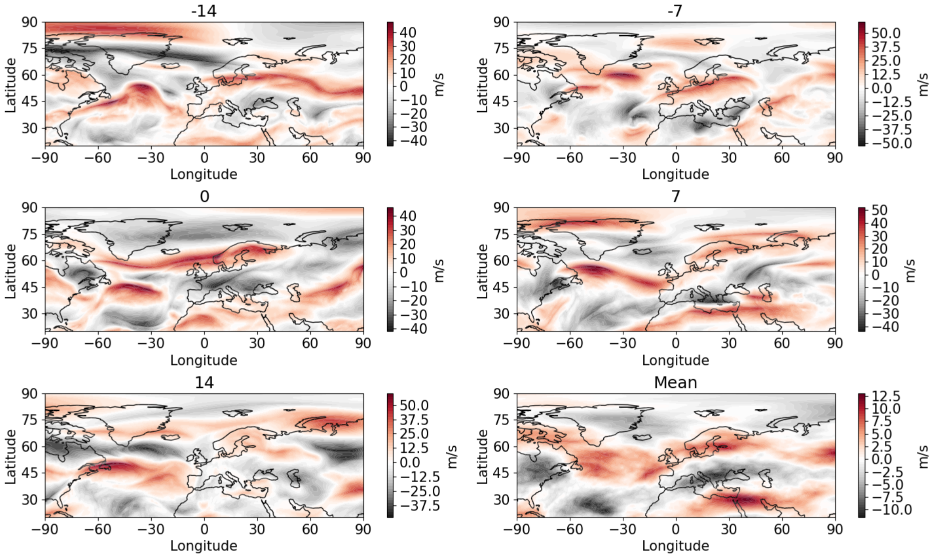

Figure 3.27: The 250 hPa zonal wind event anomaly fields for the Odda flood event for days -14, -7, 0, 7 and 14 and the 29-day mean

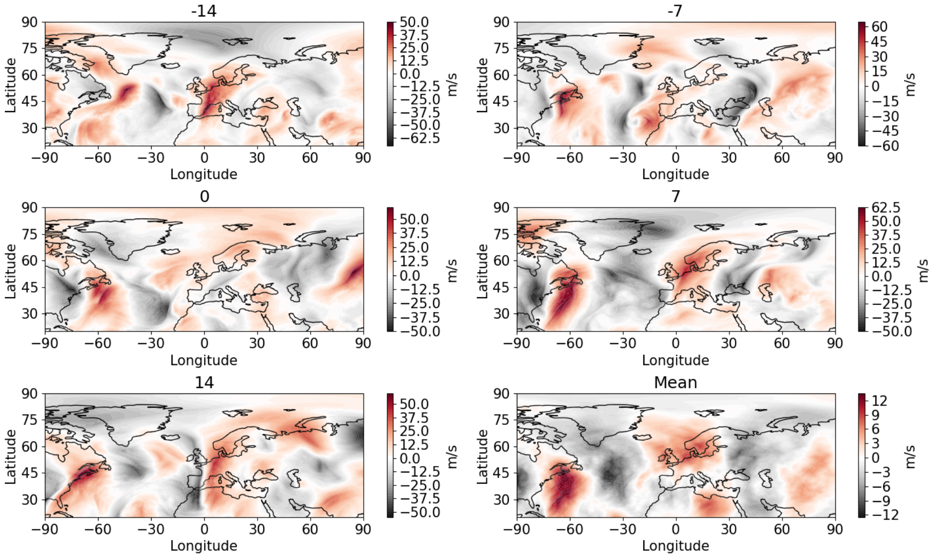

Figure 3.28: The 250 hPa meridional wind event anomaly fields for the Odda flood event for days -14, -7, 0, 7 and 14 and the 29-day mean

In the geopotential height plots in Fig. 3.26, in addition to the low pressure west of Norway that extends until Greenland, there is a high pressure starting from the eastern side of Norway. This high pressure extends to Siberia making the pressure gradient stronger and strengthening the zonally symmetric flow over Norway. The most significant feature from the zonal wind plots in Fig. 3.27 is the positive zonal wind anomaly in the 0 lag, as well as the positive anomaly seen in the mean state of the anomalies. These anomalies could have worked to bring moist and warm air from the Atlantic to the affected flood areas and enhance the precipitation rate. Looking at the meridional wind plots in Fig. 3.28, we do not see a clear wavy pattern of the anomalies, even in the mean state, suggesting the high zonal symmetry in the circulation change seen in the geopotential height plots.

3.2.3 Standardized index

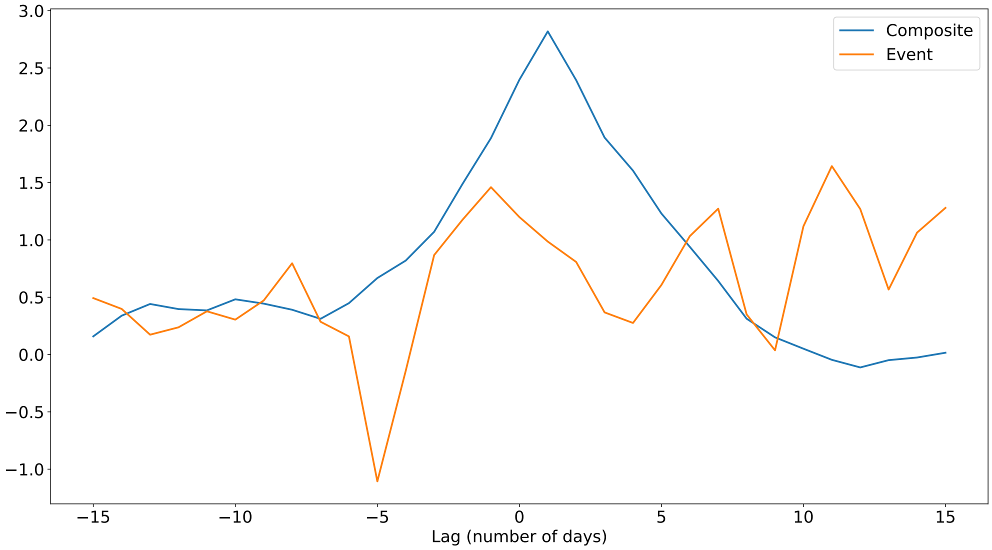

Figure 3.29: The standardized index for the Odda flood event and for the composite of the events projecting on it

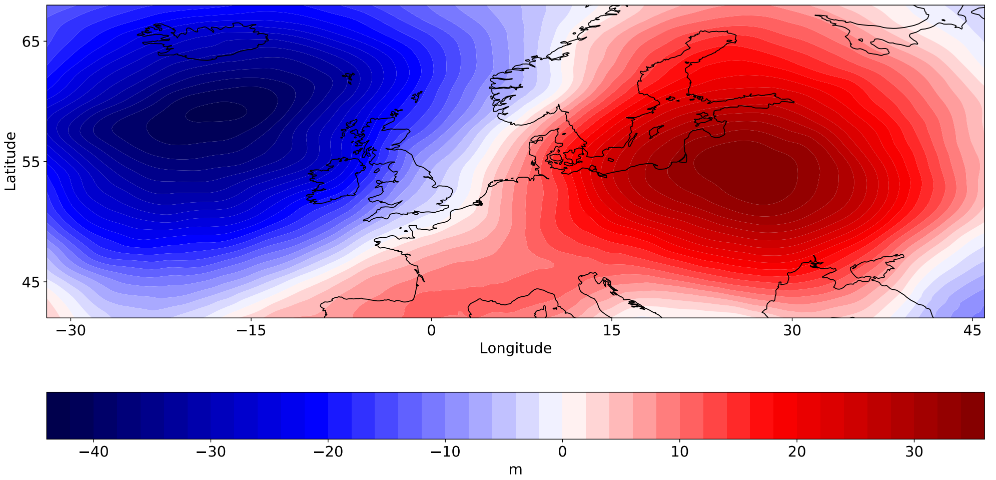

Figure 3.30: The 500 hPa geopotential height anomaly pattern for the Odda flood event

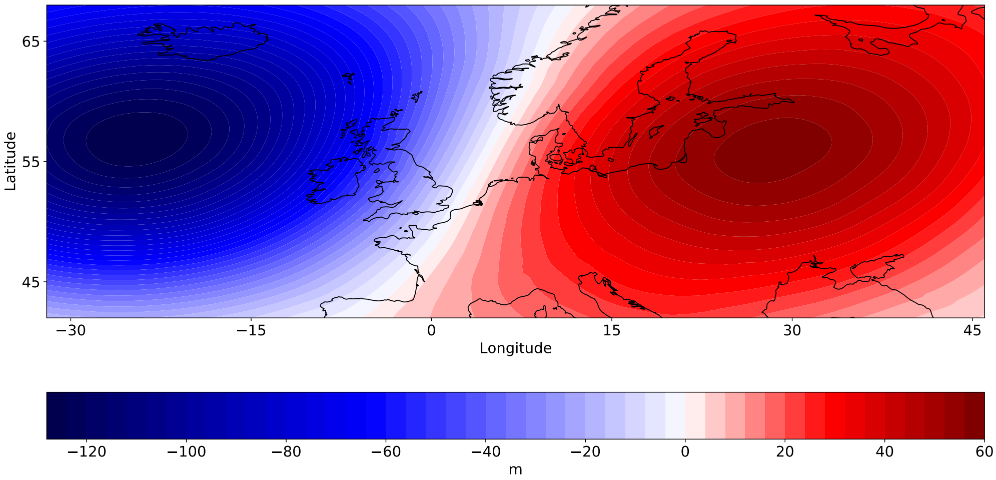

Figure 3.31: The 500 hPa geopotential height 0-day lag composites of the events projecting on the Odda flood event for days with index values above the 95th percentile

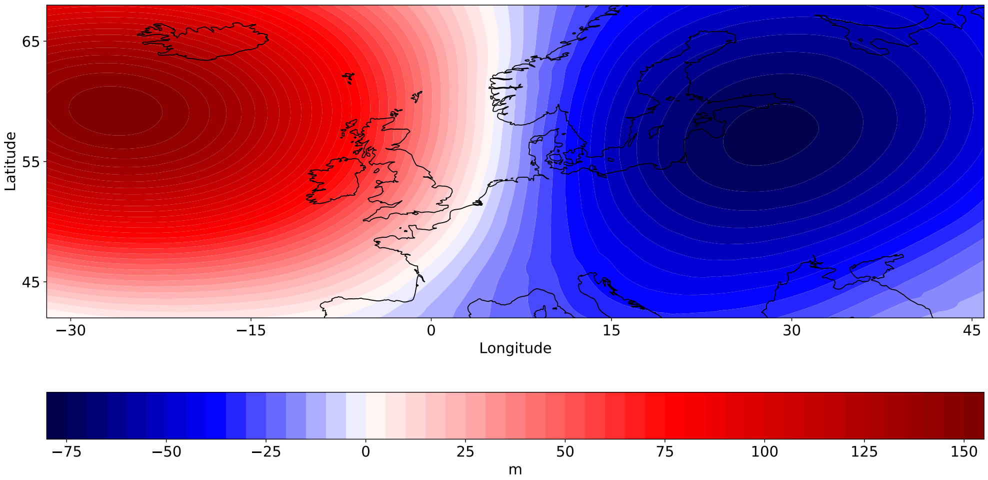

Figure 3.32: The 0-day 500 hPa geopotential height lag composites of the events projecting on the Odda flood event for days with index values below the 5th percentile

The index plot in 3.29 shows that the event index is not in a very good correlation with the index composite. The discrepancy is most seen in the middle part of the plot, where the index has much lower values than the composite, although it has a higher value in the final part. This suggests the event might not have been very strong, but just showed significant persistence. The difference between the event and composite index may also be due to the fact that this event had a slightly different pattern than the averaged event of the composite. In the anomaly pattern plot in Fig. 3.30, we see the pattern seen in the previous geopotential height plots of the different phases with a negative anomaly centered in the North Atlantic and the positive anomaly over northeastern Europe.

The 0-lag composite of all the days with values of the index above the 95th percentile in Fig. 3.31 shows very good agreement with the index anomaly pattern. This shows the validity of the index, although there are some differences to the event state. The event shows more zonal symmetry of the geopotential height gradient than in the composite, which makes the strengthening of the westerlies in the North Atlantic zonally symmetric. This can also be the cause of the difference in the evolution of the composite and event index. In Fig. 3.32, the 0-lag composite of all the maps with values of the index below the 5th percentile shows the opposite pattern, which shows the linearity in the occurrence of the pattern.

3.2.4 Autocorrelation function

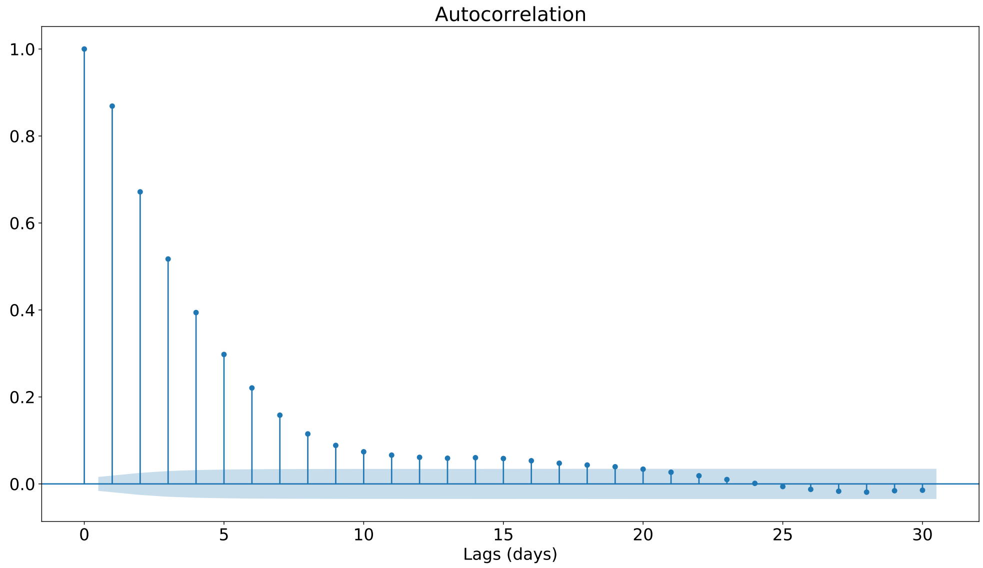

Figure 3.33: The standardized index autocorrelation function for the Odda flood event

The autocorrelation plot in 3.33 shows approximately a 20-day time scale of the event, which shows us again the event was persistent. This is in agreement with the index plot seen previously.

3.2.5 Basic variables composite maps

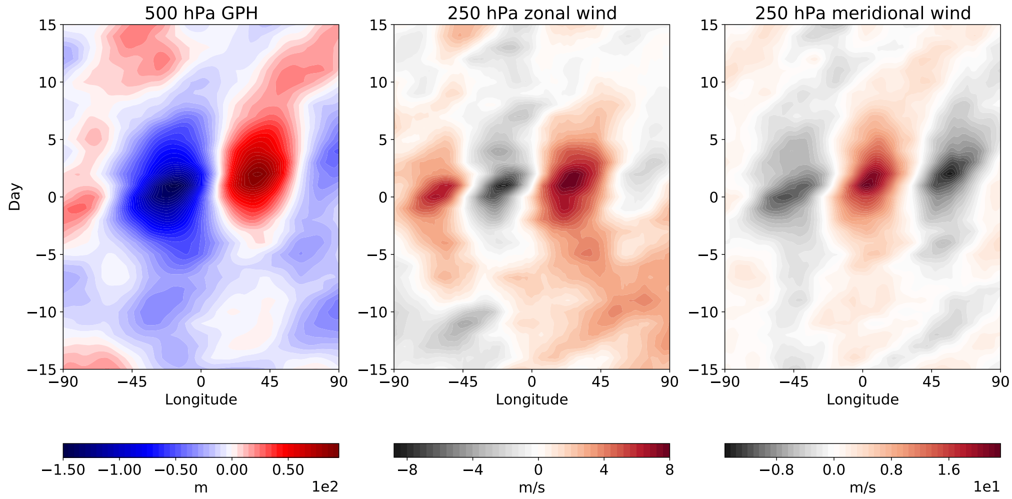

Figure 3.34: The 500 hPa geopotential height, 250 hPa zonal and meridional wind composites of the events projecting on the Odda flood event (daily anomalies) for 90°W-90°N and 55-75°N

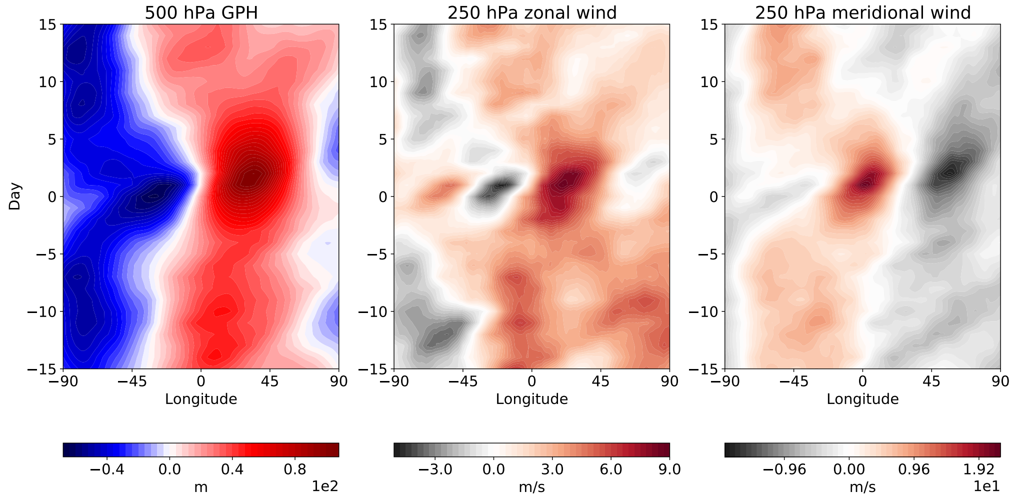

Figure 3.35: The 500 hPa geopotential height, 250 hPa zonal and meridional wind composites of the events projecting on the Odda flood event (deviations from the zonal mean) for 90°W-90°N and 55-75°N

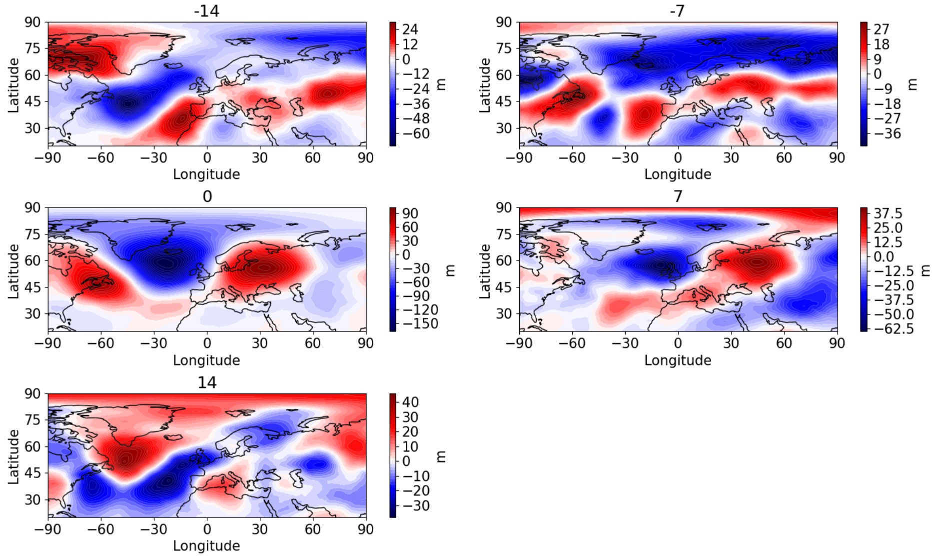

Figure 3.36: The 500 hPa geopotential height lag composites of the events projecting on the Odda flood event for lags -14, -7, 0, 7 and 14

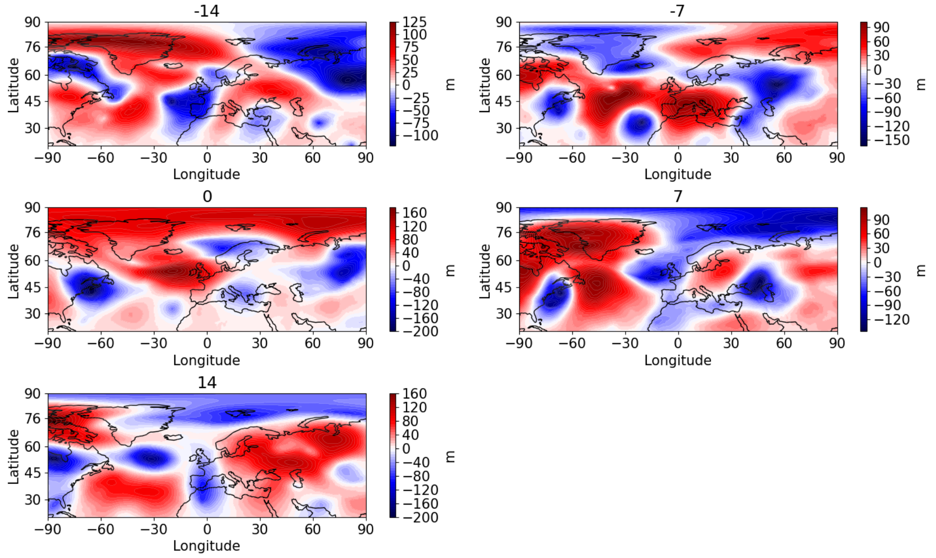

Figure 3.37: The 500 hPa geopotential height event deviations from the lag composites for the events projecting on the Odda flood event for lags and days -14, -7, 0, 7 and 14

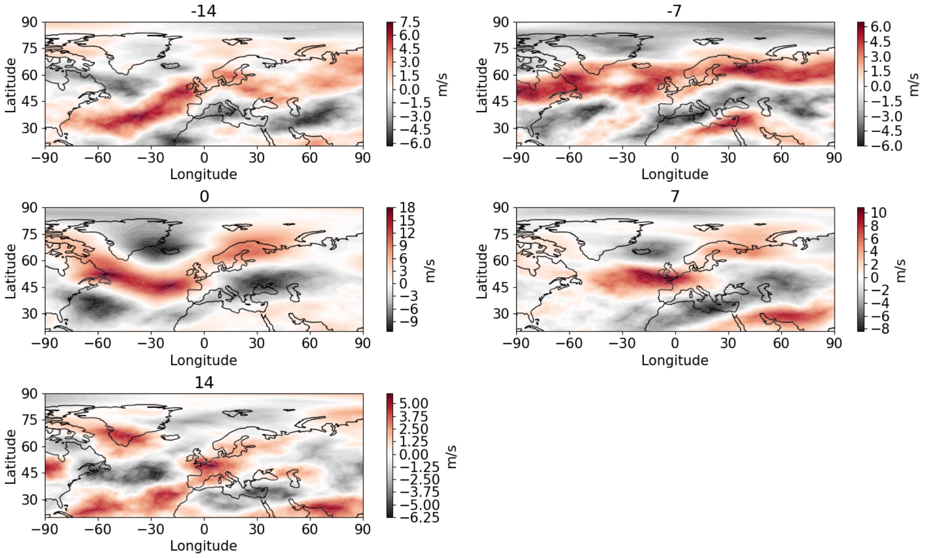

Figure 3.38: The 250 hPa zonal wind lag composites for the events projecting on the Odda flood event for lags -14, -7, 0, 7 and 14

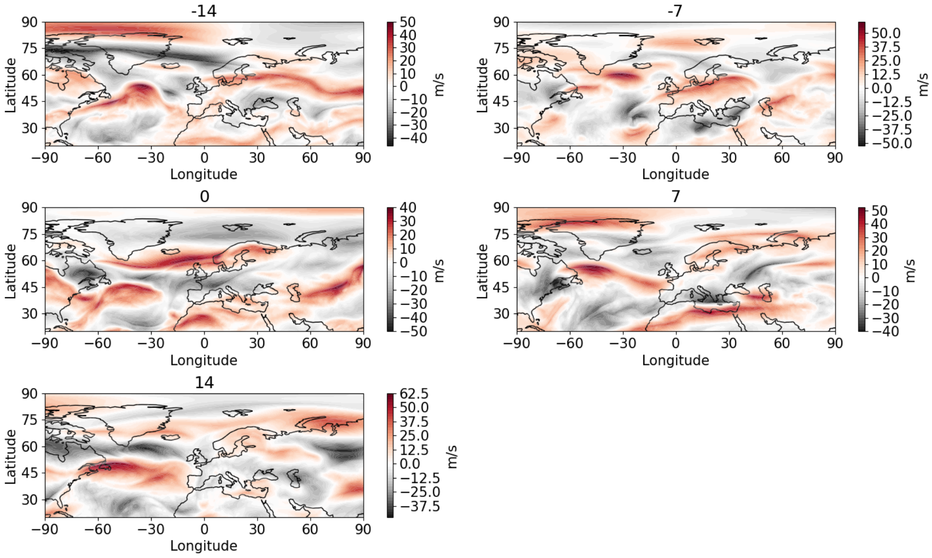

Figure 3.39: The 250 hPa zonal wind event deviations from the lag composites for the events projecting on the Odda flood event for lags and days -14, -7, 0, 7 and 14

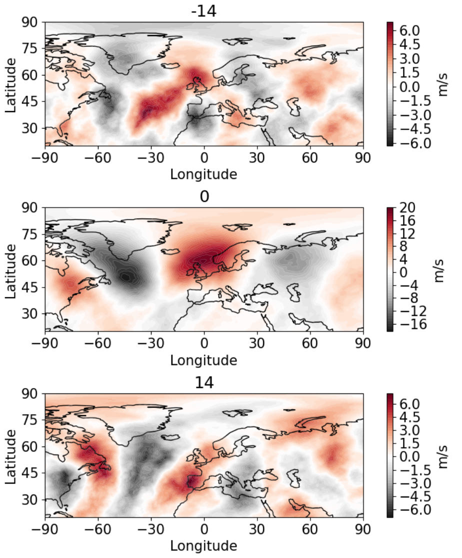

Figure 3.40: The 250 hPa meridional wind lag composites for the events projecting on the Odda flood event for lags -14, -7, 0, 7 and 14

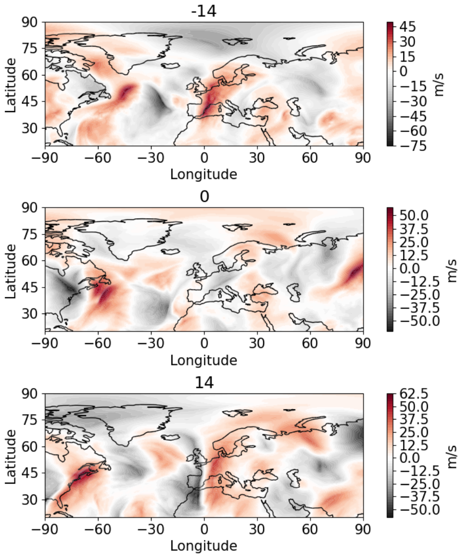

Figure 3.41: The 250 hPa meridional wind event deviations from the lag composites of the events projecting on the Odda flood event for lags and days -14, -7, 0, 7 and 14

In the composite plots of the geopotential height and zonal and meridional winds in Fig. 3.34, we see the patterns seen before with the dipole structure in the geopotential height plot and the positive zonal wind anomaly in the 0°-45°E region. The composite also shows more of a meridional slope, while the event shows more zonal symmetry as discussed before. The meridional wind plots show some differences to the event anomaly plots with clear wavy patterns indicating meandering, which supports the argument that the event was more symmetric than usual. In the zonal anomaly plots in Fig. 3.35, we see the dipole pattern in the geopotential height is more emphasized, while the positive zonal wind anomaly is more spread out throughout the time period. We also see less waviness in the meridional wind plots with only a small dipole pattern.

The plots of the different lag composites for the geopotential height in Fig. 3.36 show the aforementioned dipole pattern in lags 0 and 7. Looking at the difference plots in Fig. 3.37, we see in lag 0 how the dipole shows more of an east-west and north-south structure in the composite than in the event, which supports the enhanced eastward elongation and the quasi-symmetric structure of the westerly wind anomalies in the event.

The zonal wind lag composites in Fig. 3.38 show a positive anomaly throughout all lags in the regions of North Atlantic and around Norway. The difference plot in Fig. 3.39 shows that for lag 0, the event had a stronger zonal wind and a more zonally symmetric structure, while in the other lags we see mixed slightly positive and negative values, indicating a small difference from the lag composites.

The meridional wind plots in Fig. 3.40 show a strong positive anomaly throughout all lags around Norway, especially in lag 0. This, together with the already discussed zonal wind plots, shows us the flow in these cases is northeastward and this supports that the moist air was carried from the Atlantic towards Norway. The difference plot in Fig. 3.41 shows the meridional wind was stronger than in the composite mean (lags -14, 7 and 14) or approximately equal to the composite mean (lags -7 and 0) for the area around Norway.

3.2.6 Precipitation rate

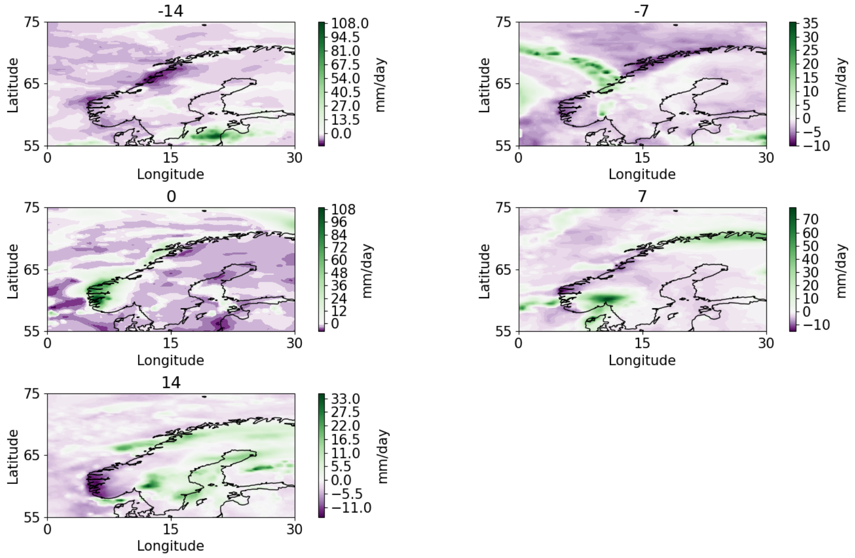

Figure 3.42: The precipitation rate event anomaly fields for the Odda flood event for days -14, -7, 0, 7 and 14

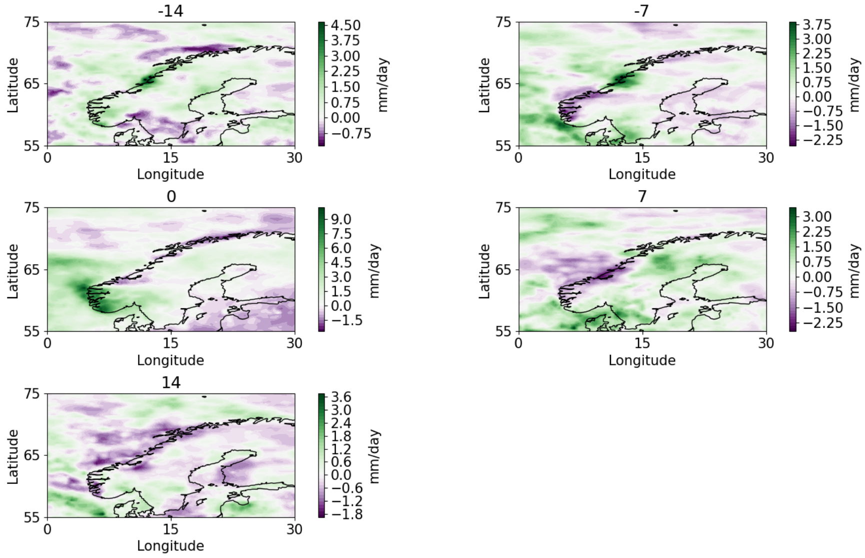

Figure 3.43: The precipitation rate lag composites of the events projecting on the Odda flood event for lags -14, -7, 0, 7 and 14

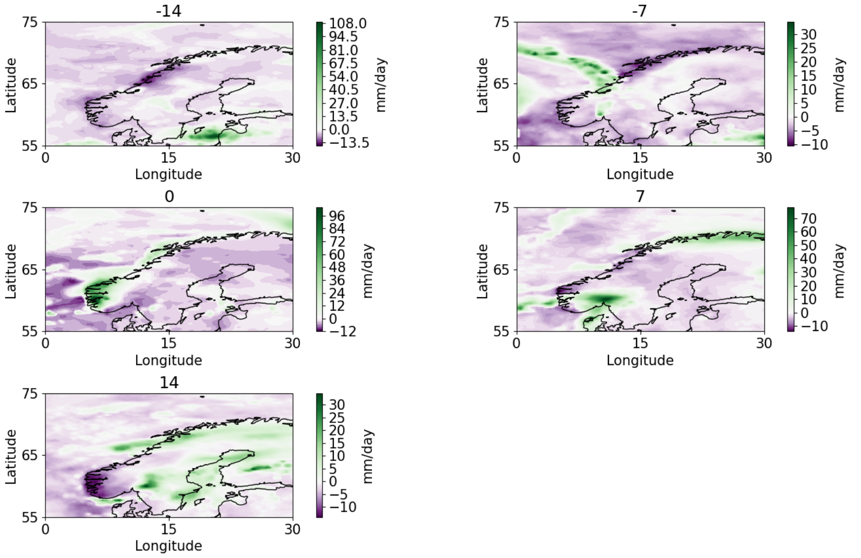

Figure 3.44: The precipitation rate event deviations from the lag composites of the events projecting on the Odda flood event for lags and days -14, -7, 0, 7 and 14

Since this event was a flood, we look into the precipitation rate as one of the key variables for determining its nature. The precipitation anomaly phase plots in Fig. 3.42 show us a strong positive anomaly in day 0, while we see a negative anomaly or values close to zero in other lags for the area of western Norway. This indicates the extreme precipitation event was not long-lasting.

Looking at the lag composites in Fig. 3.43, we see once again a very strong positive anomaly in lag 0, with negative anomalies in other lags for western Norway. The difference plots in Fig. 3.44 tell the anomaly for the event was stronger than for the composite, with positive values for lag 0 and negative values for the other lags for the region of interest. The enhanced precipitation in the event compared to the composite can be attributed to the stronger westerlies over Norway associated with high zonal symmetry of the circulation pattern in those regions.

3.2.7 Barotropic LWA and zonal wind

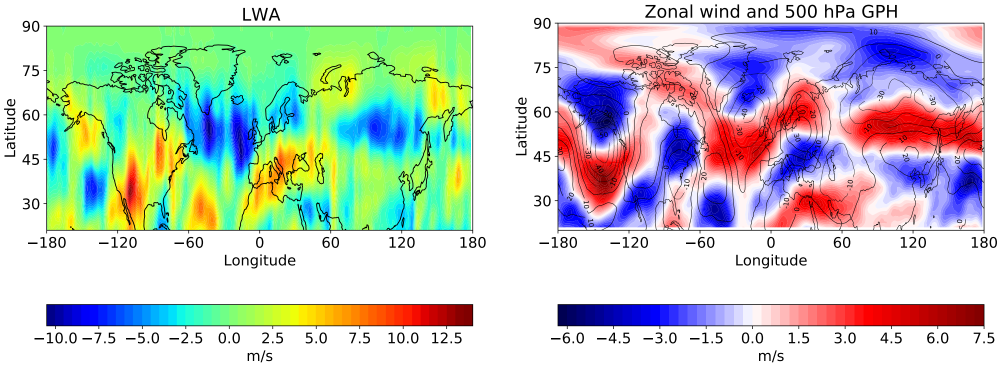

Figure 3.45: The barotropic LWA and zonal wind 29-day event anomaly means for the Odda flood event

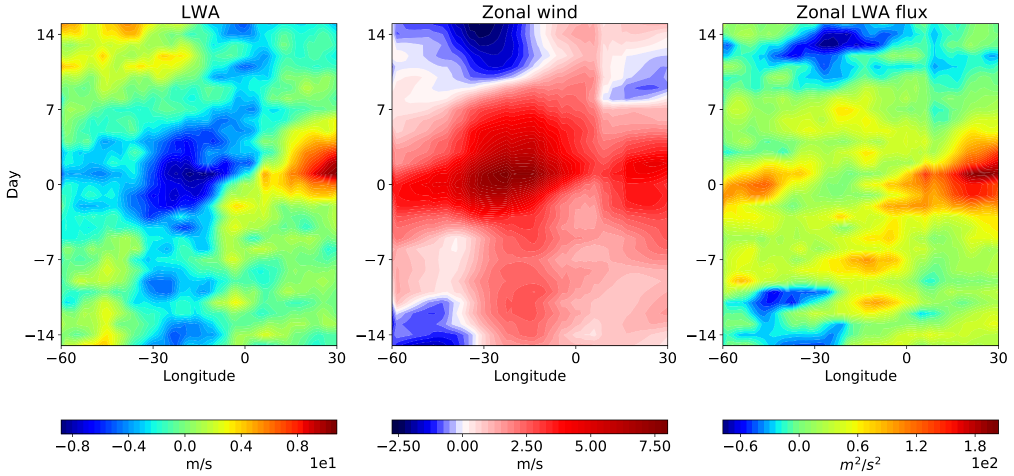

Figure 3.46: The barotropic LWA, zonal wind and zonal LWA flux composites of the events projecting on the Odda flood event for 60°W-30°E and 40-70°N

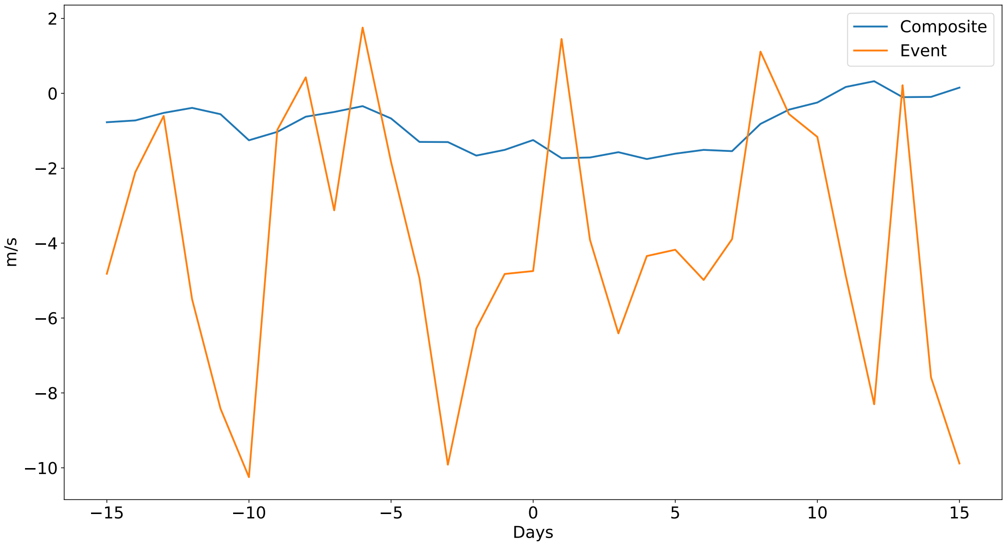

Figure 3.47: The barotropic LWA for the Odda flood event and for the composite of the events projecting on it for 60°W-30°E and 40-70°N

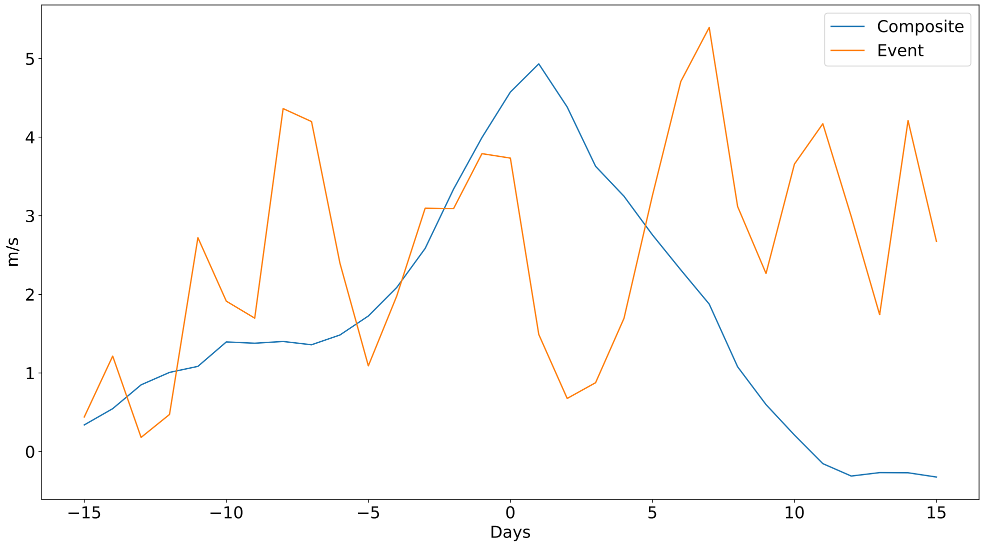

Figure 3.48: The barotropic zonal wind for the Odda flood event and for the composite of the events projecting on it for 60°W-30°E and 40-70°N

The mean state of the anomalies for the barotropic LWA and zonal wind in Fig. 3.45 shows us the positive anomaly for the zonal wind seen in the previous plots and a negative anomaly for the LWA, as expected for these two variables. The negative anomaly for the LWA can be used as a proxy for the enhanced westerlies.

Looking at the composite in Fig. 3.46, we see the positive zonal wind anomaly mentioned before, as well as the negative LWA anomaly. The zonal LWA flux composite shows slightly negative values in the early stages, with positive values developing further in time and towards the east. This shows that there was no blocking and no relation to the traffic jam conept. The region used for the composite plot was 60°W-30°E and 40-70°N based on the positive zonal wind anomaly region in Fig. 3.45, where the regions with the negative values were masked out.

For the single event in Fig. 3.47, the LWA is predominantly negative with strong fluctuation between strong negative values and values closer to zero. Consistent with this result, the westerly wind of the single event in Fig. 3.48 is predominantly positive with strong fluctuation between high positive values and values close to zero. For the composite, the LWA is predominantly negative, but the values are much weaker and smoother with the biggest negative values closer to lag 0. Consistent with that, the westerlies are predominantly positive, smoother and stronger close to lag 0 and the values are generally relatively strong. This may reflect some non-linearity in the relationship between the LWA and the westerlies and is a further proof of no blocking conditions.

3.2.8 LWA budget equation components

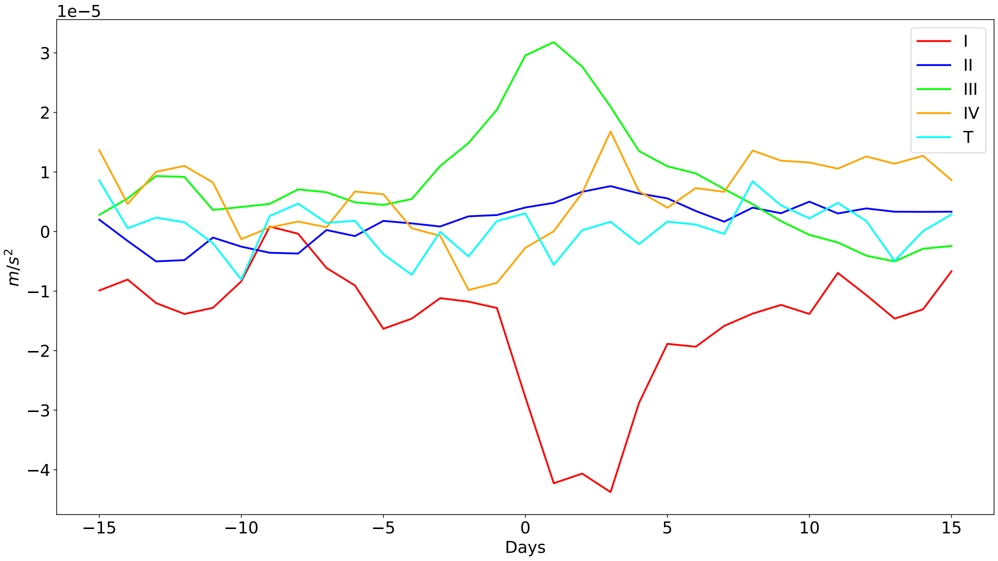

Figure 3.49: The LWA budget equation components (zonal LWA flux convergence (I), eddy meridional momentum flux divergence (II), low-level meridional heat flux (III), residual (IV) and the LWA tendency (T)) for the composite projecting on the Odda flood event for 60°W-30°E and 40°-70°N

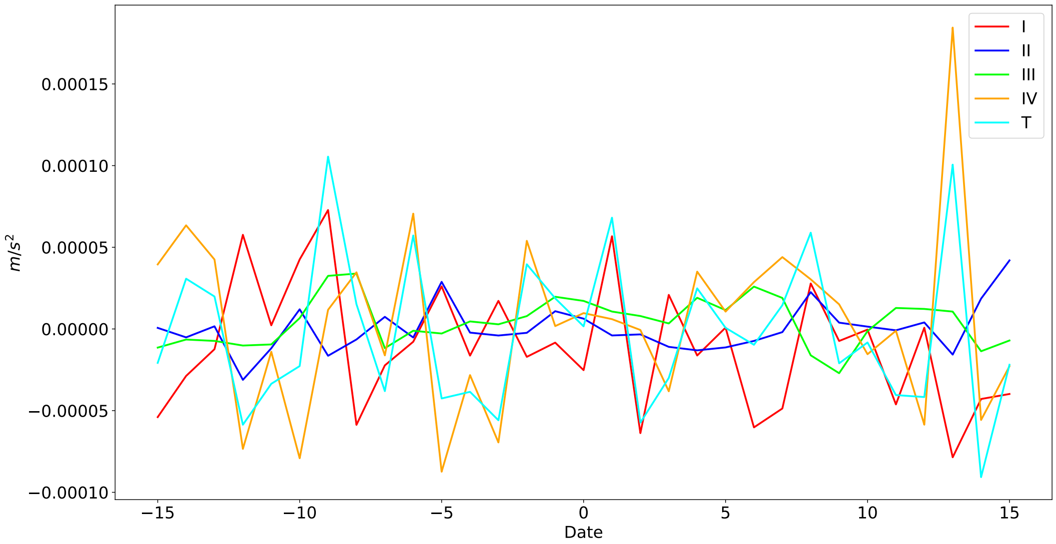

Figure 3.50: The LWA budget equation components (zonal LWA flux convergence (I), eddy meridional momentum flux divergence (II), low-level meridional heat flux (III), residual (IV) and the LWA tendency (T)) for the Odda flood event for 60°W-30°E and 40°-70°N

The line plot of the composites of the budget equation components in Fig. 3.49 shows us the biggest influence on the tendency (T) comes from the zonal advective LWA flux convergence (I) and the low-level meridional eddy heat flux (III), which enhance and dampen the tendency, respectively. Considerable influence also comes from the residual (IV) with lower values and a more stable profile throughout the time series, which also enhances the tendency. The eddy meridional momentum flux divergence (II) shows only small variation therefore we can conclude the I and III terms cancel each other out to bring the tendency around zero.

For the actual event, as we see in Fig. 3.50, the tendency (T) shows more variation where the biggest influence comes from the residual (IV), suggesting a high impact of non-conservative processes (diabatic sources and sinks of LWA) on the atmospheric circulation and dynamics at the time. This term dampens the tendency, but at the end it increases it. The zonal LWA flux convergence (I) also shows a significant impact, but less than the residual. This term exchanges between enhancing and dampening the tendency. Also, the single event shows a lot of fluctuation, while the composite shows smoother profiles as seen in the LWA and westerlies plots before.

3.3 Petra flood event

3.3.1 General event description

In August and September 2015, an extreme weather event named Petra affected a lot of the regions in southern and southeastern Norway. It was a flooding event with heavy precipitation occurring multiple days in a row in many places. The event caused significant damage to the areas affected. The peak of the event came mid-September (NRK, 2015).

3.3.2 Basic variables anomaly fields

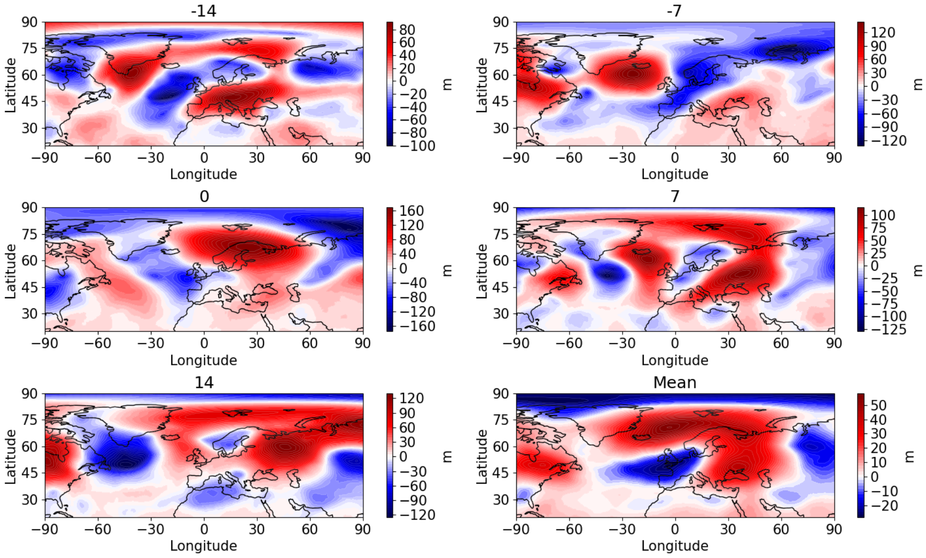

Figure 3.51: The 500 hPa geopotential height event anomaly fields for the Petra flood event for days -14, -7, 0, 7 and 14 and the 29-day mean

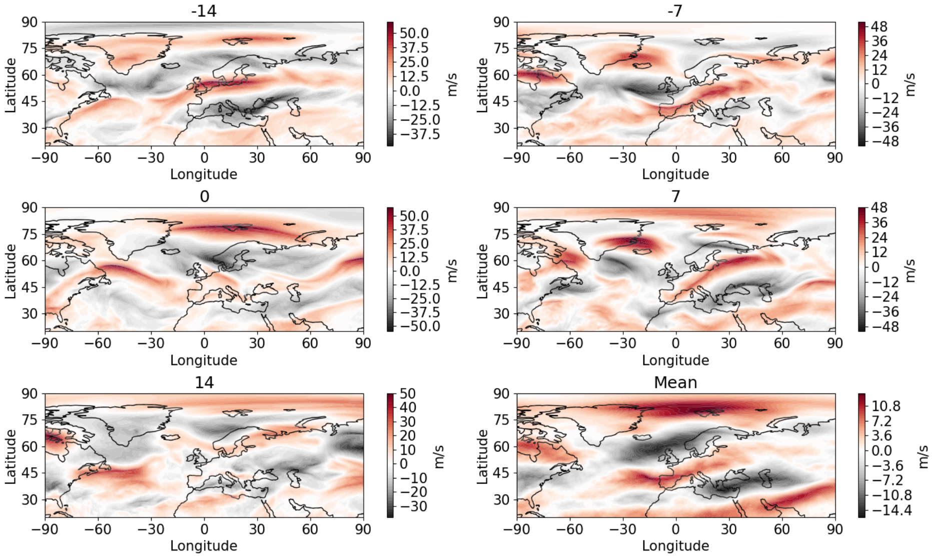

Figure 3.52: The 250 hPa zonal wind event anomaly fields for the Petra flood event for days -14, -7, 0, 7 and 14 and the 29-day mean

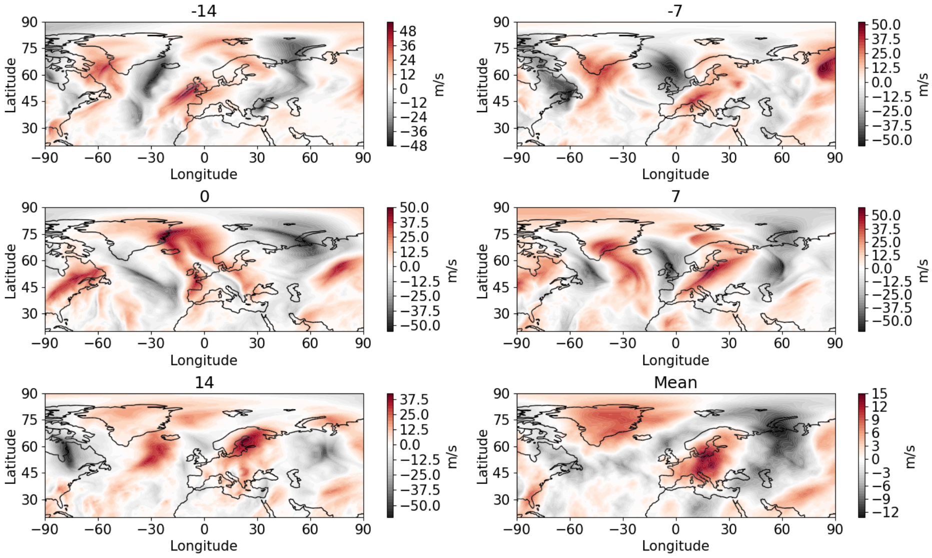

Figure 3.53: The 250 hPa meridional wind event anomaly fields for the Petra flood event for days -14, -7, 0, 7 and 14 and the 29-day mean

Looking at the geopotential height plots in Fig. 3.51, in day 0 and in the average state along the whole event we see a prominent positive anomaly over Norway with a negative anomaly over western Europe. Normally this kind of persistent pattern leads to dry conditions. In this case, the low pressure over the eastern Atlantic and northwestern Europe may have contributed to the transport of moist and warm air from the sub-tropical North Atlantic and

Mediterranean to the south of Norway.

The zonal wind plots in Fig. 3.52 show us a negative anomaly in most of the days for the region around Norway, especially in the mean state. This weakening in the westerly gives us a basis for the persistence and blocking argument.

For the meridional wind in Fig. 3.53, we can see some wavy structures in most of the lags indicating meandering of the jet stream. In the mean state we see a prominent positive anomaly over Europe which supports the idea of moisture being transported from the Mediterannean and subtropical Atlantic.

3.3.3 Standardized index

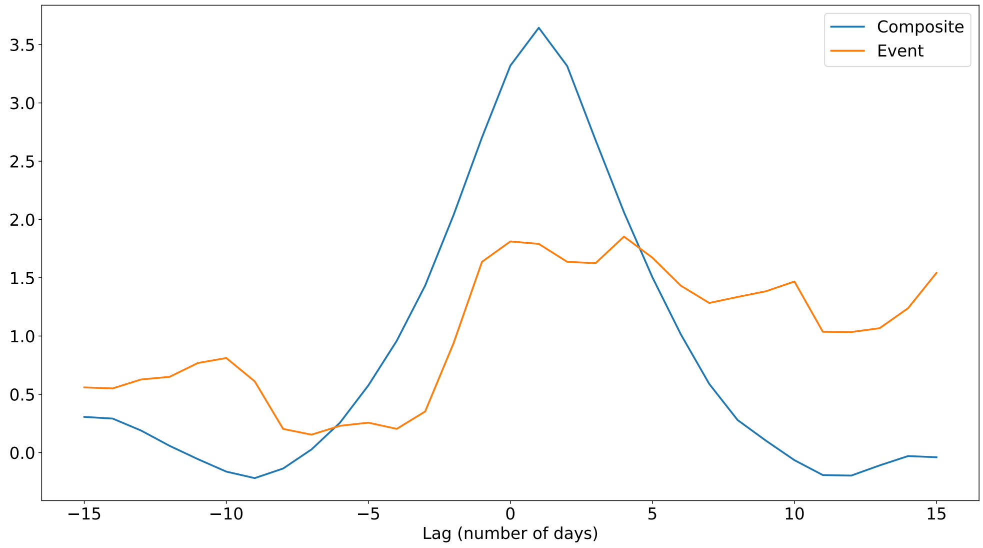

Figure 3.54: The standardized index for the Petra flood event and for the composite of the events projecting on it

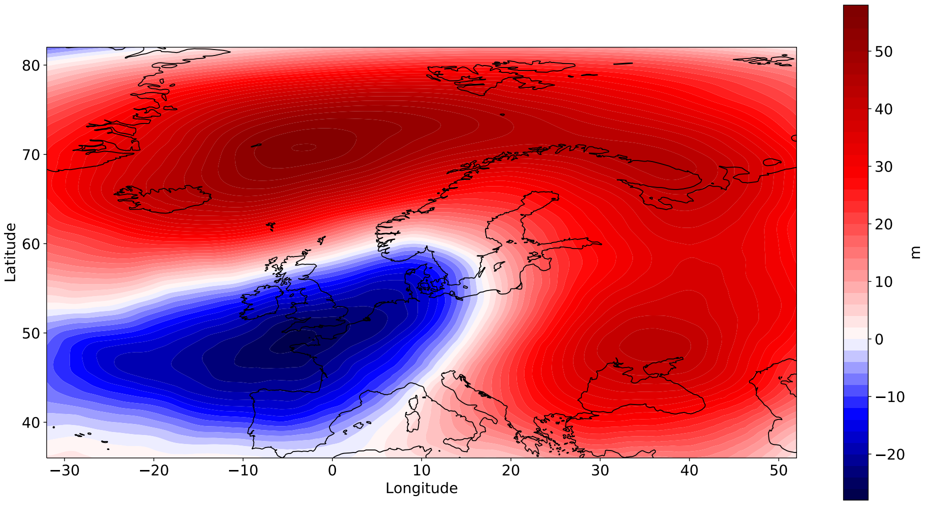

Figure 3.55: The 500 hPa geopotential height anomaly pattern for the Petra flood event

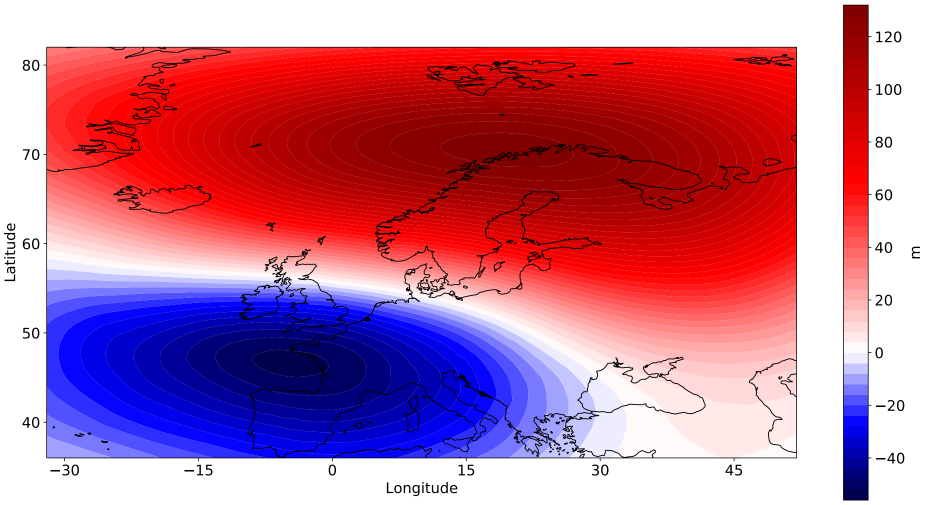

Figure 3.56: The 500 hPa geopotential height 0-day lag composites of the events projecting on the Petra flood event for days with index values above the 95th percentile

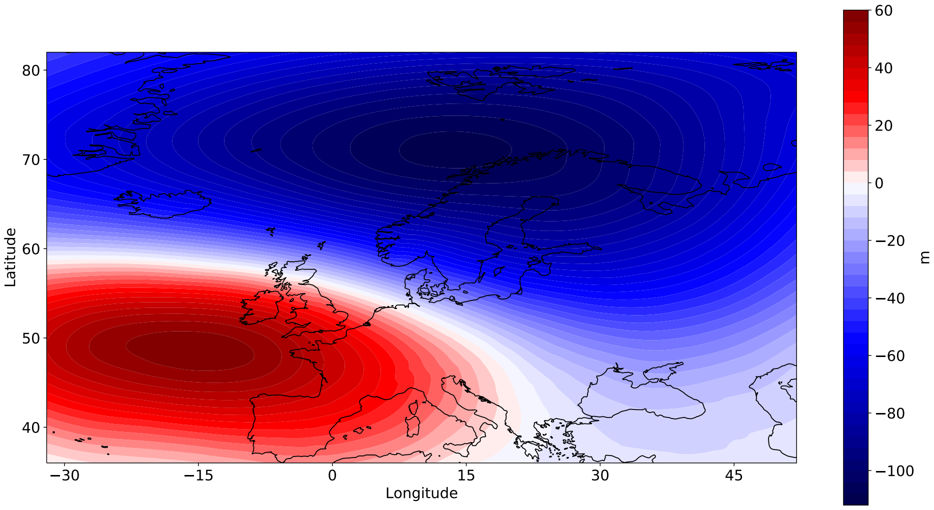

Figure 3.57: The 500 hPa geopotential height 0-day lag composites of the events projecting on the Petra flood event for days with values below the 5th percentile

The index plot shown in Fig. 3.54 shows us the event was weaker than the composite for the days around the event owing to the fact that the pattern for the event slightly differed from the pattern of the averaged composite, but at the beginning and end the index shows higher values than the composite. This suggests it was more persistent than the composite. The anomaly pattern shown in Fig. 3.55 shows an asymmetric pattern with somewhat of a double, coupled positive anomaly with distinct centers in North Atlantic and in Russia, while a negative anomaly is situated over western Europe.

The 0-day lag composite of all fields with index values larger than the 95th percentile in Fig. 3.56 shows a good agreement with the index pattern attesting to the validity of the index, although the positive anomaly isn't exactly replicated due to its asymmetry. The low pressure in the event is more isolated and it may enable better transport of sub-tropical North Atlantic and Mediterranean moist and warm air into the south of Norway. The opposite 0-day lag composite in Fig. 3.57 shows the opposite pattern meaning there is linearity in the occurrence of the pattern.

3.3.4 Autocorrelation function

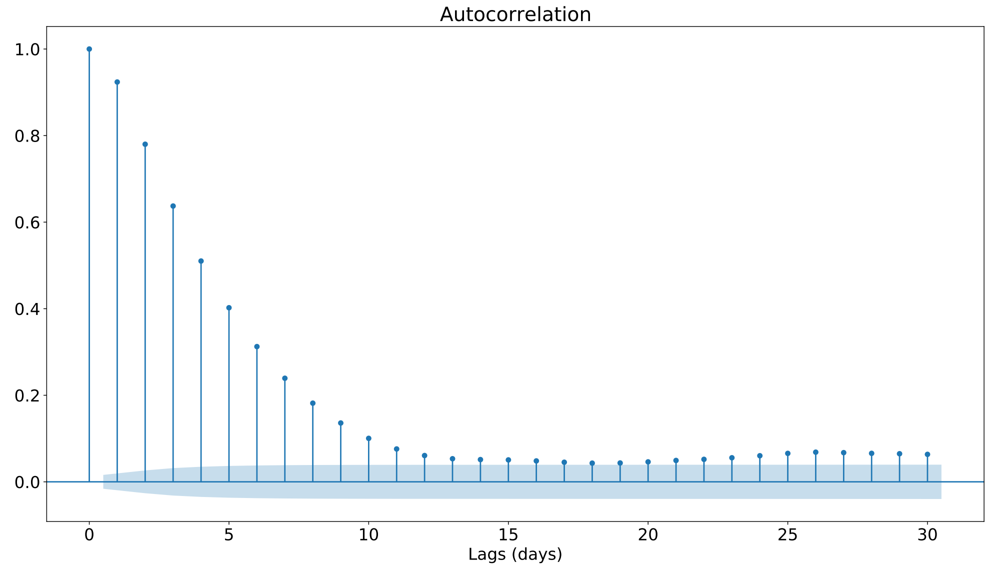

Figure 3.58: The standardized index autocorrelation function for the Petra flood event

The autocorrelation plot in Fig. 3.58 shows approximately a 15-day time scale of the event showing a quite high persistence. We can also note how around day 20 the correlation starts to increase again, indicating high persistence.

3.3.5 Basic variables composite maps

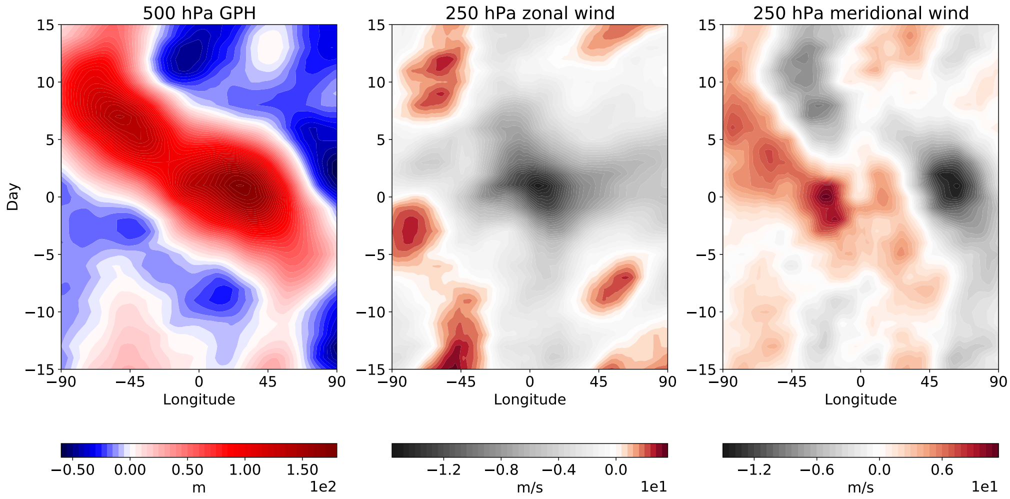

Figure 3.59: The 500 hPa geopotential height, 250 hPa zonal and meridional wind composites of the events projecting on the Petra flood event (daily anomalies) for 90°W-90°N and 55°-75°N

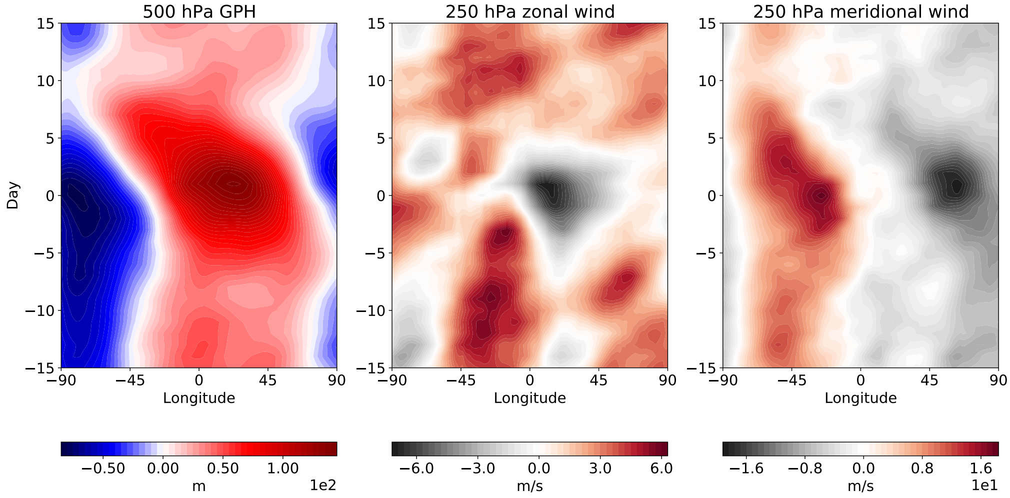

Figure 3.60: The 500 hPa geopotential height, 250 hPa zonal and meridional wind composites of the events projecting on the Petra flood event (deviations from the zonal mean) for 90°W-90°N and 55°-75°N

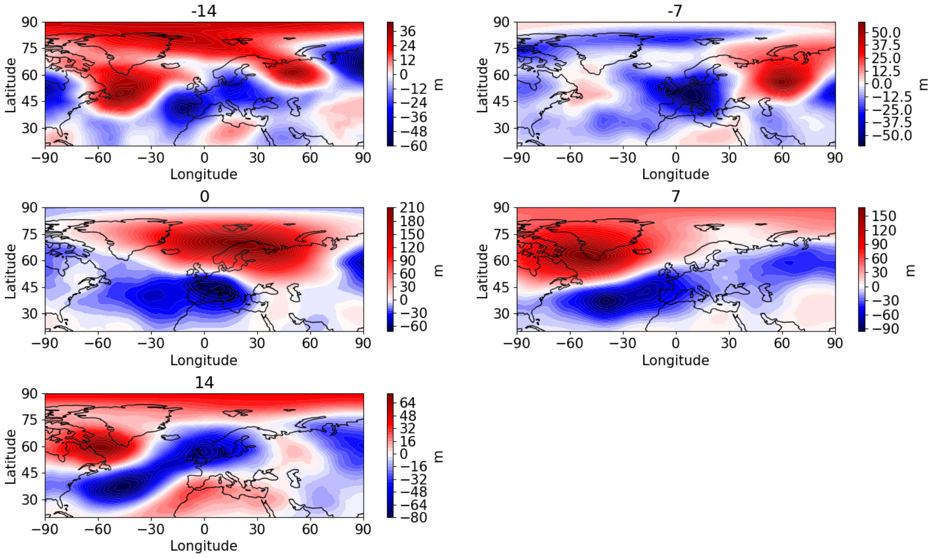

Figure 3.61: The 500 hPa geopotential height lag composites of the events projecting on the Petra flood event for lags -14, -7, 0, 7 and 14

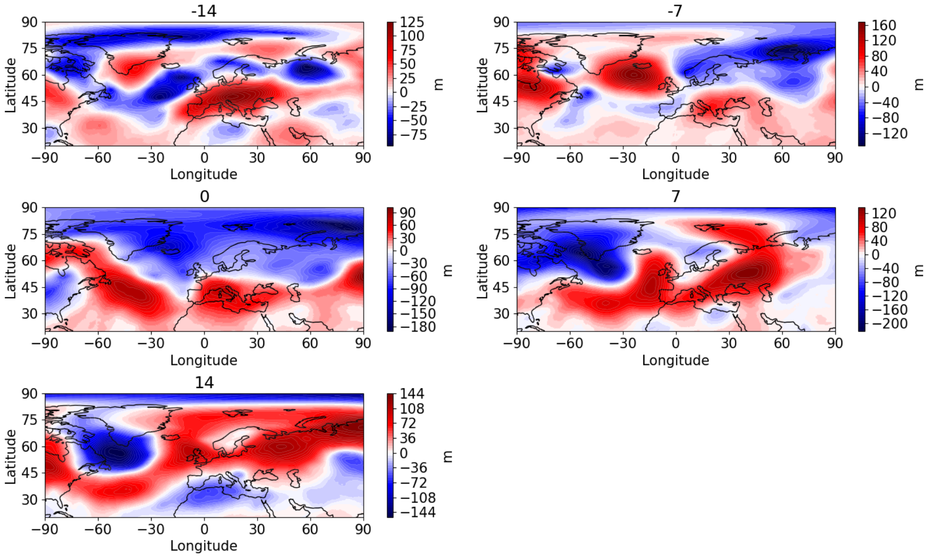

Figure 3.62: The 500 hPa geopotential height event deviations from the lag composites of the events projecting on the Petra flood event for lags and days -14, -7, 0, 7 and 14

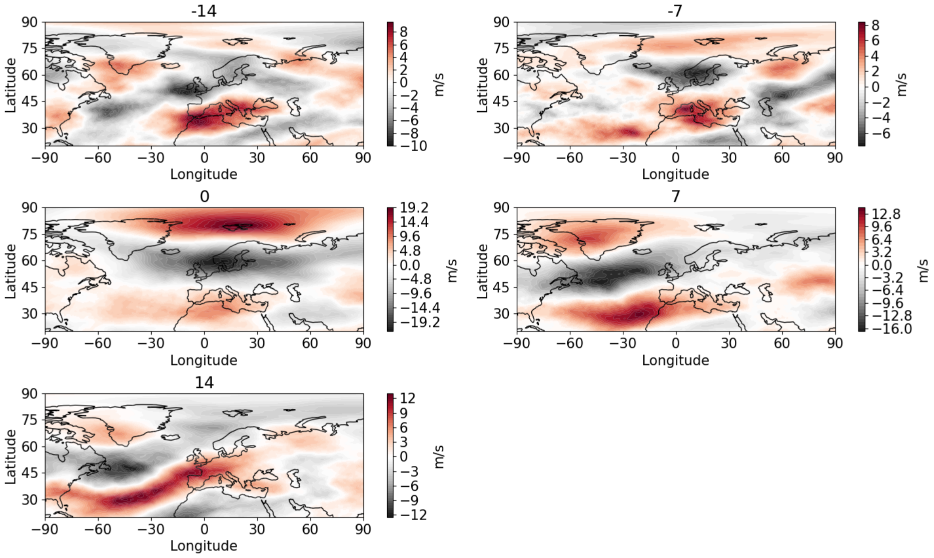

Figure 3.63: The 250 hPa zonal wind lag composites of the events projecting on the Petra flood event for lags -14, -7, 0, 7 and 14

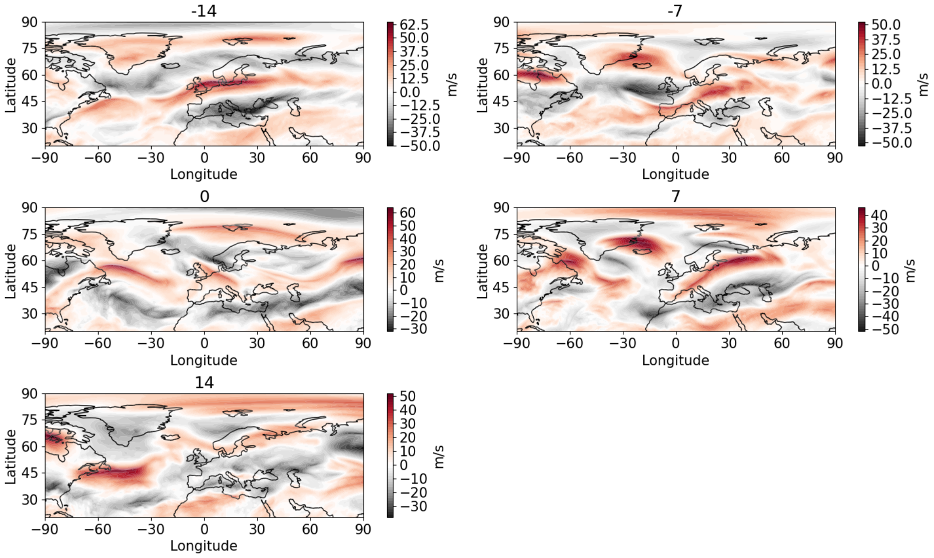

Figure 3.64: The 250 hPa zonal wind event deviations from the lag composites of the events projecting on the Petra flood event for lags and days -14, -7, 0, 7 and 14

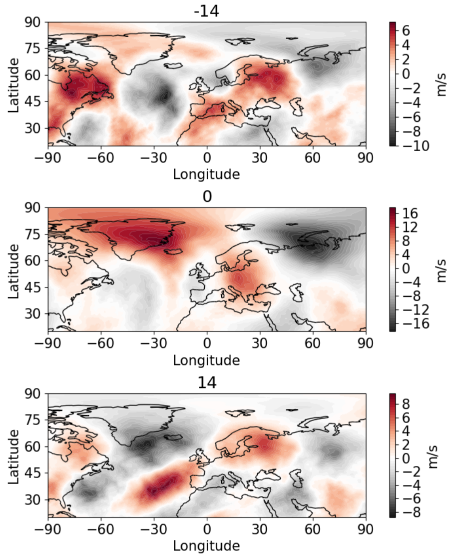

Figure 3.65: The 250 hPa meridional wind lag composites of the events projecting on the Petra flood event for lags -14, -7, 0, 7 and 14

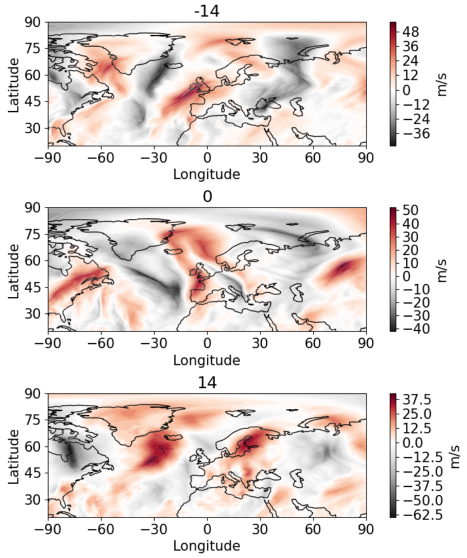

Figure 3.66: The 250 hPa meridional wind event deviations from the lag composites of the events projecting on the Petra flood event for lags and days -14, -7, 0, 7 and 14

The composite plot in Fig. 3.59 shows the dominant positive anomaly for the geopotential height with significant westward propagation. The zonal wind plot shows the negative anomaly, while the meridional wind shows the positive anomaly. These patterns can be efficient in advecting warm and moist air from the subtropical North Atlantic and the Mediterranean to the south of Norway. In the deviations from the zonal mean composite in Fig. 3.60, we see similar structures with the exception of the geopotential height positive anomaly being more prominent and some differences in the distribution of the wind anomalies. We can also see how the negative geopotential height anomaly is less isolated.

The individual lag composites in Fig. 3.61 do not show a lot of persistence with the pattern of interest only clearly visible in lag 0. In lag -7, we can see the formation of the mentioned pattern, while in lag 7 we see it gradually drifting away. In the difference plots in Fig. 3.62, we can see how the event was weaker than the composite, especially in lags 0, 7 and 14. This is in agreement with the index plot.

For the zonal wind lag composites in Fig. 3.63, we can see a persisting negative anomaly in all lags around the region of Norway. This indicates persistence and is in agreement with the previous plots. In the difference plots in Fig. 3.64, we see how the event had stronger negative anomalies than the composite, with some local exceptions for the region of interest around Norway.

The meridional wind lag composites in Fig. 3.65 show a positive anomaly in all lags in the region of interest, in agreement with the previous composite plots. The difference plots in 3.66 show the winds in the event were stronger than in the composite, just like the zonal wind, indicating stronger flow contributing to the previously mentioned moist air advection.

3.3.6 Precipitation rate

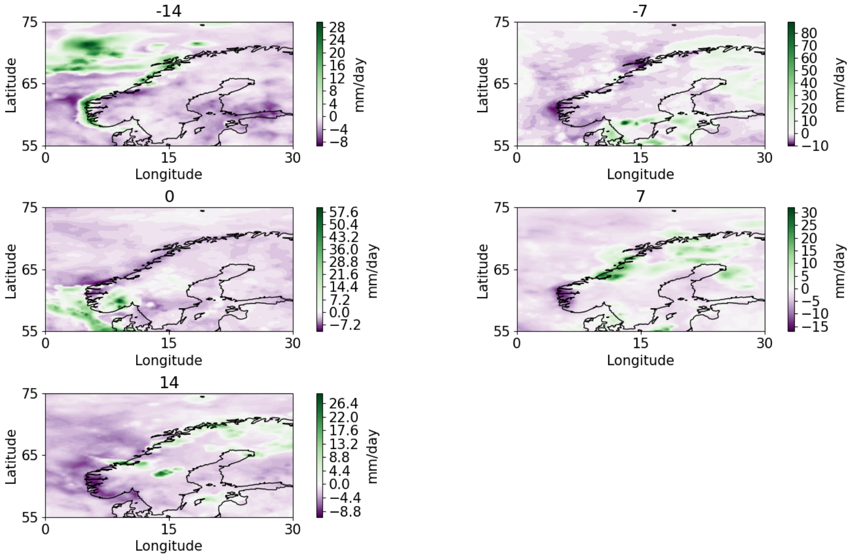

Figure 3.67: The precipitation rate event anomaly fields for the Petra flood event for days -14, -7, 0, 7 and 14

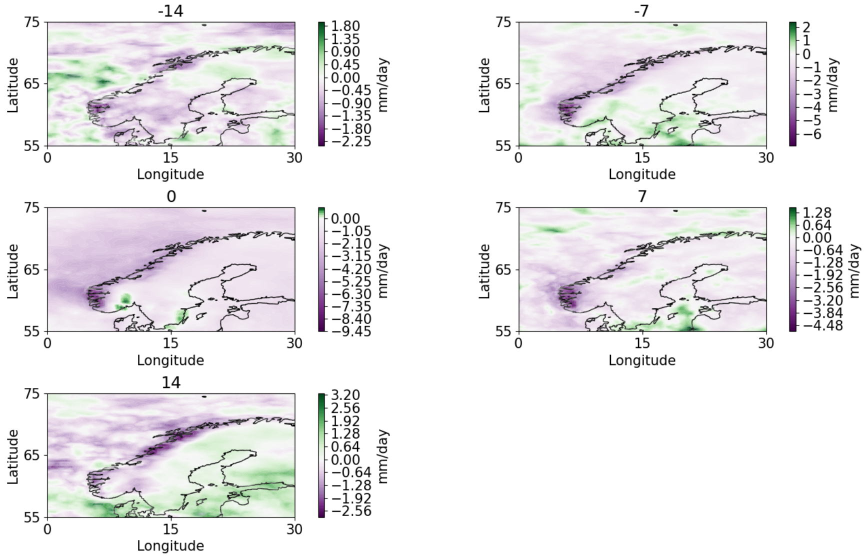

Figure 3.68: The precipitation rate lag composites of the events projecting on the Petra flood event for days -14, -7, 0, 7 and 14

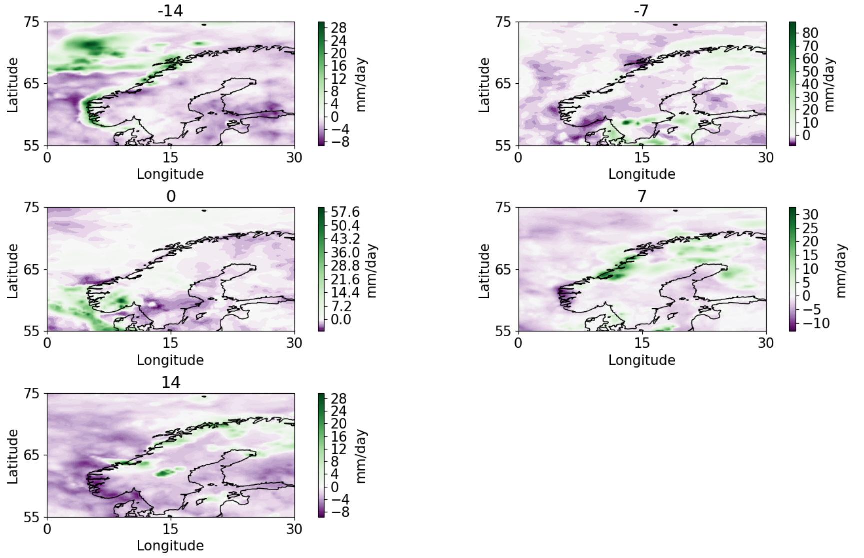

Figure 3.69: The precipitation rate event deviations from the lag composites of the events projecting on the Petra flood event for lags and days -14, -7, 0, 7 and 14

Since this event was a flood, we look into precipitation rate once again as one of the key variables for determining its nature. For the anomaly fields on different days of the event in Fig. 3.67, we see a distinct positive anomaly on day 0 for the region of interest in the south of Norway, while on other days we see values close to zero or negative values indicating the extreme precipitation event was not long-lasting. The lag plot in Fig. 3.68 shows a positive anomaly in the region of interest in lags 0 and 7, while the other lags show negative anomalies or values close to zero. The difference plot in Fig. 3.69 shows the event was stronger than the composite looking at the region of interest in lag 0. This can be contributed to the circulation, which shows a more isolated low-pressure system for the event that can transport the North Atlantic and Mediterranean moist and warm air more effectively.

3.3.7 Barotropic LWA and zonal wind

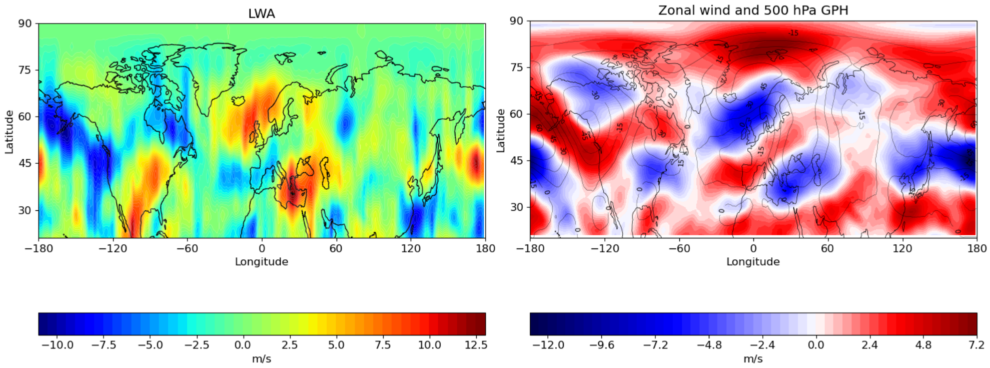

Figure 3.70: The barotropic LWA and zonal wind event 29-day anomaly means for the Petra flood event

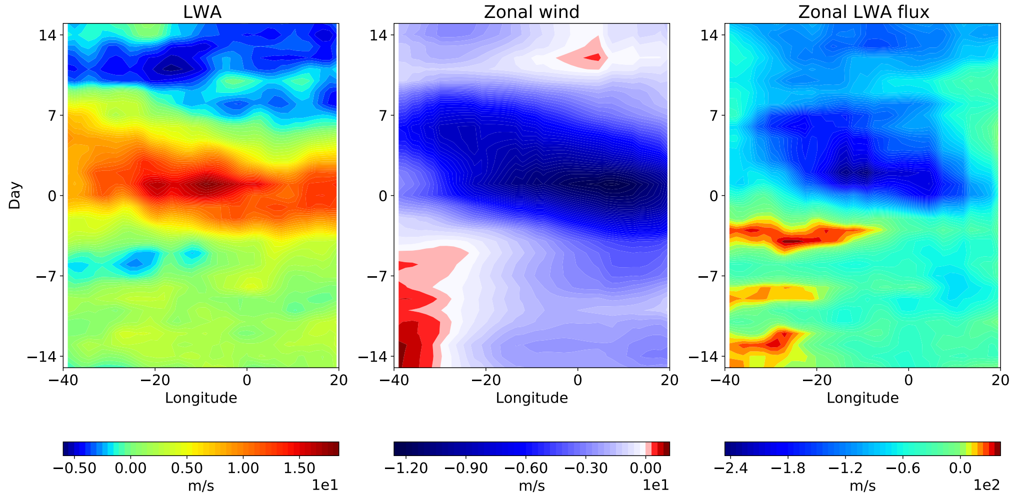

Figure 3.71: The barotropic LWA, zonal wind and zonal LWA flux composites of the events projecting on the Petra flood event for 40°W-20°E and 50-70°N

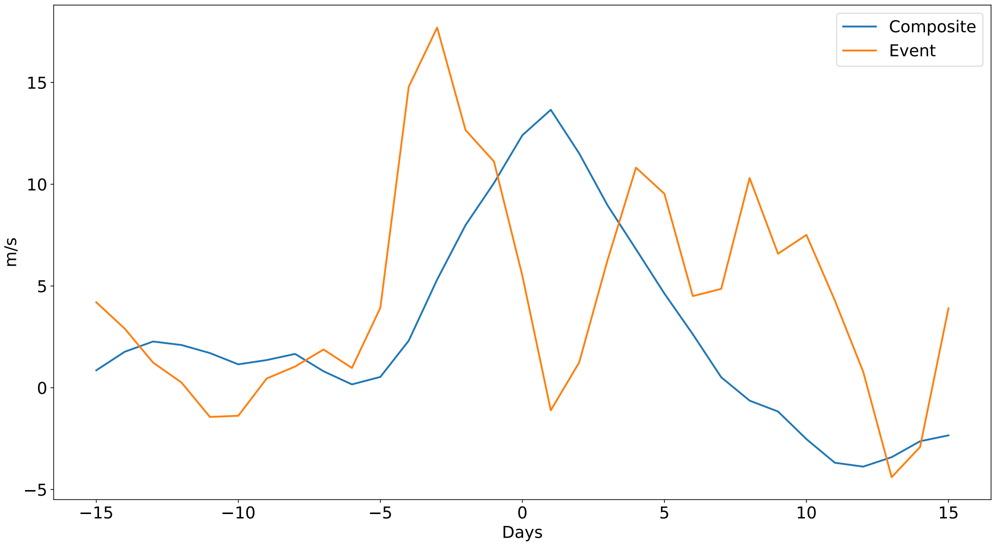

Figure 3.72: The barotropic LWA for the Petra flood event and for the composite of the events projecting on it for 40°W-20°E and 50-70°N

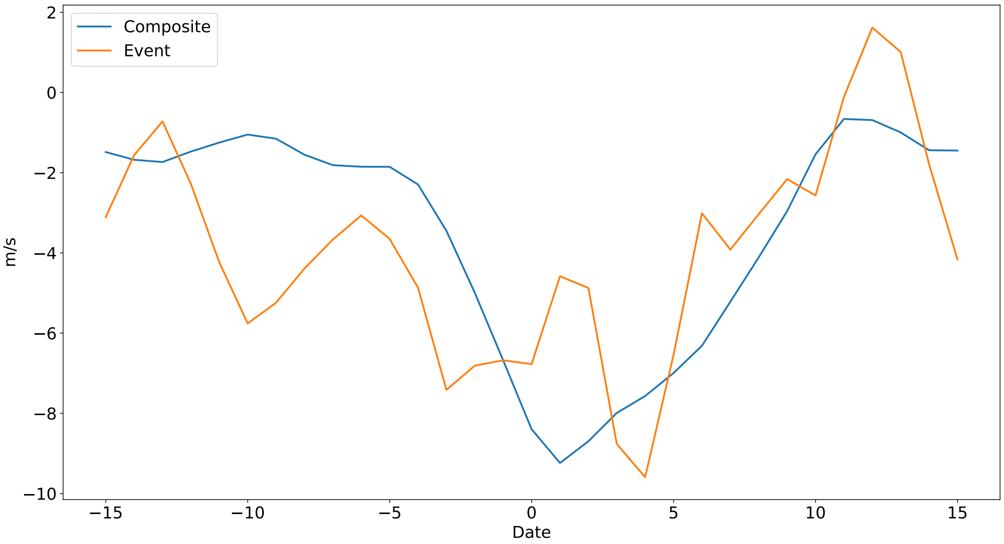

Figure 3.73: The barotropic zonal wind event for the Petra flood event and for the composite of the events projecting on it for 40°W-20°E and 50-70°N

In the plots of the mean state of the barotropic LWA and zonal wind in Fig. 3.70, we see a strong positive anomaly of LWA in the North Atlantic correlated with a strong negative anomaly in the zonal wind, suggesting blocking. The composite plot shown in Fig. 3.71 shows the prominent positive anomaly in the LWA and negative anomaly in the zonal wind from lags 0 to 7, as seen in the mean anomaly plots. The zonal LWA flux composite shows distinct positive values in the onset and maturation stages of the event. Here we can again make the connection with the traffic jam concept from (Nakamura and Huang, 2018), with the jet stream having a capacity for the LWA flux. This is further proof of the appearance of blocking. After the capacity is exceeded, blocking occurs. The region used for the composite calculation was 40°W-20°E and 50-70°N based on the negative wind anomaly region in Fig. 3.70.

From the LWA line plot in Fig. 3.72, we see that the values for the event mostly follow the composite with a slight imbalance around the central day. The values are positive throughout. For the zonal wind in Fig. 3.73, we again see how the values for the event closely follow the composite while they are mostly negative. Also, the values for the composite are much smoother than for the single event, as expected.

3.3.8 LWA budget equation components

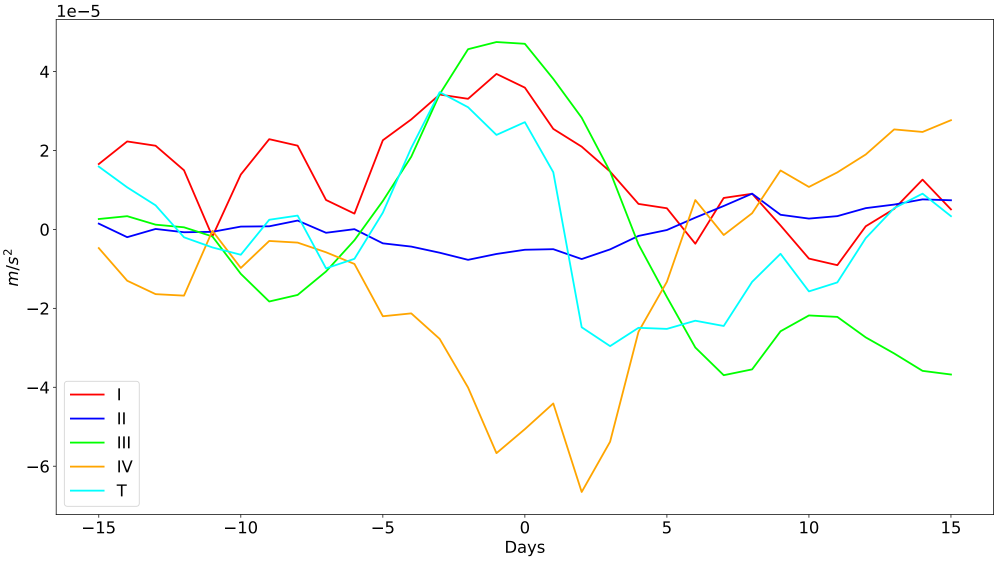

Figure 3.74: The LWA budget equation components (zonal LWA flux convergence (I), eddy meridional momentum flux divergence (II), low-level meridional heat flux (III), residual (IV) and the LWA tendency (T)) for the composite of the events projecting on the Petra flood event for 40°W-20°E and 50-70°N

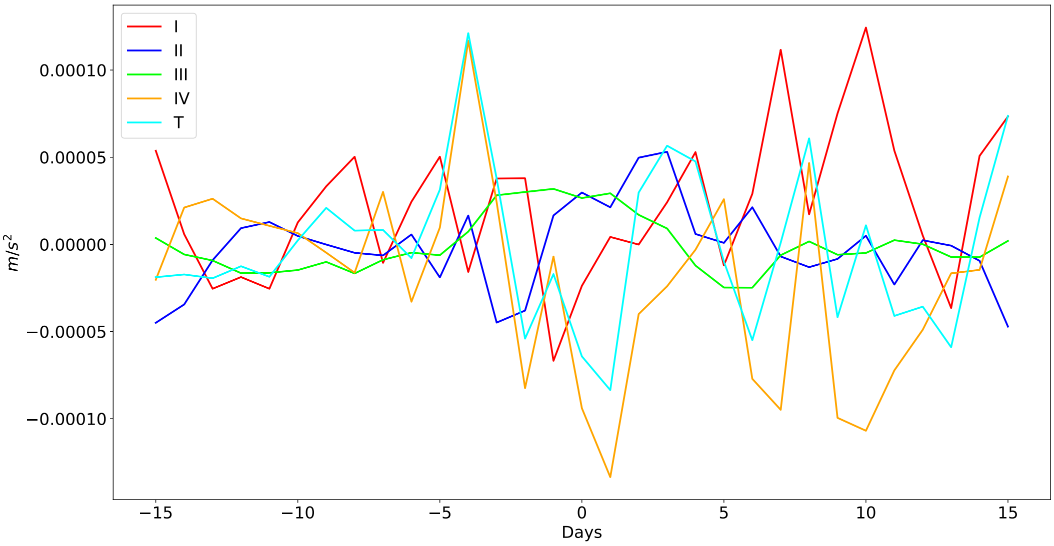

Figure 3.75: The LWA budget equation components (zonal LWA flux convergence (I), eddy meridional momentum flux divergence (II), low-level meridional heat flux (III), residual (IV) and the LWA tendency (T)) for the Petra flood event for 40°W-20°E and 50-70°N

The line plot of the composites of different budget equation components in Fig. 3.74 shows the biggest contributors to the tendency are the zonal LWA flux convergence (I) and the low-level meridional heat flux (III), which help to increase the LWA. The shape of the tendency (T) follows these two as well. Another contribution is the residual (IV), which has the opposite pattern and it dampens the LWA. The eddy meridional momentum flux divergence (II) again does not have a significant contribution.

For the actual event shown in Fig. 3.75, the plot shows more fluctuation in the tendency with generally positive values where the biggest contributors are the zonal LWA flux convergence (I) and the residual (IV), which have a similar impact in the first part of the time series and an opposing one in the other part. The eddy meridional momentum flux divergence (II) and low-level meridional heat flux (III) have some influence on the budget in the central part of the time series where they increase the LWA, while the residual mostly helps to dampen the tendency. The spikes of the zonal LWA flux convergence in the beginning of the time series are in agreement with the zonal LWA flux composite in Fig. 3.71, showing their influence on the blocking from the early stages. The zonal LWA flux convergence also helps to maintain the positive LWA in the remainder of the time series, showing high persistence. This is another example of the analogy to the traffic jam.

3.4 Finsland snowfall event

3.4.1 General event description

In January and February 2018, heavy snowfall affected the region of Sørlandet in Norway. There were many days with power outages which caused significant damage to the residents of this area. The meteorological station in Finsland measured the highest snowfall height ever recorded in its operating history (Breiteig, 2018).

3.4.2 Basic variables anomaly fields

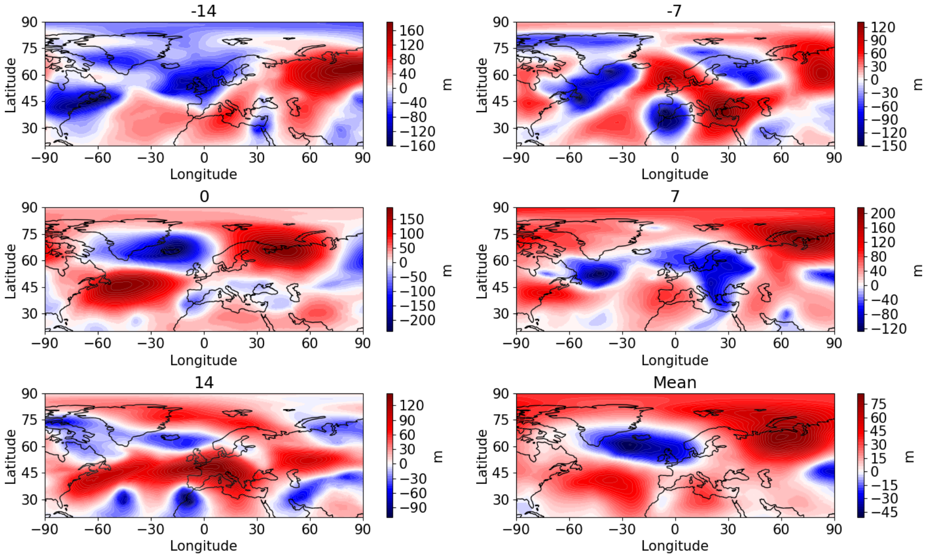

Figure 3.76: The 500 hPa geopotential height event anomaly fields for the Finsland snowfall event for days -14, -7, 0, 7 and 14 and the 29-day mean

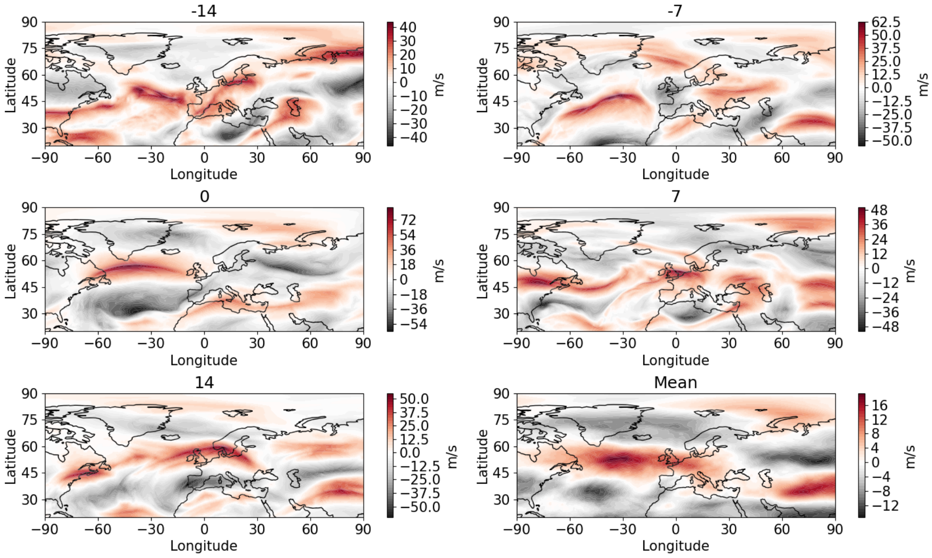

Figure 3.77: The 250 hPa zonal wind event anomaly fields for the Finsland snowfall event for days -14, -7, 0, 7 and 14 and the 29-day mean

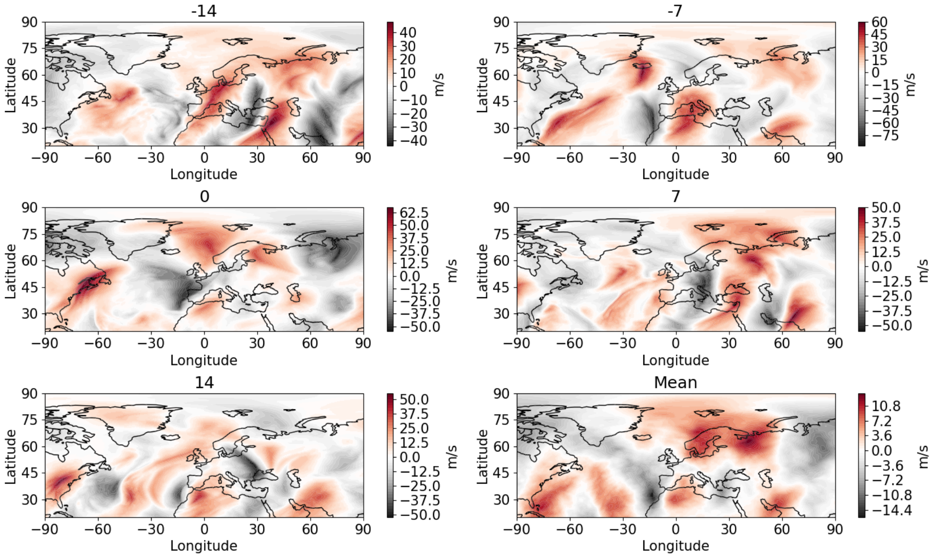

Figure 3.78: The 250 hPa meridional wind event anomaly fields for the Finsland snowfall event for days -14, -7, 0, 7 and 14 and the 29-day mean

Looking at the geopotential height plots in Fig. 3.76, we see a prominent negative anomaly in the North Atlantic seen in all days besides day -7. The pattern seen in the mean state with the positive anomaly situated over western Russia together with the mentioned negative anomaly is the pattern of interest for this event. The zonally symmetric dipole helped to strengthen the zonally symmetric flow over Norway.

The zonal wind plots in Fig. 3.77 show positive anomalies in the North Atlantic in all lags and the mean state, similar to the Odda case. The stronger westerly could have brought the moist air from the Atlantic and accompanied by the lower temperatures, contributed to the heavy snowfall. However, there were also strong negative zonal wind anomalies between Norway and Greenland north of the low-pressure anomalies. The meridional wind plots in Fig. 3.78 show some wavy structures possibly related to meandering and a prominent positive anomaly in the mean state around Norway.

3.4.3 Standardized index

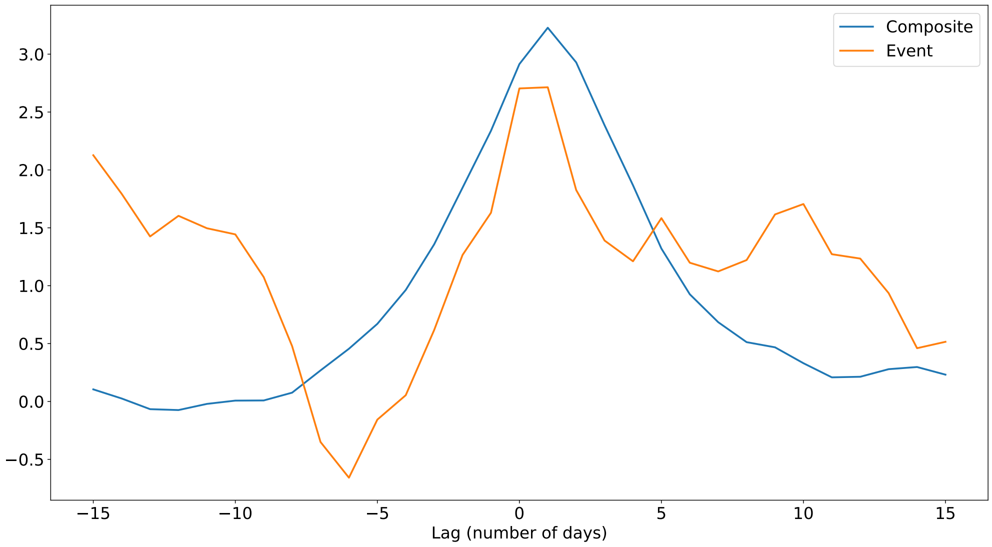

Figure 3.79: The standardized index for the Finsland snowfall event and for the composite of the events projecting on it

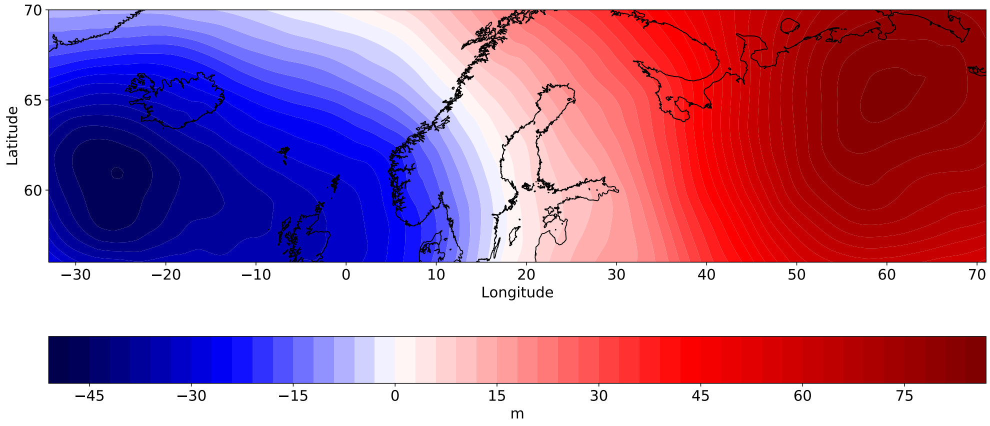

Figure 3.80: The 500 hPa geopotential height anomaly pattern for the Finsland snowfall event

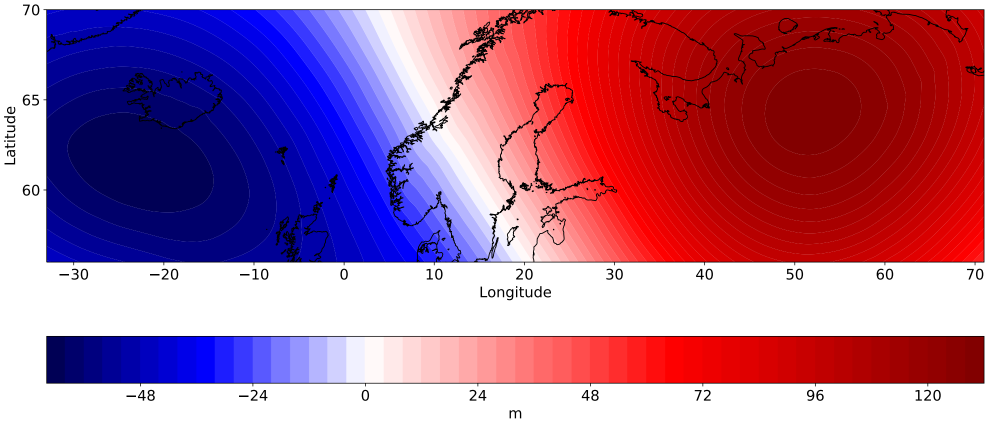

Figure 3.81: The 500 hPa geopotential height 0-day lag composites of the events projecting on the Finsland snowfall event for days with index values above the 95th percentile

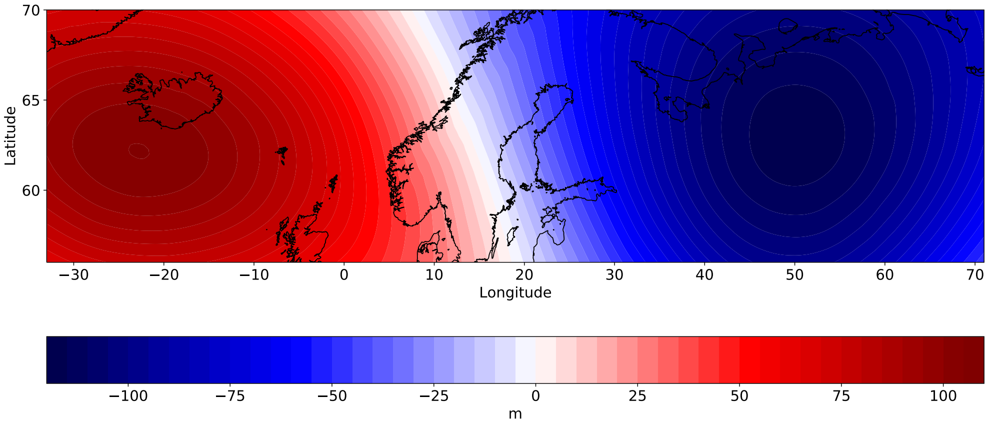

Figure 3.82: The 500 hPa geopotential height 0-day lag composites of the events projecting on the Finsland snowfall event for days with values below the 5th percentile

The index plot in Fig. 3.79 shows a good agreement between the event index and its composite. In the central days the event index is only slightly weaker than the composite and at the beginning and end it is stronger, with a slight discrepancy prior to the central days. This indicates it was much more persistent than the composite. The anomaly pattern in Fig. 3.80 shows the pattern seen in the previous plots with a negative anomaly over the North Atlantic and a positive one over Russia.

For the 0-day lag composite for days with values of the index over the 95th percentile, we see very good agreement with the anomaly pattern in Fig. 3.81. The 0-day lag for the days with index values below the 5th percentile shows an opposite, symmetric pattern in Fig. 3.82, which means there is linearity in the occurrence of the pattern.

3.4.4 Autocorrelation function

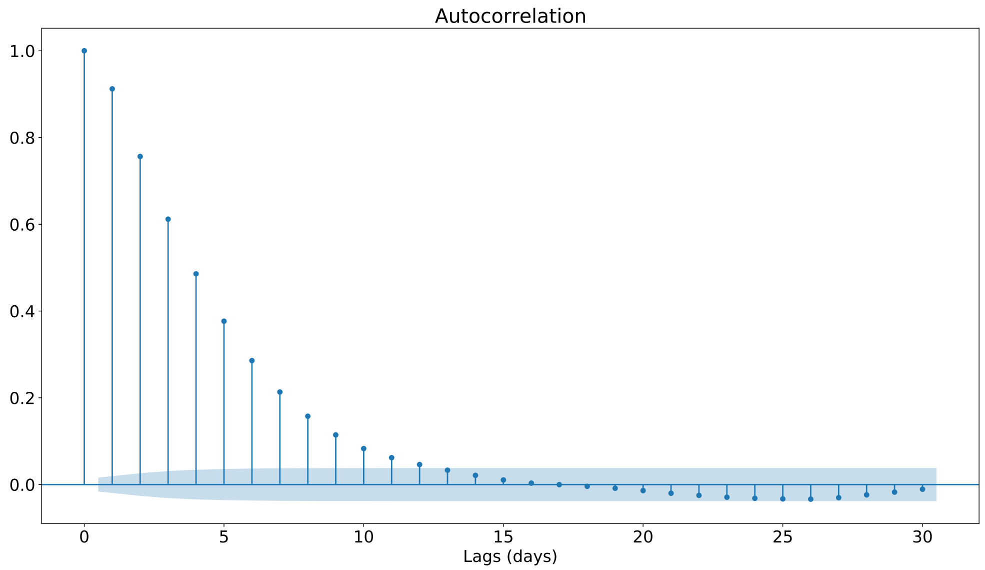

Figure 3.83: The standardized index autocorrelation function for the Finsland snowfall event

The autocorrelation plot in Fig. 3.83 in this case shows approximately a 12-day time scale of the event, which is less than in other cases, but still a significant amount for the persistence argument.

3.4.5 Basic variables composite maps

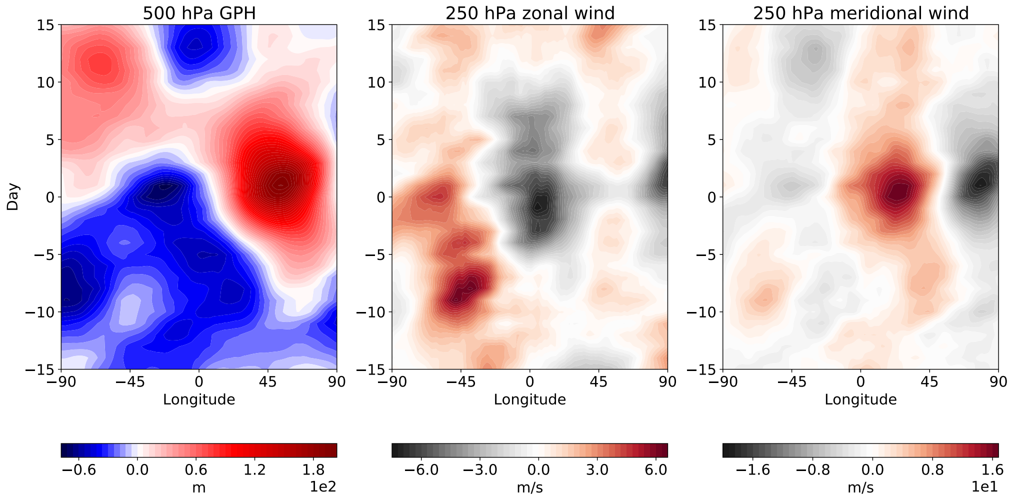

Figure 3.84: The 500 hPa geopotential height, 250 hPa zonal and meridional wind composites of the events projecting on the Finsland snowfall event (daily anomalies) for 90°W-90°N and 55°-75°N

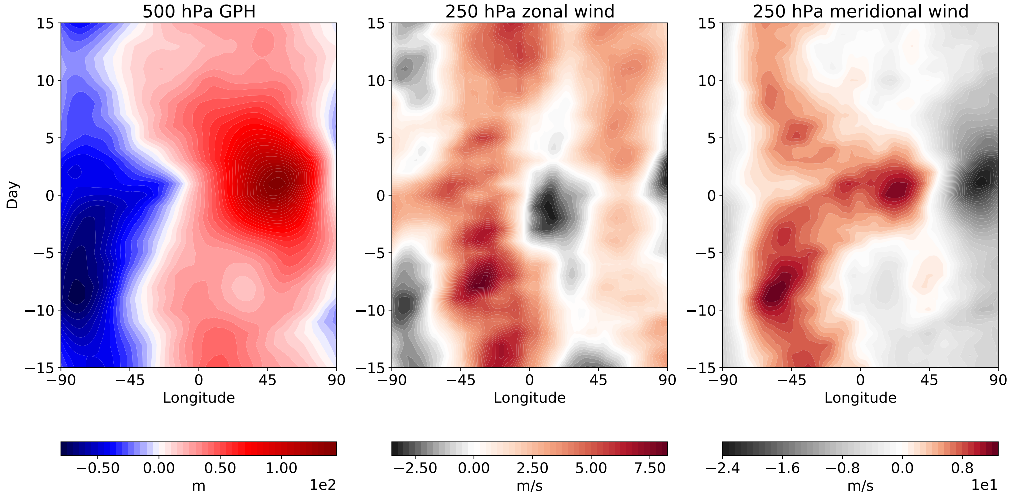

Figure 3.85: The 500 hPa geopotential height, 250 hPa zonal and meridional wind composites of the events projecting on the Finsland snowfall event (deviations from the zonal mean) for 90°W-90°N and 55°-75°N

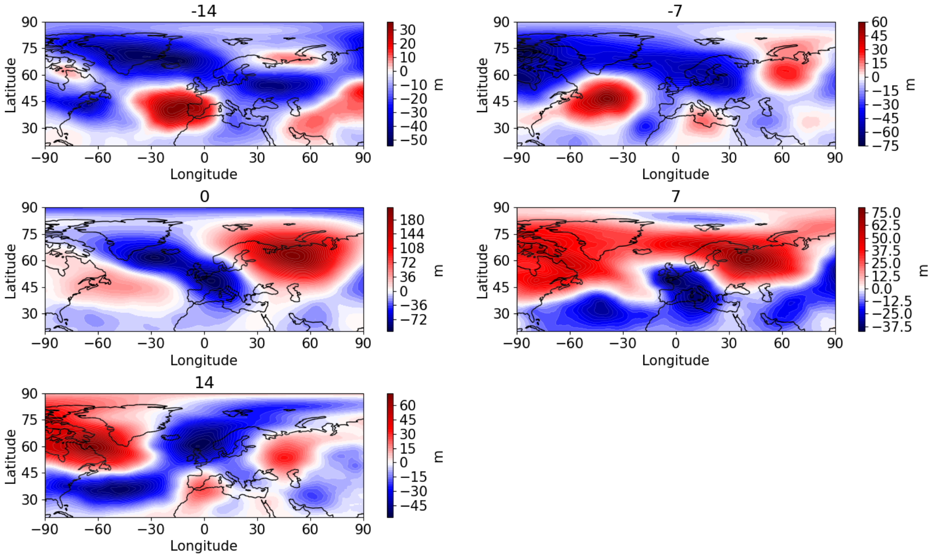

Figure 3.86: The 500 hPa geopotential height lag composites of the events projecting on the Finsland snowfall event for lags -14, -7, 0, 7 and 14

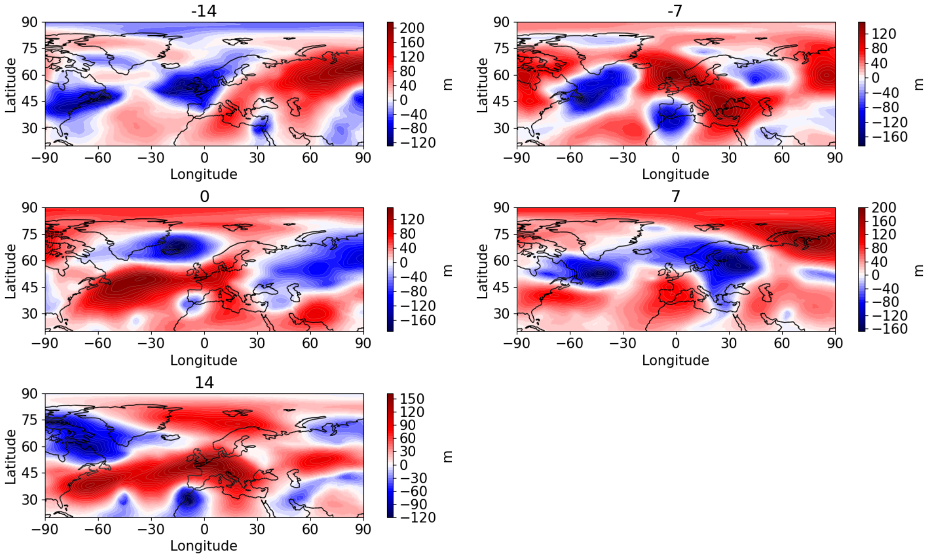

Figure 3.87: The 500 hPa geopotential height event deviations from the lag composites of the events projecting on the Finsland snowfall event for lags and days -14, -7, 0, 7 and 14

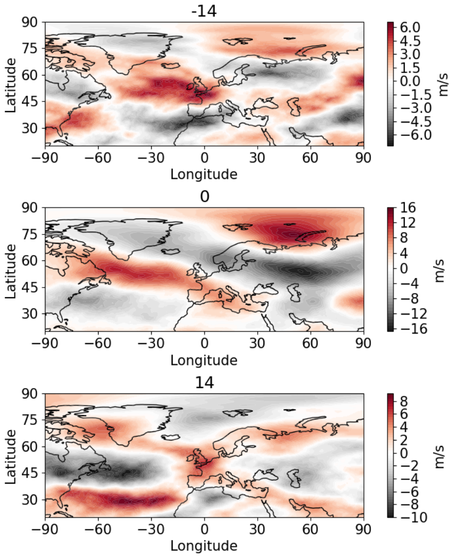

Figure 3.88: The 250 hPa zonal wind event lag composites of the events projecting on the Finsland snowfall event for lags -14, -7, 0, 7 and 14

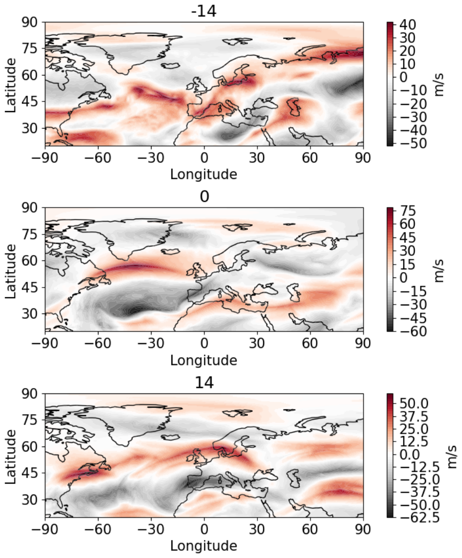

Figure 3.89: The 250 hPa zonal wind event deviations from the lag composites of the events projecting on the Finsland snowfall event for lags and days -14, -7, 0, 7 and 14

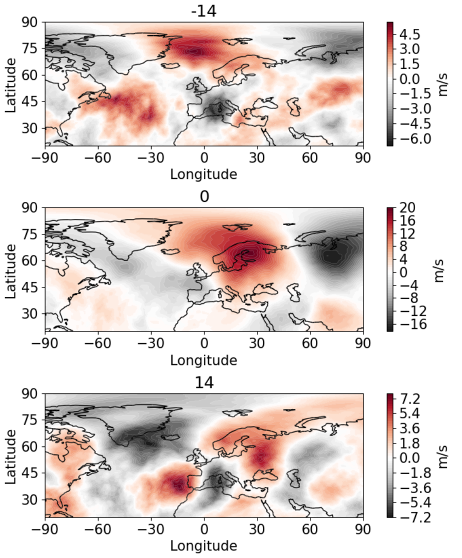

Figure 3.90: The 250 hPa meridional wind lag composites of the events projecting on the Finsland snowfall event for lags -14, -7, 0, 7 and 14

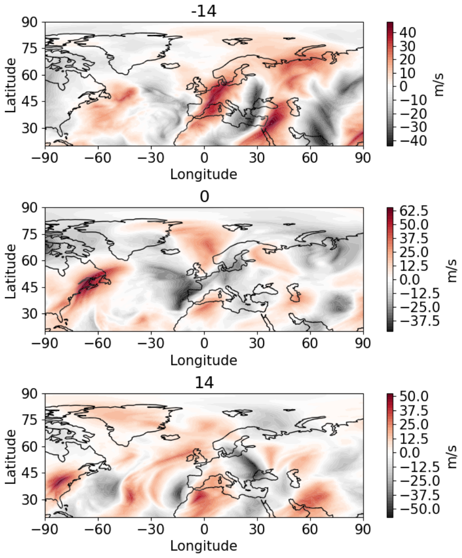

Figure 3.91: The 250 hPa meridional wind event deviations from the lag composites of the events projecting on the Finsland snowfall event for lags and days -14, -7, 0, 7 and 14

The composite plots in Fig. 3.84 show the previously seen dipole pattern for the geopotential height in Fig. 3.80 as well as a similar pattern for the zonal wind. The meridional wind shows a distinct positive anomaly, which is also seen in the previous anomaly plots. The composites for the deviations from the zonal mean in Fig. 3.85 show the aforementioned anomalies more prominently, especially the positive zonal wind anomaly spread out throughout the whole time domain as well as the dipole pattern in the geopotential height.

In the lag composites for the geopotential height in Fig. 3.86, we see the persistence in the negative anomaly pattern prior to the central lag and the persistence in the positive anomaly after the central lag. In the difference plots in Fig. 3.87, we can see how the event is slightly weaker than the composite in all lags, which is in agreement with the index and its composite, but only for the lags -7, 0 and 7. This pattern shows lower pressure in the Arctic and higher wind anomalies between Greenland and Norway. This may be due to the fact that the Arctic region was not considered in the area used for the index.

The zonal wind lag composites in Fig. 3.88 show the prominent positive anomaly as seen in the previous plots over the North Atlantic. The difference plots in Fig. 3.89 show the winds are slightly stronger than the composite mean, as opposed to the situation for the geopotential height. The negative wind anomalies between Greenland and Norway are also reproduced, but weaker.

The plots for the lag composites of the meridional wind in Fig. 3.90 show the prominent positive anomaly over the region of Norway as seen in the previous plots. Judging from the differences in Fig. 3.91, we see there is mostly no significant change for the area of interest, suggesting the same strength of the event winds to the composite.

3.4.6 Snowfall rate

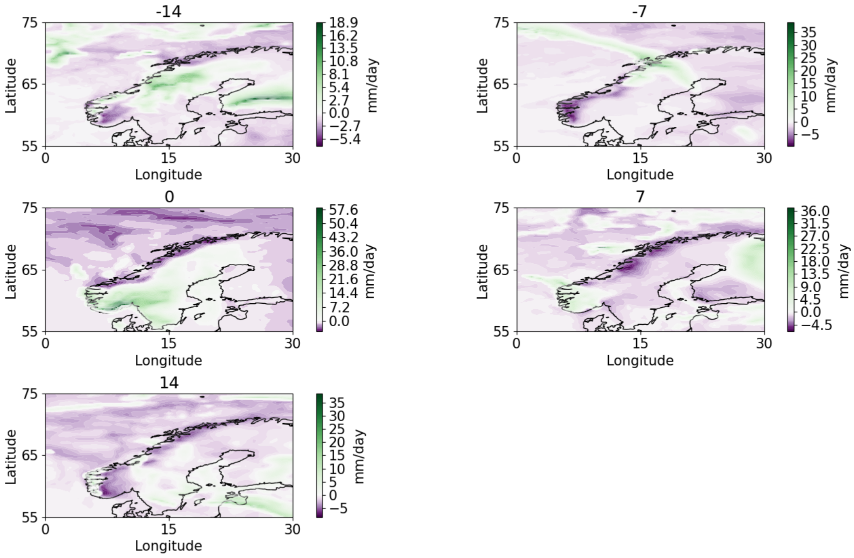

Figure 3.92: The snowfall rate anomaly fields for the Finsland snowfall event for days -14, -7, 0, 7 and 14

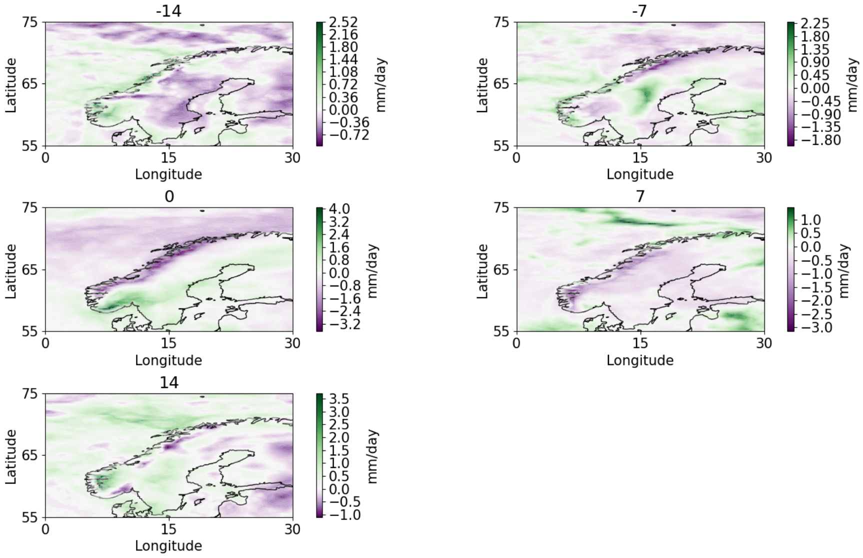

Figure 3.93: The snowfall rate lag composites of the events projecting on the Finsland snowfall event for lags -14, -7, 0, 7 and 14

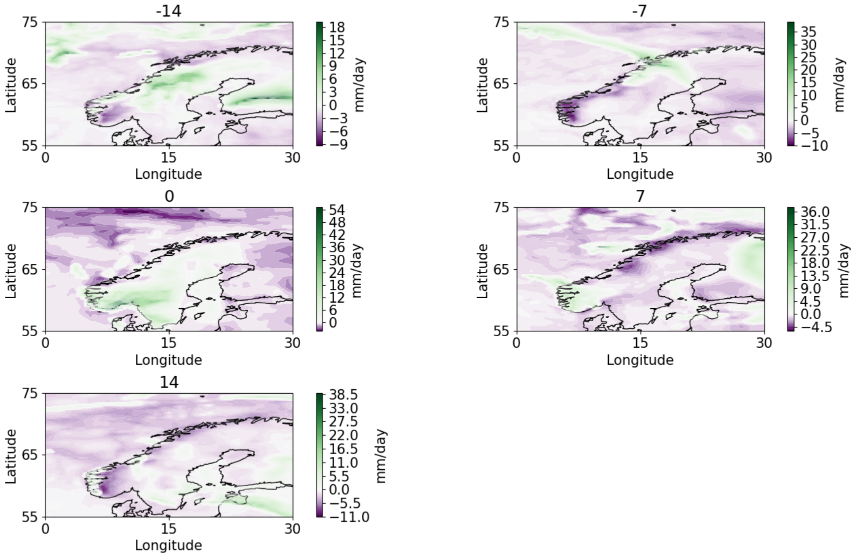

Figure 3.94: The snowfall rate event deviations from the lag composites of the events projecting on the Finsland snowfall event for lags and days -14, -7, 0, 7 and 14

This event was related to extreme snowfall so we look into the plots of the mean snowfall rate. For the snowfall rate related to the actual event in Fig. 3.92, a positive anomaly in the region of interest in the south of Norway is seen in days 0 and 7, indicating persistence of these conditions, which was crucial for the impact of this event, similar to the Lærdal drought case. For the lag composites in Fig. 3.93, we see positive values for all lags for the region of interest besides lag 14. The difference plots in Fig. 3.94 show positive values at lags 0 and 7, similar to the actual days of the event, indicating the strength of the event snowfall compared to the composite.

3.4.7 Barotropic LWA and zonal wind

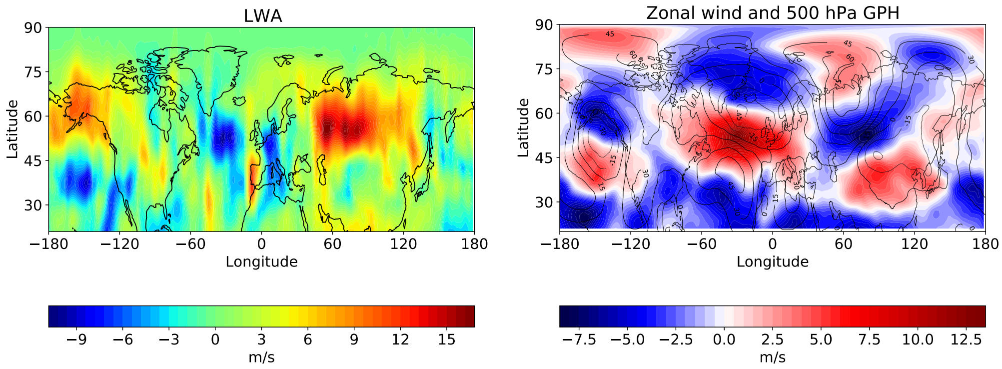

Figure 3.95: The barotropic LWA and zonal wind 29-day event anomaly means for the Finsland snowfall event

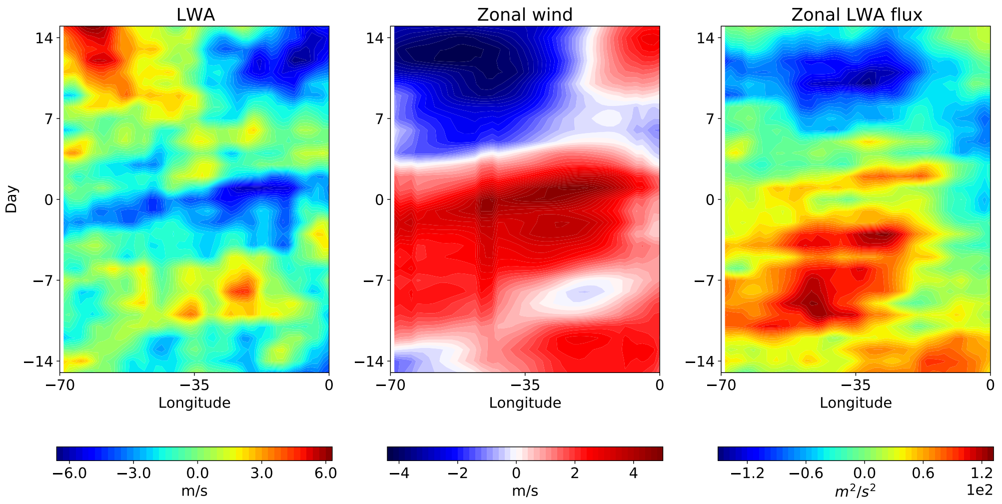

Figure 3.96: The barotropic LWA, zonal wind and zonal LWA flux composites of the events projecting on the Finsland snowfall event for 70°W-0° and 40-60°N

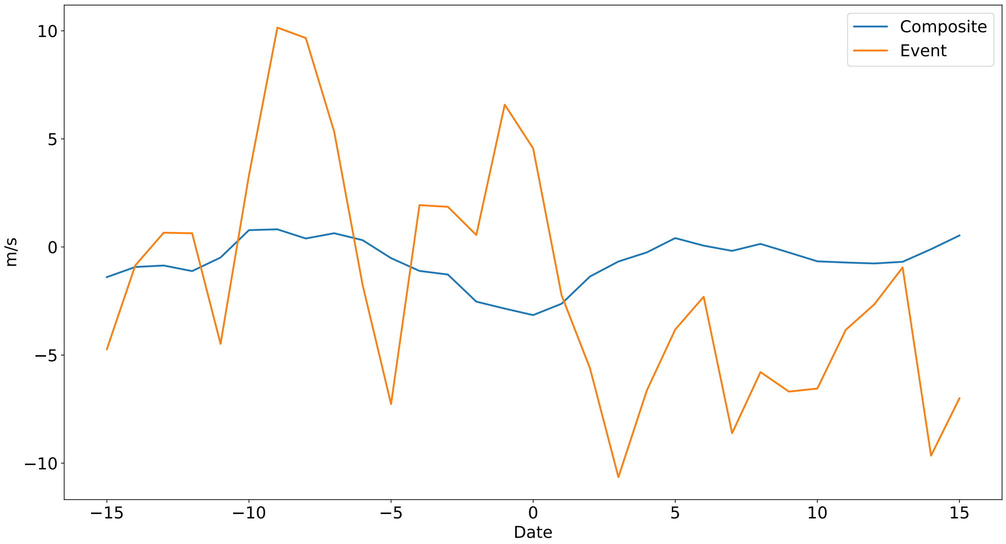

Figure 3.97: The barotropic LWA for the Finsland snowfall event and for the composite of the events projecting on it for 70°W-0° and 40-60°N

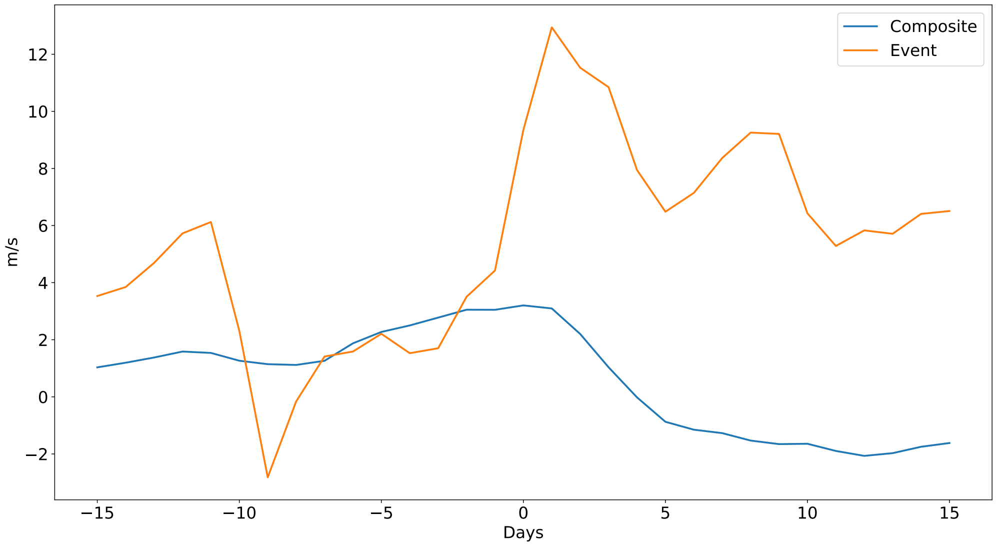

Figure 3.98: The barotropic zonal wind for the Finsland snowfall event and for the composite of the events projecting on it for 70°W-0° and 40-60°N

For the barotropic LWA and zonal wind anomaly mean states for the event shown in Fig. 3.95, we see a negative LWA anomaly over the North Atlantic and some parts of central Europe corresponding to the positive wind anomaly over that region. This indicates this event was not related to blocking. It is also interesting to note there's quite a spacious positive LWA anomaly further away from the region of interest over Siberia. The region of 70°W-0° and

40-60°N was then used for the composite calculation, excluding the negative values with a mask.

In the composite plot in Fig. 3.96, we see the negative LWA anomaly and positive wind anomaly in the maturation phase (close to lag 0). The zonal LWA flux composite shows us a large positive anomaly occurring at the same time, preceeding the negative zonal wind and positive LWA further in the time series, showing again there was no blocking since the influence of the flux came later into the event and not in its early stages, which is crucial for fulfilling the blocking conditions.

As far as the line plots for the barotropic LWA and zonal wind are concerned, in Fig. 3.97, we can see how the LWA (with large fluctuations) has mostly positive values before the central day and then negative values suggesting more or less an agreement with the composite. The zonal wind in Fig. 3.98 shows a much higher value than the composite, where the positive anomalies persist more in the positive lags than in the composite. These results together with the composite and the mean anomaly state suggest this event was not related to a blocking pattern. They also suggest a lot of non-linearity between the LWA and the zonal wind.

3.4.8 LWA budget equation components

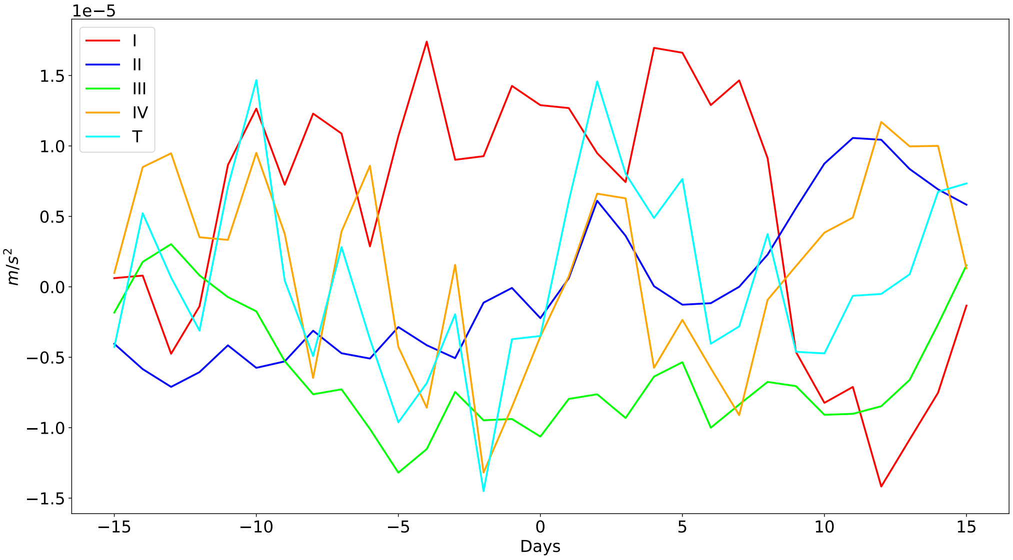

Figure 3.99: The LWA budget equation components (zonal LWA flux convergence (I), eddy meridional momentum flux divergence (II), low-level meridional heat flux (III), residual (IV) and the LWA tendency (T)) for the composite of the events projecting on the Finsland snowfall event for 70°W-0° and 40-60°N

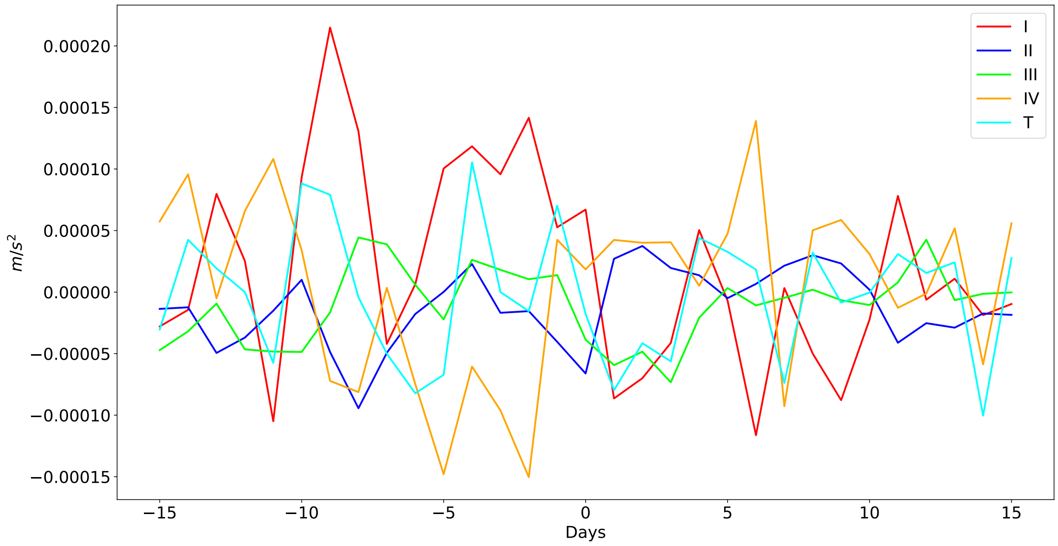

Figure 3.100: The LWA budget equation components (zonal LWA flux convergence (I), eddy meridional momentum flux divergence (II), low-level meridional heat flux (III), residual (IV) and the LWA tendency (T)) for the Finsland snowfall event for 70°W-0° and 40-60°N

For the LWA budget equation components, the line plot of the composites in Fig. 3.99 shows us the fluctuating nature of all components with all of them having a strong impact. The zonal LWA flux convergence helps to enhance the tendency and at the end it starts to dampen it. The residual exchanges between enhancing and dampening. The heat flux dampens it throughout the time series, while the momentum flux dampens it in the first part and then enchances it in the second. For the actual event in Fig. 3.100, we can see the biggest contributions to the tendency (T) come from the zonal LWA flux convergence (I), which enchances it, and the residual (IV), which dampens it. The significant influence of the residual is not a surprise considering the non-linearity seen in the LWA and zonal wind plots.

3.5 Mykland heatwave event

3.5.1 General event description

In May and June 2018, a heatwave affected southern Norway. Days of higher than normal temperatures contributed to fires spreading throughout the region. This was also helped by the lack of precipitation in this time period. There was also a lot of damage to agricultural crops as well. The temperatures measured in these two months in the area were the highest ever measured in history at that time. The large-scale circulation in this event was a persisting high-pressure pattern, which caused the high temperatures and low precipitation

(Breiteig, 2018; Arnesen, 2018).

3.5.2 Basic variables anomaly fields

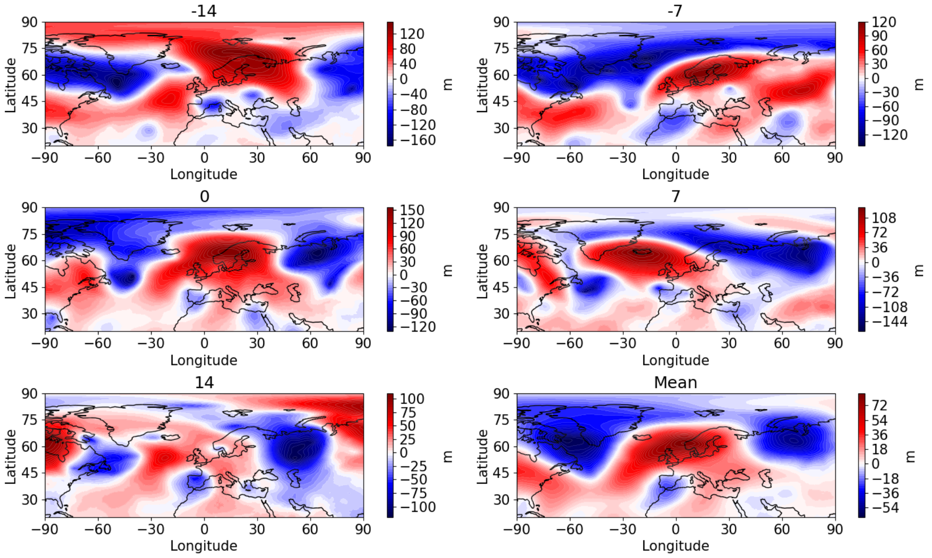

Figure 3.101: The 500 hPa geopotential height event anomaly fields for the Mykland heatwave event for days -14, -7, 0, 7 and 14 and the 29-day mean

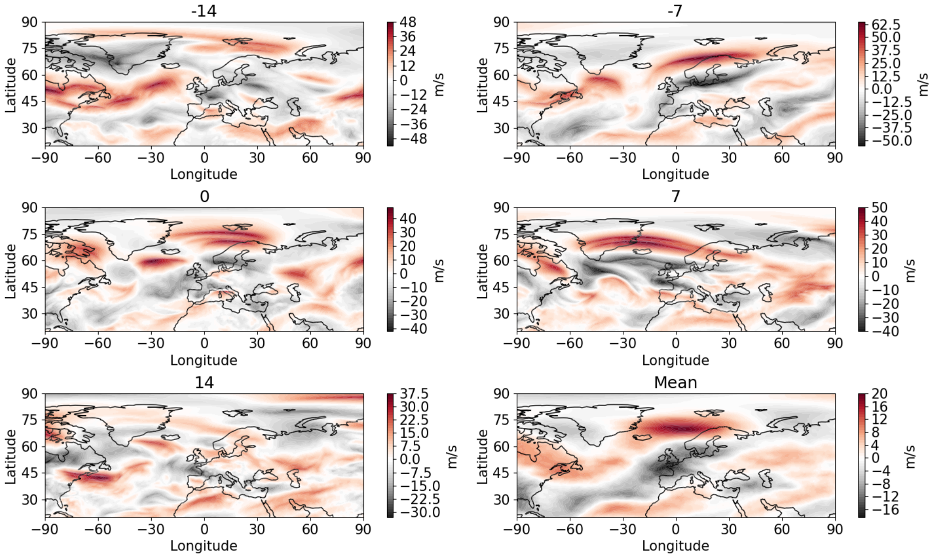

Figure 3.102: The 250 hPa zonal wind event anomaly fields for the Mykland heatwave event for days -14, -7, 0, 7 and 14 and the 29-day mean

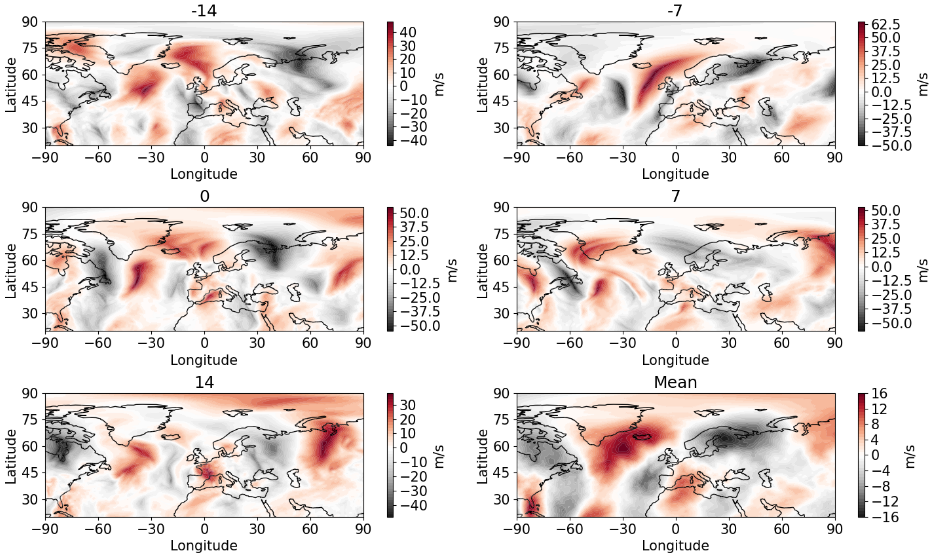

Figure 3.103: The 250 hPa meridional wind event anomaly fields for the Mykland heatwave event for days -14, -7, 0, 7 and 14 and the 29-day mean

The geopotential height plots in Fig. 3.101 show us a distinct positive anomaly situated over Norway. The anomaly only loses its strength in the last days indicating potential for dry and warm conditions. In the mean state, we see a dipole pattern between the mentioned positive anomaly and a negative anomaly east of it with a center over Siberia.

For the zonal wind in Fig. 3.102, we see a negative anomaly in all days which is especially seen in the mean state, indicating a persistence and blocking pattern coming from weakened westerlies. The meridional wind plots in Fig. 3.103 show some waviness in different lags indicating meandering, but the most compelling feature is the dipole pattern seen in the mean state with Norway approximately finding itself at the separation of the two patterns.

3.5.3 Standardized index

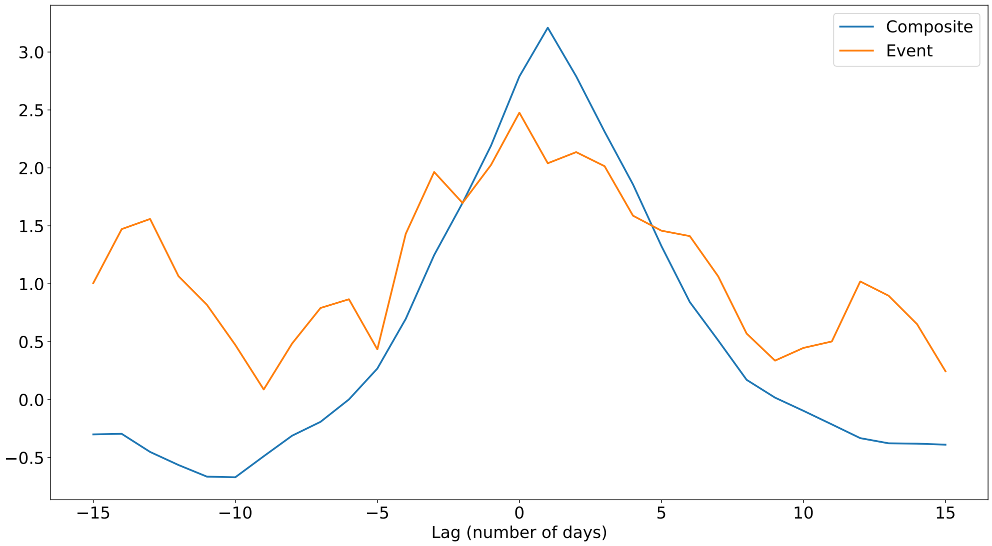

Figure 3.104: The standardized index for the Mykland heatwave event and for the composite of the events projecting on it

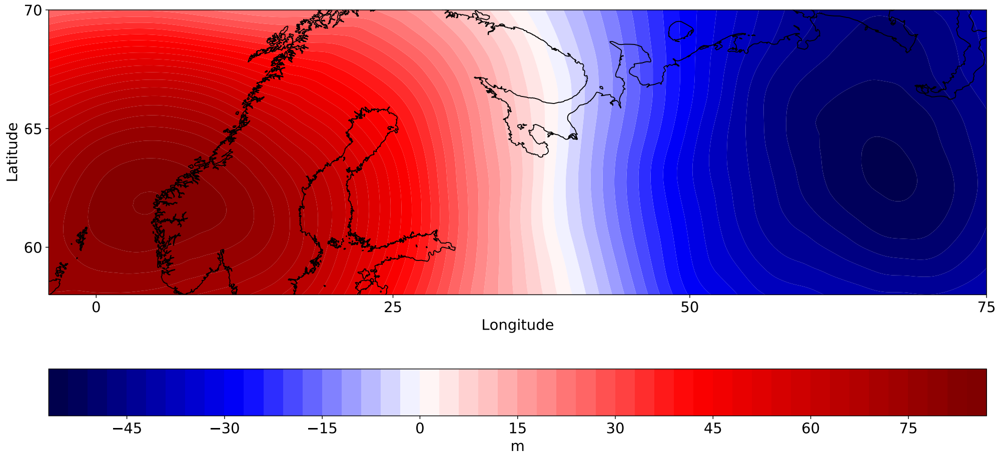

Figure 3.105: The 500 hPa geopotential height anomaly pattern for the Mykland heatwave event

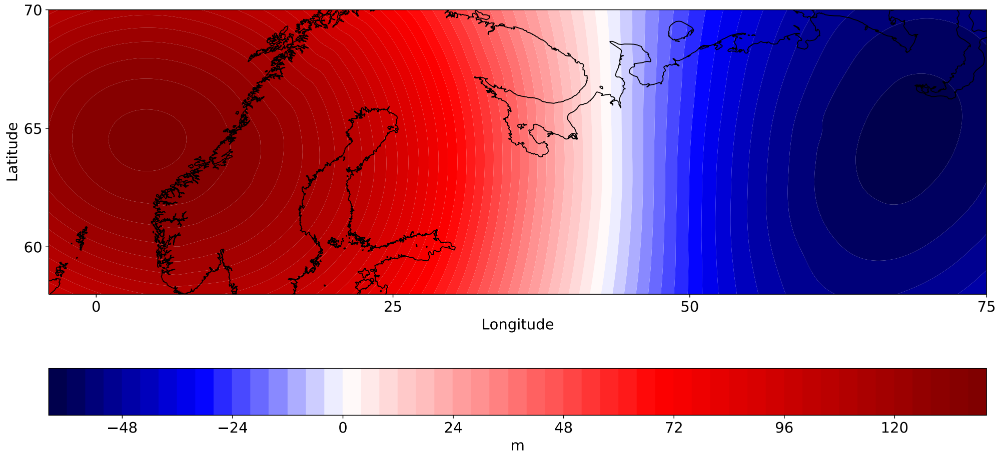

Figure 3.106: The 500 hPa geopotential height 0-day lag composites of the events projecting on the Mykland heatwave event for days with index values above the 95th percentile

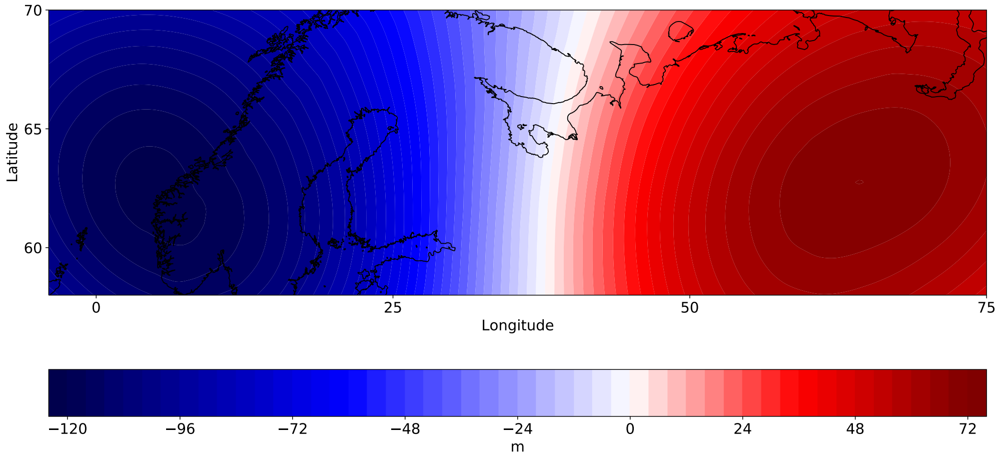

Figure 3.107: The 500 hPa geopotential height 0-day lag composites of the events projecting on the Mykland heatwave event for days with values below the 5th percentile

The index plot shown in Fig. 3.104 gives a very good agreement of the index with its composite. The event index has slightly lower values in the central days of the event, but has higher values at the beginning and end. This indicates it was much more persistent than the composite. The anomaly pattern used for the calculation in Fig. 3.105 shows the dipole pattern seen in previous plots with the positive anomaly centered around western Norway and the negative anomaly centered over Siberia. The zonal symmetry of the pattern helped to strengthen the zonal flow over Norway.

In Fig. 3.106, we see the 0-day lag composite of all the fields with values of the index above the 95th percentile. There is a very good agreement with the anomaly pattern for the index. For the case of 0-day lag composite of all fields with values of the index below the 5th percentile in Fig. 3.107, we see the opposite pattern meaning there is linearity in the occurrence of the pattern.

3.5.4 Autocorrelation function

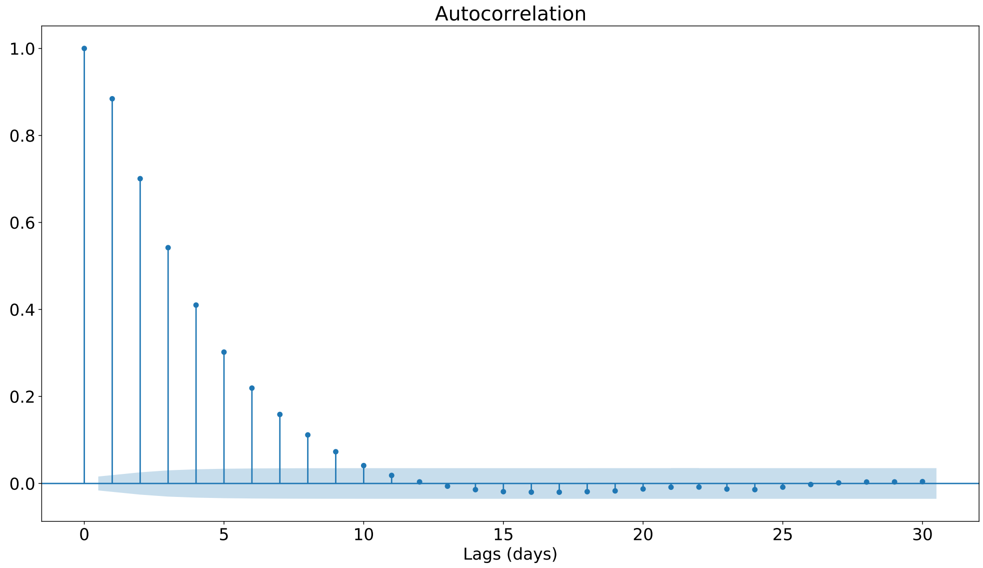

Figure 3.108: The standardized index autocorrelation function for the Mykland heatwave event

The autocorrelation plot in Fig. 3.108 in this case shows approximately a 10-day time scale of the event which is less than in other cases, but still a significant amount. This indicates also that the extreme might have been even stronger due to its shorter time scale.

3.5.5 Basic variables composite maps

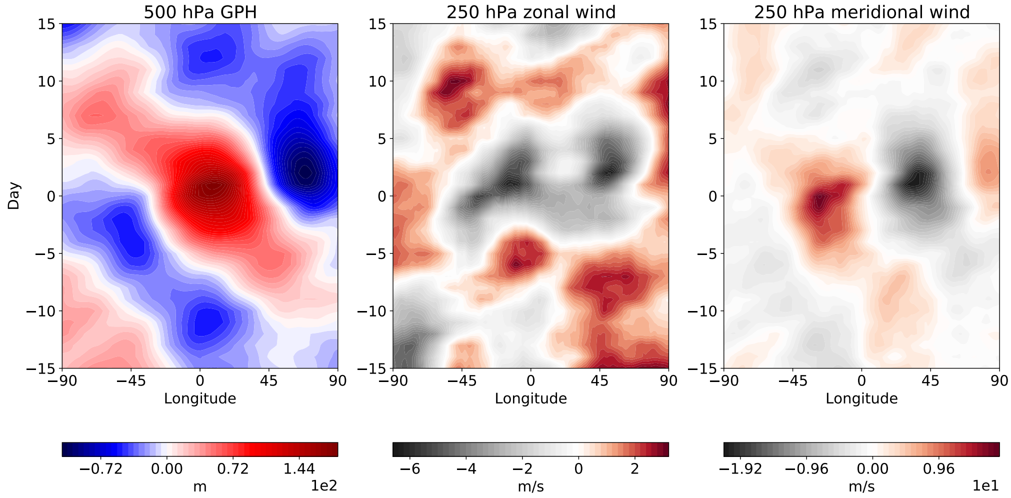

Figure 3.109: The 500 hPa geopotential height, 250 hPa zonal and meridional wind composites of the events projecting on the Mykland heatwave event (daily anomalies) for 90°W-90°N and 55°-75°N

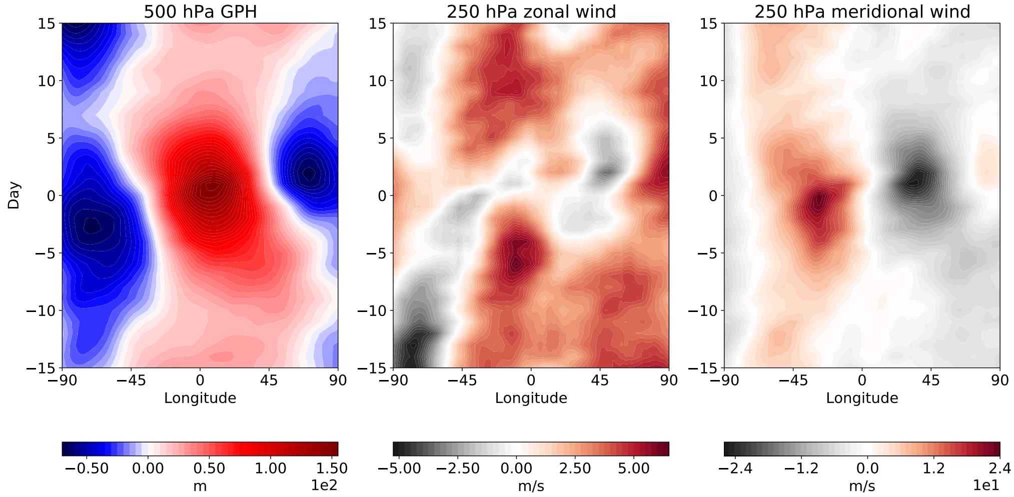

Figure 3.110: The 500 hPa geopotential height, 250 hPa zonal and meridional wind composite of the events projecting on the Mykland heatwave event (deviations from the zonal mean) for 90°W-90°N and 55°-75°N

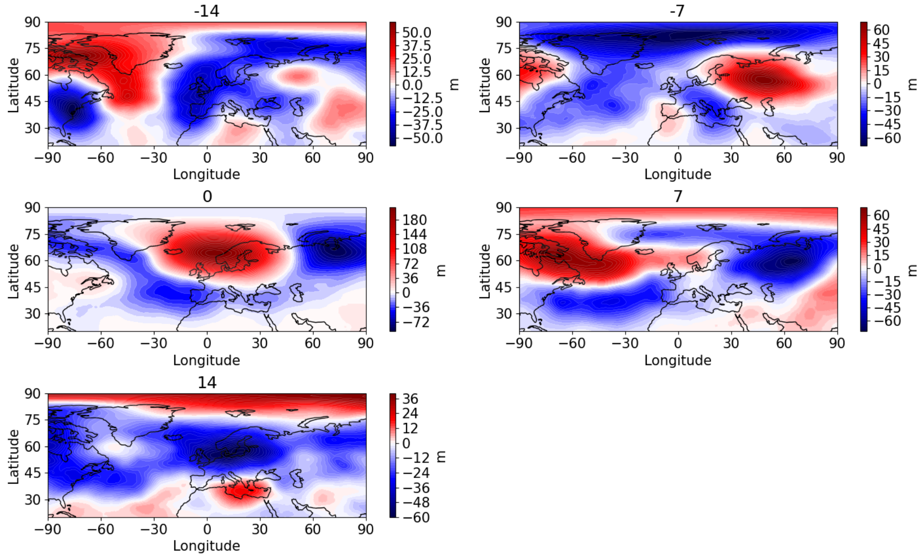

Figure 3.111: The 500 hPa geopotential height lag composites of the events projecting on the Mykland heatwave event for lags -14, -7, 0, 7 and 14

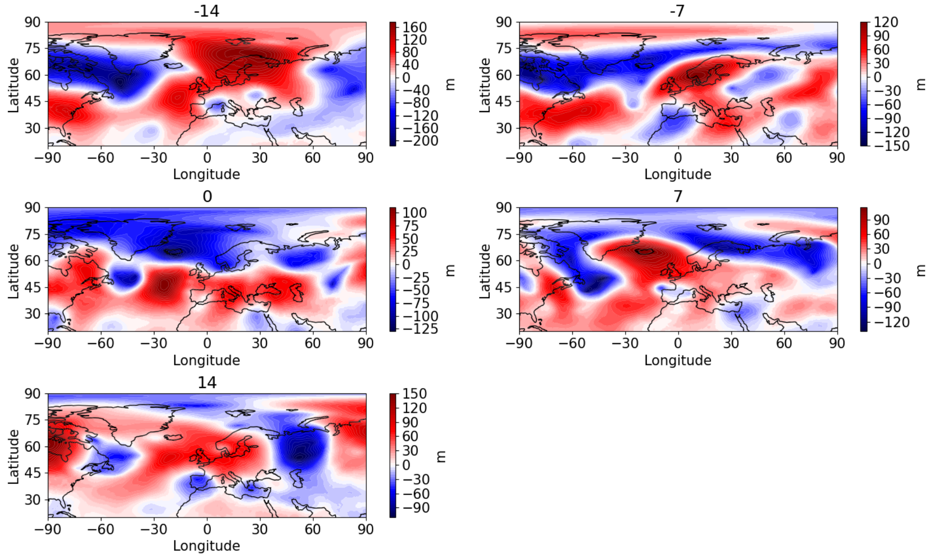

Figure 3.112: The 500 hPa geopotential height event deviations from the lag composites of the events projecting on the Mykland heatwave event for lags and days -14, -7, 0, 7 and 14

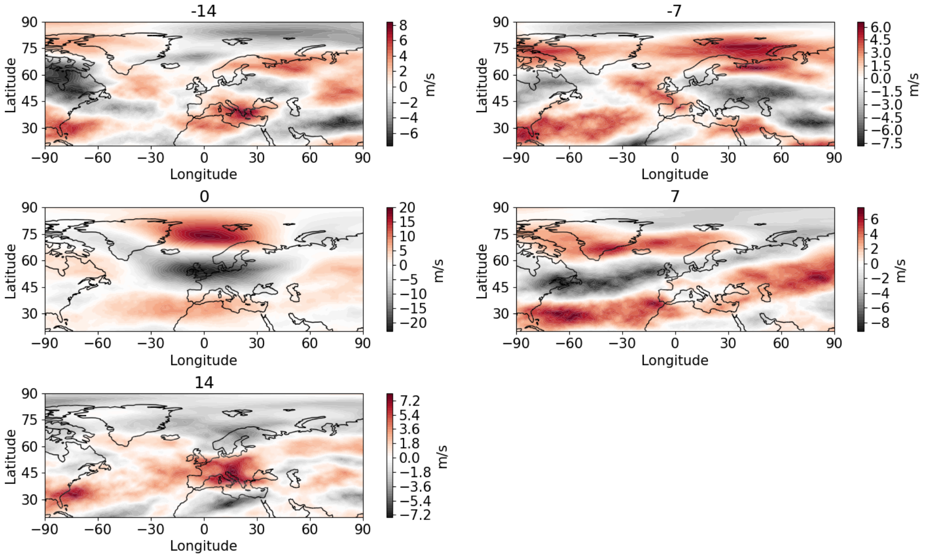

Figure 3.113: The 250 hPa zonal wind lag composites of the events projecting on the Mykland heatwave event for lags -14, -7, 0, 7 and 14

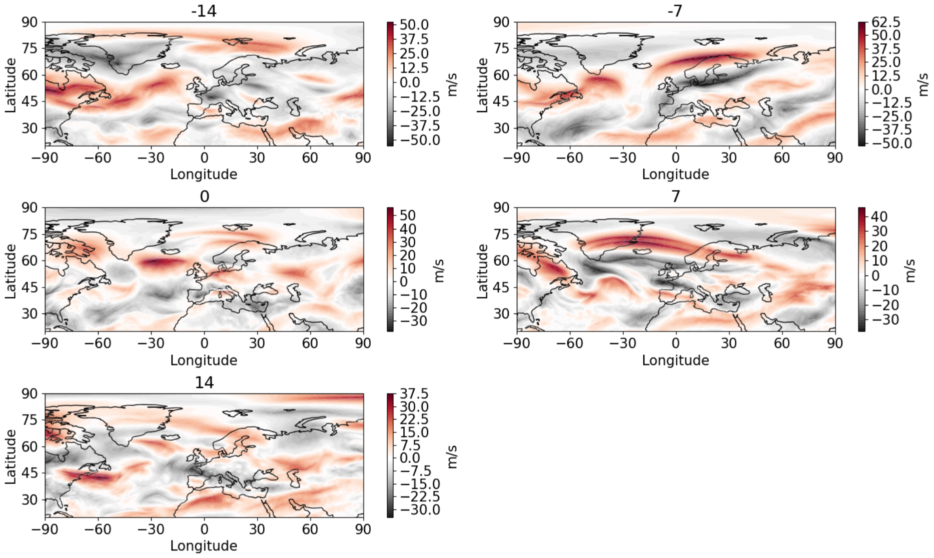

Figure 3.114: The 250 hPa zonal wind event deviations from the lag composites of the events projecting on the Mykland heatwave event for lags and days -14, -7, 0, 7 and 14

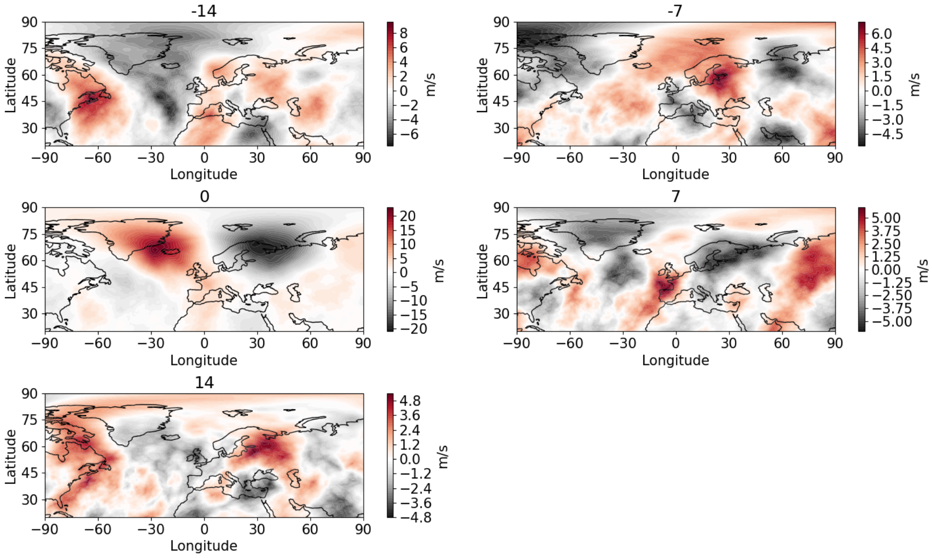

Figure 3.115: The 250 hPa meridional wind lag composites of the events projecting on the Mykland heatwave event for lags -14, -7, 0, 7 and 14

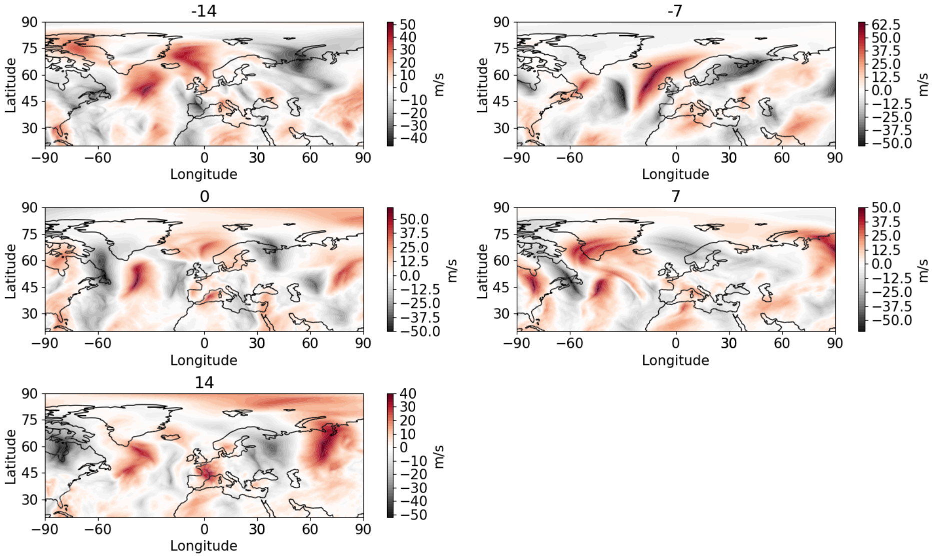

Figure 3.116: The 250 hPa meridional wind event deviations from the lag composites of the events projecting on the Mykland heatwave event for lags and days -14, -7, 0, 7 and 14

Looking at the composite plots of the geopotential height in Fig. 3.109, we see the previously mentioned persistent positive anomaly as well as the negative zonal wind anomaly. There is also significant westward propagation throughout the time series for the geopotential height. The meridional wind plot also shows a dipole pattern similar to the one in the event anomalies. For the composites made from the deviations from the zonal mean in Fig. 3.110, the geopotential height pattern is more prominent and persistent, while the zonal wind doesn't clearly show the negative anomaly. The meridional wind plot is similar to the previous one.

For the geopotential height lag composites in Fig. 3.111, in lag 0 we see the pattern from the previous plots. Looking at the whole series we can see the formation and evolution of it with the positive anomaly forming in the east and then moving to the west, while the negative anomaly moved to the east in lags 0 and 7. From the difference plots in Fig. 3.112, we can see how the event was weaker than the composite, especially in lag 0, in agreement with the index.

For the lag composites of the zonal wind in Fig. 3.113, the previously mentioned negative anomaly is seen only in the 0 and 7 lag. The difference plots in Fig. 3.114 show us how the winds were slightly stronger than in the composite mean.

Looking at the meridional wind plots in Fig. 3.115, we see the prominent dipole pattern at lag 0, while the other lags show some waviness, although there is a lot of scatter between the patterns. The differences in Fig. 3.116 show the winds were slightly weaker or similar to the composite mean.

3.5.6 Surface temperature

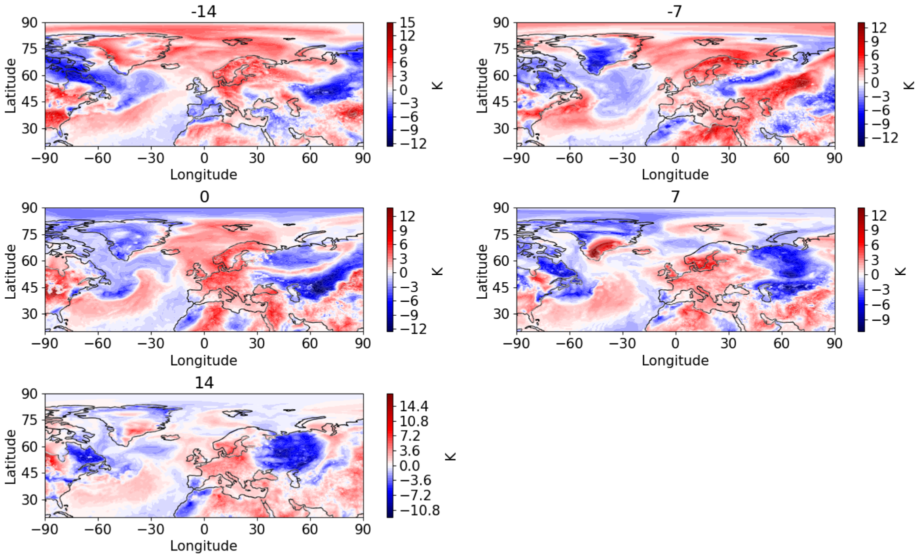

Figure 3.117: The surface temperature event anomaly fields for the Mykland heatwave event for days -14, -7, 0, 7 and 14

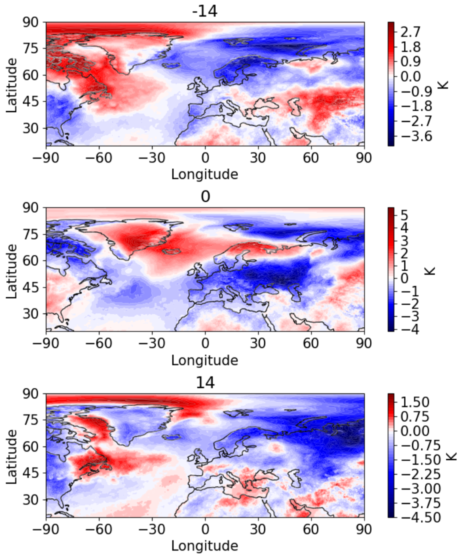

Figure 3.118: The surface temperature lag composites of the events projecting on the Mykland heatwave event for lags -14, -7, 0, 7 and 14

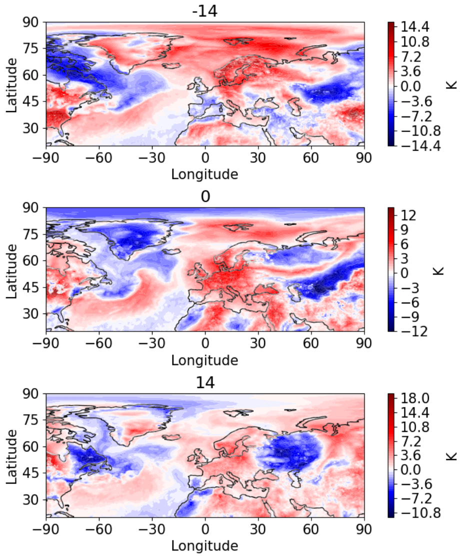

Figure 3.119: The surface temperature event deviations from the lag composites of the events projecting on the Mykland heatwave event for lags and days -14, -7, 0, 7 and 14

Since this event was a heatwave, we look into the surface temperature as the key variable for determining its nature. Looking at the phases of the event in Fig. 3.117, we see how the positive anomaly persists over all phases of the event. From the lag composites in Fig. 3.118, we see how the anomaly is actually negative over the region of interest. In the difference plot in Fig. 3.119, we see how the event was much stronger than the composite mean. This persistence of the positive anomaly was the key of the impact of this event, similar to the Lærdal and Finsland cases.

3.5.7 Barotropic LWA and zonal wind

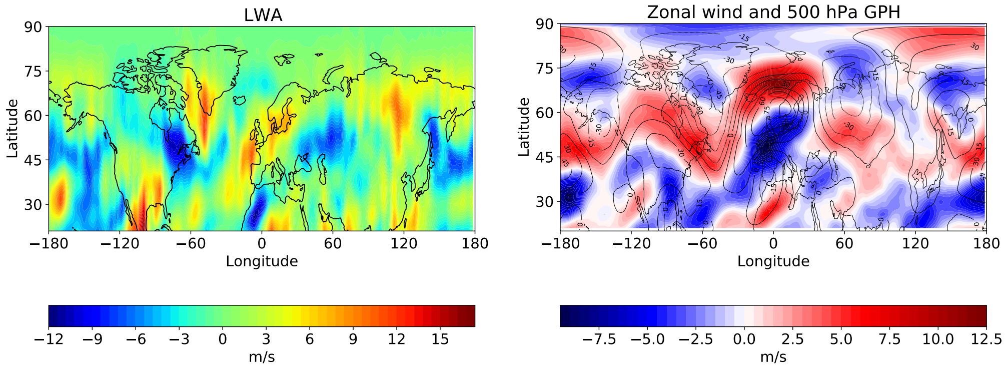

Figure 3.120: The barotropic LWA and zonal wind 29-day event anomaly means for the Mykland heatwave event

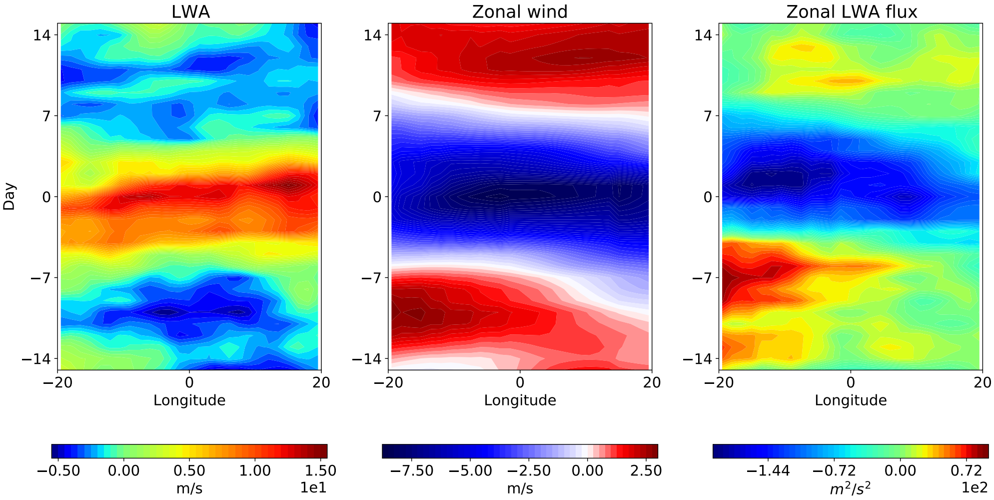

Figure 3.121: The barotropic LWA, zonal wind and zonal LWA flux composites of the events projecting on the Mykland heatwave event for 20°W-20°E and 40-65°N

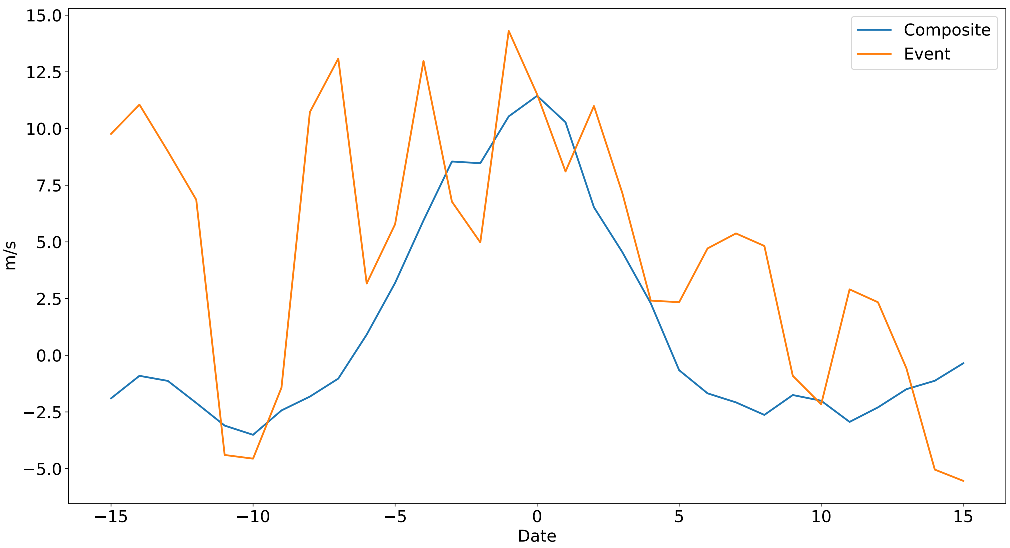

Figure 3.122: The barotropic LWA for the Mykland heatwave event and for the composite of the events projecting on it for 20°W-20°E and 40-65°N

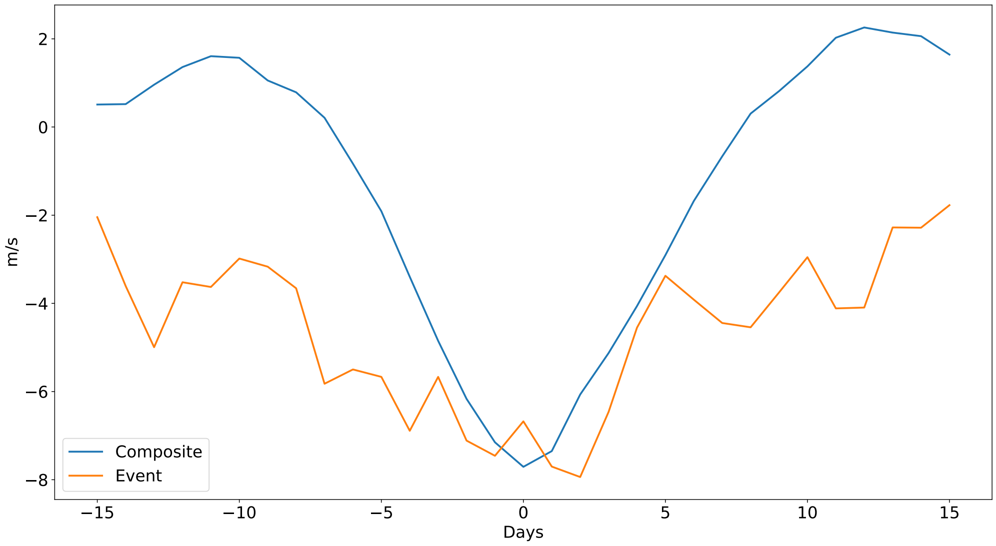

Figure 3.123: The barotropic zonal wind event for the Mykland heatwave event and for the composite of the events projecting on it for 20°W-20°E and 40-65°N

Looking at the mean state of the anomalies for the event in Fig. 3.120, we see a positive LWA anomaly corresponding to a negative zonal wind anomaly over Europe. This indicates conditions for blocking. The region of 20°W-20°E and 40-65°N was used for the composite calculation, while masking out the positive values.

In the composite plot in Fig. 3.121, we see the positive LWA anomaly from lag -5 to 5 with the negative zonal wind anomaly from lag -7 to 7 as seen in the previous plots. Prior to the establishment of these patterns, we see the positive values of the zonal LWA flux in the early lags, indicating the onset of blocking and jet stream meandering in this event. This is another analogy with the traffic jam concept where the LWA flux in the early stages indicates blocking after the capacity for the flux is exceeded.

Looking at the line plot for the LWA in Fig. 3.122, we see how the event LWA closely follows the composite with quite high values. The zonal wind in Fig. 3.123 also follows the composite closely while having stronger negative values, further cementing the argument for blocking conditions.

3.5.8 LWA budget equation components

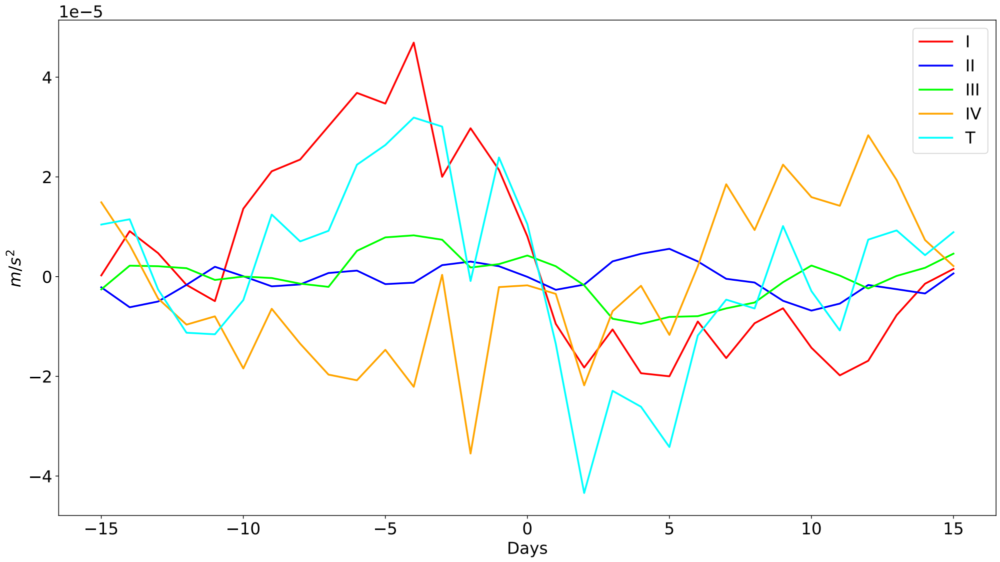

Figure 3.124: The LWA budget equation components (zonal LWA flux convergence (I), eddy meridional momentum flux divergence (II), low-level meridional heat flux (III), residual (IV) and the LWA tendency (T)) for the composite of the events projecting on the Mykland heatwave event for 20°W-20°E and 40-65°N

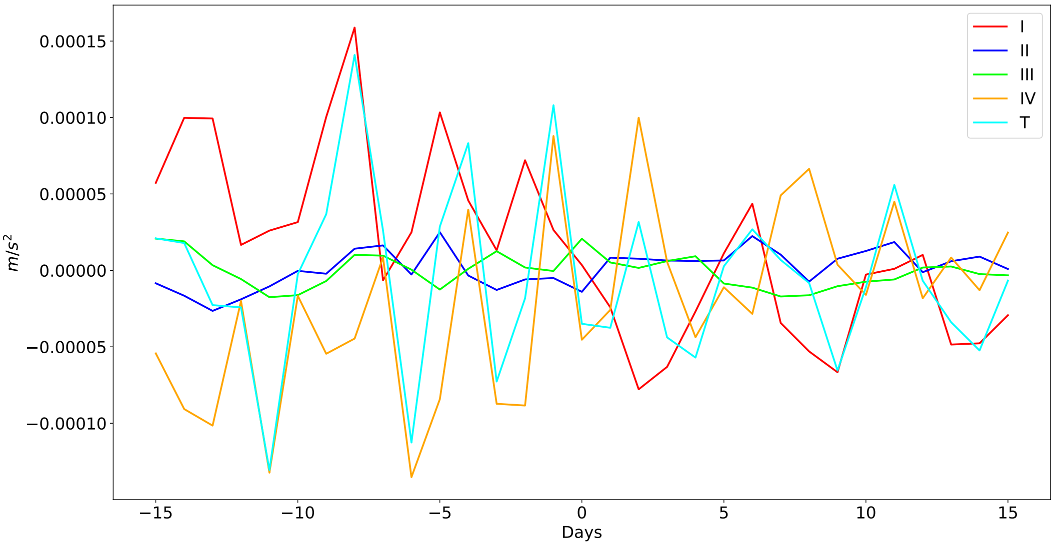

Figure 3.125: The LWA budget equation components (zonal LWA flux convergence (I), eddy meridional momentum flux divergence (II), low-level meridional heat flux (III), residual (IV) and the LWA tendency (T)) for the Mykland heatwave event for 20°W-20°E and 40-65°N

For the budget equation components line plot of the composite in Fig. 3.124, we can see how the tendency (T) changes from positive values in the beginning to negative values in the other part. The main drivers of the tendency are the zonal LWA flux convergence (I) and the residual (IV), where they enhance and dampen the LWA in the different halves of the time series, while the eddy meridional momentum flux divergence (II) and the low-level meridional heat flux (III) have a lesser impact.

For the actual event in Fig. 3.125, we can see how the tendency is very fluctuant with the zonal LWA flux convergence and the residual as the biggest contributors. The momentum and heat flux (II and III) have a very small impact as seen already in the composite. The zonal LWA flux convergence helps to maintain a positive LWA with its early onset and agreement with the zonal LWA flux composite in Fig. 3.121. We can again relate this situation to the traffic jam analogy.

Chapter 4

Discussion

4.1 Introduction

In this study, five extreme events that have occurred in the past seven years in the area of south and southwestern Norway have been investigated. The goal of the thesis was to understand the different dynamical mechanisms influencing the large-scale circulation throughout the time period of the events, find ways to identify and predict the events and identify the influence of the events on the meteorological variables relevant for energy production in Norway. The first assumption of the cause of these events was a link with high-amplitude quasi-stationary Rossby waves and the resonance between free and forced waves, which amplified the Rossby waves (Kornhuber et al., 2017; Coumou et al., 2014). The approach in most of the recent literature related to such Northern Hemisphere mid-latitude extremes has been linked to wave number decomposition of the previously mentioned anomalous Rossby waves (Kornhuber et al., 2017; Coumou et al., 2014). In this thesis, some interesting findings have been obtained while focusing on a completely different analysis using the LWA diagnostic and its budget components. This method was used since the resonance mechanism is only valid for summer events, while in this case the investigated events occurred in all seasons. The LWA is a good tool for forecasting blocking events with its flux being a key aspect of the analysis as proposed by the traffic jam concept in (Nakamura and Huang, 2018). The jet stream has a capacity for the LWA flux and when the capacity is exceeded, blocking occurs. This process is analogous to the process of the occurrence of a traffic jam after a highway exceeds its capacity for the number of vehicles (Nakamura and Huang, 2018). The emergence of the flux in the early stages of the event makes it a useful tool for the prediction of such events. The different components of the LWA budget equation 1.6 help to pinpoint the exact dynamical mechanisms influencing the events.

4.2 Results summary

First, a summary of the most significant results for all the events is given. For the five events in question, three of them were related to blocking, while the other two were not. The Lærdal fire event, Petra flood event and the Mykland heatwave event all showed significant enhanced LWA and weakened westerlies with early onsets of the LWA flux indicating blocking, seen in Figs. 3.21, 3.71 and 3.121. The biggest influence on the enhancement of the LWA came from the zonal LWA flux convergence as seen in Figs. 3.25, 3.75 and 3.125, where its early onset is in agreement with the early onset of the LWA flux. In the case of the Odda flood event and the Finsland snowfall event, enhanced westerlies with dampened LWA were dominant. These events were not related to a blocking pattern. The biggest contributor to dampening the LWA were the non-conservative processes in the residual (diabatic sources and sinks), as seen in Figs. 3.50 and 3.100. As far as the large-scale circulation is concerned, Odda, Finsland and Mykland cases all exhibited zonally symmetric pressure dipole patterns, as seen in Fig. 3.30, 3.80 and 3.105, which helped to strengthen the zonally symmetric flow over Norway. In the case of Odda and Finsland, the westerly flow brought the moisture from the Atlantic which contributed to the wet conditions, while for Mykland the easterly flow helped the high-pressure anomaly bring dry and warm conditions. For Lærdal and Petra, different northeast-southwest oriented pressure anomaly patterns, seen in Figs. 3.5 and 3.55, were related to weaker westerlies and blocking. For Lærdal, which occurred in winter, this led to an extreme drought and fires, while for Petra, which occurred in late summer/early autumn, it led to extreme precipitation and flooding caused by the advection of the moist air from the subtropical Atlantic and the Mediterannean by the isolated low-pressure anomaly.

4.3 Analysis and comparison

4.3.1 Basic variables anomaly fields

Second, the events and their results are compared between each other as well as the aspects of the different types of results themselves. The initial anomaly fields of the variables, such as the 500 hPa geopotential height and the 250 hPa zonal and meridional winds have offered a clear insight into the dominating circulation patterns that occurred during the periods of the extreme events. In all of the cases, a distinct circulation pattern from the 500 hPa geopotential height was indicative of the conditions that have led to the extreme events. However, certain constraints were present in terms of choosing the right time period used to determine the extreme event. After checking the previous forecasts and news reports of the events, an appropriate time interval of 29 days was selected. The central day was chosen on the basis of the geopotential height maps in the days leading up to the event and after it to determine in which day was the relevant circulation pattern the most prominent or visible. While this approach was a good way to set up a basis for the possible mechanisms and causes of the event, a further generalization to similar events before and after the exact event was needed in order to obtain more substantial means of identifying the mechanisms for this class of event. Other issues occurring in checking these anomaly fields were related to not being able to pinpoint exactly that the certain event was related to a persistent or blocking circulation pattern. If we compare the 500 hPa geopotential height patterns for each event in Figs. 3.1, 3.26, 3.51, 3.76 and 3.101, we can see that in almost all cases negative anomalies are present around the region of the North Atlantic. Positive anomalies are present in the northern seas and oceans or around a continental area. The Mykland case is the one that stands out the most, since its negative anomaly pattern is the only one that isn't situated somewhere over the North Atlantic and its positive anomaly is the only one that is situated exactly around Norway. From these characteristics, we can already make assumptions on the different types of patterns related to these extreme events.

For the zonal wind patterns in Figs. 3.2, 3.27, 3.52, 3.77 and 3.102, we can see that the Lærdal, Odda and Finsland cases have similar patterns in the mean state, with negative anomalies in the subpolar and subtropical Atlantic Ocean and positive anomalies in the mid-latitude Atlantic Ocean. These three cases have all had different types of events (drought, flood and heavy snowfall, respectively), therefore from that we can assume different large-scale mechanisms have caused the events. It is also important to note that they happened in winter or autumn (mid-January, late October and mid-January respectively). We can also see similarities between the Petra and Mykland cases, where we have a negative anomaly over western Europe/North Atlantic and a positive anomaly in the northern Norwegian sea/Arctic Ocean. This is another interesting result, since these two events were also of different nature (flood and heatwave, respectively) and they happened in the spring and summer (August/September and May/June respectively). Regarding the meridional wind, for the Lærdal and Odda cases we can see some clear, wavy structures with positive anomalies over Norway (Figs. 3.3, 3.28, 3.53, 3.78 and 3.103). The other cases don't show the same wavy pattern, but some specific, singular patterns of anomalies. The Petra and Finsland case again show a positive pattern over Norway, while Mykland is the only case of the five that shows a negative pattern over the same region.

4.3.2 Standardized index

The standardized index was used as a simple, but powerful tool in indicating the strength and persistence of the events. Through the comparison of the event index with its composite over a large number of events throughout the time series, we see how from the projected anomaly state we can 'look' into previous and following similar extreme events and form a strong argument for the mechanisms underlying events of this class. This technique allowed to connect the conditions occurring in a particular event with the previously mentioned similar events before and after it in the whole time series. The full set of the chosen events gives a credibility to the obtained results and is a good foundation and basis for further analysis. Some of the limitations occurring with this method came from the selection of the region determined for the analysis. It was very important to test different regions to get the best possible representation of the extreme event in question, but also of similar previous and following events. The typical issue occurring throughout the analysis was an anomaly pattern that was not suited for projection to the daily anomalies, therefore resulting in an index pattern that would not be representative of the event and of its prior and future analogues. However, it was also very important to choose a distinct circulation pattern that could be related to the event in question, so some precision may have been lost in this procedure.

One of the most important results in this part of the analysis were the 0-day lag composites of the different sets of the events. In all cases for days with an index value above the 95th percentile, as seen in Figs. 3.6 and 3.7, 3.31 and 3.32, 3.56 and 3.57, 3.81 and 3.82 and 3.106 and 3.107, we have seen how the index was able to replicate the anomaly pattern used for the index calculation, while also producing an opposite pattern for the days with index values below the 5th percentile. The Petra case is the only one that stands out, due to the unusual shape of the positive anomaly in its pattern and the isolation of the negative anomaly, but it still showed considerable agreement. The testing of the index through the 95th percentile was a crucial part of the analysis since it showed the credibility of the index. On the other hand, the 0-day composite lags based on the days with index values below the 5th percentile were important in showing the linearity in the occurrence of the selected anomaly pattern for the index calculation.

The indices themselves, in Figs. 3.4, 3.29, 3.54, 3.79 and 3.104, have all shown that the events have lower values than their composites around the central day and have much more irregular shapes. This comes from the fact that the composite comes from a large number of the strongest events (in terms of having the biggest index values), therefore it is to be expected that the single event may be weaker. The smooth shape of the composite comes from the averaging, while there is a lot of noisiness in the event index time series causing its shape to be more irregular. We can also see how for most of the cases the index shows higher values than the composite at the beginning and end of the time series, suggesting higher persistence than in the composite mean for all events. This also suggests that the persistence of the events can play a crucial role in the manifestation of such extremes. The aforementioned lesser values around the central days are especially seen in the Odda and Petra cases, where in the central days the values for the index are almost two times less than the composite mean. However, all of these circumstances are to be expected when comparing a single event to a mean consisting of a very high number of events with the biggest index values. Therefore we can conclude more analysis is needed to ascertain the exact situation of the event and its impact.

4.3.3 Autocorrelation

From the autocorrelation plots, we have seen different time scales of the events. Through this diagnostic we were able to see how some events were more persistent than others. This has provided valuable information that was lacking in the previous anomaly fields or index time series on the persistence of the events and how they compare with each other in that regard. While in the geopotential height and wind anomaly fields we could have seen the evolution of a certain circulation pattern, we were not able to pinpoint when exactly has a certain pattern started to develop or how far back is it connected to the previous days' patterns. This diagnostic gives us a concrete value to which we can relate the persistence of the different patterns for the events. From the plots in Figs. 3.8, 3.33, 3.58, 3.83 and 3.108, we see there's quite a lot of variations in the autocorrelations of the events. The Lærdal, Odda and Petra events show quite large time scales (15 days or more), while Finsland and Mykland show time scales of around 10 days, giving us the picture on the lengthiness of the assumed persistence in these cases. It is important to note that the significant correlations are the one outside the shaded tail around the x-axis. Some other interesting features are the rises in the autocorrelation appearing in the Lærdal and Petra cases after the autocorrelation hits a low point, which gives even more of an argument for persistent conditions. In the cases of Odda, Finsland and Mykland, the situation is the opposite, where we see an anticorrelation after a while. This indicates lesser persistence and the beginning of a shift in the previous dominant circulation pattern.

4.3.4 Composites

Composite plots of the different variables give us an insight into the atmospheric circulation occurring during the exact event and all the similar past and following events. While the circulation situation becomes more clear, there is certain challenges to pinpoint the exact conditions that led to a certain event, again mainly coming from the usage of the region for the calculation. One of the most useful aspects of this analysis is to be able to separate the event into different phases and to see when and where do we expect to have the start and end of the impact. It is as well possible to see when do the biggest changes occur in the whole time series. They also give input on whether the related circulation pattern was stationary and persistent or was there significant zonal propagation, which is one of the things investigated when determining whether an event showed persistence and blocking patterns.

Comparing the different composite plots for the events in Figs. 3.9, 3.10, 3.34, 3.35, 3.59, 3.60, 3.84, 3.85, 3.109 and 3.110 yields some interesting remarks. All of the cases besides Petra and Mykland show a significant amount of stationarity for all variables with slight propagations in some cases. This is seen for both the composites made from the daily anomalies and from the daily deviations from the zonal mean. The Petra and Mykland cases are the most interesting one as they show significant westward propagation of the relevant pattern for the geopotential height. This indicates their persistence in opposing the usual eastward propagation of such circulation systems. They are also the cases in which the dominant pattern is the most long-lasting, with a time frame of approximately from lag -10 to 10. In other cases, the time frame is mostly around lag -5 to lag 5. These results show us that the 10-day before and after time period is the most important time period in which the events have their biggest impact and are the most related to the circulation patterns that caused them. However, the persistence can still be occurring in a bigger time period, but with a smaller impact, as seen from the autocorrelation results.

When generally comparing the plots made from the daily anomalies and from the daily deviations from the zonal mean, we can see how there is much less noisiness in the case with the deviations from the zonal mean. The patterns are much more ’regular’ and ’spread out’ throughout the time frame, as opposed to the first case. Therefore in this case it is easier to deduce the shape of the pattern as well as its influence and time frame. However, they do not show the propagations as efficient as the daily anomalies. It is also visible that for the case of the deviations from the zonal mean, we see much more positive anomalies in the zonal wind plots than for the other case.

Another valuable input comes from seeing the difference of the circulation for a specific event and for the composite mean, giving us the heads up on how strong and what kind of an impact did the event have compared to the others. One downside of this is that the composite mean may have significantly lower values due to the fact that the days used for the lag composites were chosen based on the index made from the 500 hPa geopotential height. However, this is not the case for plots of the geopotential height. The composite also always tends to give lower values due to the averaging over a large number of events. For this reason, the difference plots for the 500 hPa geopotential height and other variables may not be in agreement. Some plots may show the events were weaker than the composite, while the others may show it was stronger. This is because the prominent geopotential height patterns may not be in the same region as the prominent patterns for other variables. It is also quite subjective and not very precise to try to determine the extent of the difference in this way by just examining the map plots. Therefore it was possibly better to perform this kind of evaluation in a different way. One way to do this would be to select specific regions and use field means of those.

The connection of these difference plots with the plots of the index and its composite were another good test for the validity of the index and the compositing, as well as for the expected outcome of the whole analysis. These plots, however, are still not conclusive as they do not reveal much on the influence of the eddy circulation components and the non-conservative forcing (diabatic sources and sinks) influencing the events, which could turn out to be crucial for their understanding.

For each event, a different variable shows us the direct impact of the event, in these cases drought, floods and heatwaves. Through the difference of the events to the composite mean of the specific variables we can directly judge the impact of the event. Once again, the impact of the event can also be linked to the impacts of previous and following events through the composite mean to further solidify the arguments. In these differences, there can also be deviations from the real state due to the averaging present in the lag composites as discussed in the previous paragraph. Another useful purpose of these results is that we were able to see the exact region in which the event happened. This is especially seen in the drought, extreme precipitation and extreme snowfall cases. In the cases of Lærdal, Odda, Petra and Finsland this is visible in Figs. 3.17, 3.19, 3.42, 3.44, 3.67, 3.69, 3.92 and 3.94, mostly in lag 0. For these particular plots it was very important to use a smaller region to adjust the scale due to the noisiness of the precipitation and snowfall rate data. For the Mykland case in Figs. 3.117 and 3.119, the data is less noisy but there is still the issue with the reduced values in the composite mean. In this case also, the region affected is bigger due to the plotting properties of temperature as opposed to the precipitation rate and the snowfall rate.

4.3.5 LWA, zonal wind and zonal LWA flux

The key part of the results is the analysis of the barotropic LWA and zonal wind, the zonal LWA flux and the components of the LWA budget equation. The LWA gives a clear picture on whether an event was related to a blocking pattern or not, as opposed to the other results so far. Its anticorrelation to the barotropic zonal wind, where the weakening of the zonal wind was directly connected to the aforementioned blocking patterns, further strengthens the argument for this narrative. However, the property of the LWA flux being a blocking indicator in the early stages of the event and the analogy of the blocking to a traffic jam has proven to be the most relevant feature by which blocking is evaluated. A positive LWA flux always causes a positive LWA and negative zonal wind anomaly later in time (Nakamura and Huang,

2018) and is an indicator of blocking. For the Lærdal, Petra and Mykland cases, as seen in Figs. 3.20, 3.70 and 3.120, there was a positive anomaly of LWA and negative anomaly of the zonal wind. In all of these cases the aforementioned anomalies were present in the North Atlantic/European sector around the regions of interest in Norway. Since the LWA tells us about the distortions of the quasi-geostrophic potential vorticity contours (Nakamura and Huang, 2018), we can deduce from this there was significant meandering that contributed to the blocking and persistence conditions. In the cases of Odda and Finsland, we could see a negative LWA anomaly and positive zonal wind anomaly, as seen in Figs. 3.45 and 3.95. These showed that the event indeed was not related to a blocking pattern. After this, we have a clear picture on which events presented blocking patterns and which didn't. Then we can go further into the analysis with the evolution of the barotropic LWA and zonal wind for specific regions.

When focusing on the line plots of the barotropic LWA and zonal wind for different regions, we are able to get more information than just from the previously mentioned mean plots. The regions used in each case were the same ones used for the composites of the barotropic LWA, zonal wind and the zonal LWA flux. In the cases of barotropic LWA and zonal wind for Lærdal and Mykland, as seen in Figs. 3.22, 3.23, 3.122 and 3.123, we see how both events are stronger than the composite, while the composite have their regular shapes with peaks in the middle and lower values at the beginning and end. We can also see a lot of noisiness in the event plots. For each case, we can make a comparison with their respective index plots in Figs. 3.4 and 3.104, where we see that the patterns are quite similar between the two sets of plots for each event.

In the case of Petra, in Figs. 3.72 and 3.73, we again see the regular, expected shapes for the composite, while the event plots show lower values around the central days and somewhat larger values at the beginning and end. Here we can also draw a parallel to the index plot in Fig. 3.54, where we see a similar pattern.

In the case of Odda, as seen in Figs. 3.47 and 3.48, we can see for the LWA how the composite does not have the regular expected shape, but rather has an almost constant value centered around zero or slightly negative. The event plot shows quite a lot of fluctuation, with mostly large negative values and a few positive values, therefore it is difficult to deduce a lot from it. For the zonal wind, we see a regular shape for the composite, and the event again shows noisiness with larger values at the beginning and end with lower values around the central day. There is also a generally upward trend throughout the time series. The slight upward trend and the larger values at the beginning and end can be somewhat compared to the index plot in Fig. 3.29.

The most peculiar case is the Finsland one, where we see in Figs. 3.97 and 3.98 how both composites have a constant value around zero, while the event plots are quite noisy and show clear trends. The LWA is trending from positive to negative values, while the zonal wind is trending from negative to positive, which we expect from these two variables considering their general relationship. While this pattern is not what we expect for an extreme event with a clear growth, peak and decay, the anticorrelation between the two is a good sign for the analysis. There is also no similarity with the index plot in Fig. 3.79, indicating strong non-linearity for this case.

It is also useful to note that the cases that we have related to persistence and blocking as per the discussion in the previous paragraph (Lærdal, Petra, Mykland), have shown the most appropriate and expected patterns in these plots, while the cases that we could not relate to the aforementioned conditions (Odda and Finsland), have shown results with significant discrepancies and irregularities, even looking past the fact that we didn't get the expected pattern of the positive LWA and negative zonal wind. This suggests a lot of non-linearity was involved in the Odda and Finsland cases.

Next, we look into the composites of the barotropic LWA and zonal wind as well as the zonal LWA flux. We can see similar outcomes for these plots as we have seen for the line plots of the composites and the events in the previous paragraph. For example, the Lærdal, Petra and Mykland cases show the most regularity and the most expected results. As we can see in Figs. 3.21, 3.71 and 3.121, there is a positive LWA anomaly correlated with the negative zonal wind anomaly around the central days in the same region. In each case, there is also a positive LWA flux prior to the establishment of the aforementioned pattern. The circulation is thought to have a capacity for the LWA flux and when that capacity is exceeded, blocking appears, as reported by (Nakamura and Huang, 2018). For the Lærdal and Mykland cases, the flux is quite prominent, while for the Petra case we see separated clusters of the flux. There is also a different type of pattern showing up in the Lærdal case to the west of the plot, with a negative LWA and positive zonal wind anomaly, but that is further away from the region of interest, so it does not affect the argument for persistent and blocking conditions. In (Nakamura and Huang, 2018), it is shown that the LWA flux is biggest at a medium value of the LWA and then it decreases, while the LWA further increases. This is in agreement with these plots. It is also important to note that the slowing down of the winds caused by waves limits the growth of the LWA flux, which is the effect of non-linear modification by the large-amplitude waves (Nakamura and Huang, 2018).

The Odda and Finsland cases in Figs. 3.46 and 3.96 show different patterns with negative LWA and positive zonal wind anomalies around the central days in agreement with the plots discussed in the previous paragraph. In the Odda case, there's a positive flux around the central day to the east, which could be related to the small region of positive LWA and negative zonal wind in the later part of the plot. For Finsland, there is a quite prominent positive flux in the initial stages, which only results in a positive LWA and negative zonal wind towards the end of the time series. We can also see how in the plots for the Lærdal, Petra and Mykland cases, there is much more correlation between the positive LWA, negative zonal wind and negative LWA flux in the same regions and time periodes of the plot. For the Odda and Finsland cases, there is much more noisiness and inconsistency between the three and less correlation similar to the plots discussed in the previous paragraph.

4.3.6 LWA budget equation components

Decomposing the LWA budget into its components tells us about the different small-scale contributions leading to the creation of the conditions for a certain event. For a thorough analysis, it is important to master these parts of the circulation on a smaller spatial scale in order to have a full understanding of the whole case. The small-scale circulation patterns offer the final conclusive input that is not available from the analysis of the large-scale circulation in the 500 hPa geopotential height and the 250 hPa meridional and zonal winds. Once all the components have been evaluated, it is easy to see which one is the most important and significant for contributing to the outcome and effect of the extreme event. From the plots presented, it is easily seen that the biggest contributions come from the zonal LWA flux convergence, which enhances the LWA, and the residual, which dampens it. The significance of the residual suggests it has quite a high influence in determining the causes and outcomes of the extreme events in question.

Considering each event in Figs. 3.25, 3.50, 3.75, 3.100 and 3.125, we can confirm that the zonal LWA flux convergence (I) and the residual (IV) have the biggest influence on the tendency. They are mostly anticorrelated, where the flux convergence enhances the LWA, while the residual dampens it. It is also very clear that the eddy meridional momentum flux divergence (II) has a negligible influence on the tendency, while the low-level meridional heat flux (III) has somewhat of a bigger influence, slightly increasing the LWA.

However, there are certain differences in the composite plots for the LWA budget equation components. Judging from Figs. 3.24, 3.49, 3.74, 3.99 and 3.124, we can see how the zonal LWA flux convergence and the residual are still the biggest contributors. In all cases besides Odda, they peak in the central days with positive and negative values, respectively, and towards the end they shift their sign. The Odda case is the only one where the situation is opposite. The flux convergence and the residual also show the same anticorrelation as seen in the event line plot. Therefore we can conclude that these two definitely have the biggest influence on the LWA budget, where the flux convergence enhances the LWA tendency and the residual dampens it.

Then we take a look at the meridional heat flux. In the cases of Lærdal, Odda and Petra we see that it has quite a big influence with a typical composite shape with a positive peak in the central days. In the Finsland case it has a negative profile, while in the Mykland case its pattern is stationary around zero. These profiles are quite different than from the cases for the event plots. This could come from the fact that the composite consists of multiple events averaged together. In the Odda and Finsland cases, we can see how the zonal LWA flux convergence and the low-level meridional heat flux have opposing patterns. (Huang and Nakamura, 2017) suggest that for the Atlantic region (both regions used for the Odda and Finsland composite), a low-level poleward heat flux is mostly balanced by the zonal divergence of the LWA flux as well as an equatorward heat flux by the zonal LWA flux convergence. In the same study, it is suggested that regions with large low-level heat flux show relatively weak LWA (which is true for the Odda case), where the LWA has moved away from its source region by the zonal flux into a downstream region of convergence. It is also noteworthy to add the different profiles of the heat flux for the events in different seasons.

The eddy meridional momentum flux divergence is again mostly stationary and centered around zero, as seen in the event plots. There is only a slight upward trend seen in the Finsland case, which is the noisiest and most irregular one of all. This kind of noisiness and irregularity was also present in the composites of the LWA, zonal wind and zonal LWA flux, so it is not a surprise that this is the case here again. It is also notable to mention that the tendency is again dictated by the zonal LWA flux convergence that increases it, and the residual that dampens it, same as in the events. However, in some cases the heat flux presents a significant influence as well, attesting to its strength and relevance for the events along the main contributors of flux convergence and the residual.

4.3.7 Concluding remarks and further research suggestions

The given results give a valuable insight into different strategies on how to approach the extreme events problematic and compare it to the methods presented in previous studies. It also gives the crucial insight into the small-scale dynamical mechanisms causing the events. Further development of the results and methods given in this work can lead to a well-defined and ready-to-use concept for determining exact causes for different extreme events with as few as possible physical constraints and uncertainties. An algorithm like this, where one could predict an extreme weather event a certain amount of time before it is supposed to make an impact can save affected areas from a lot of casualties and damages to the infrastructure.

A good example of a suggestion for development of a tool for forecasting extreme events with the goal of minimizing their negative impact is a scheme in (Petoukhov et al., 2018), which is based on tracking of amplifying large-scale planetary waves on 10-day-to-monthly scales. In this study, sea-level pressure and the 500 hPa geopotential height are suggested as useful tools to predict wildfires and droughts. In (Lagerquist et al., 2017), these variables are the basis for a machine-learning model used for prediction of wildfires using self-organizing maps. A good circumstance is that the low-frequency variability of these waves makes them susceptible for long-term forecasting (more than 10 days). This could be specifically useful for preventing impacts of events like the droughts and fires in Lærdal and Mykland.

In (Liu et al., 2012), it is suggested that yearly variations of the boreal autumn sea ice could be a useful tool in predicting snowfall patterns in the following winters for North America, Europe and east Asia. This type of method could be useful for predicting events such as the Finsland snowfall. In (Jaiser et al., 2012) it is also suggested that the reduced sea ice concentration at the end of the summer can influence the large-scale circulation in the upcoming winter. This can be useful in seasonal forecasting for the Northern Hemisphere winter.

Finally, the results in this thesis and in (Nakamura and Huang, 2018) have also shown that the zonal LWA flux can be a good predictor of different extreme weather events related to blocking in all seasons and not only in summer. The property of the jet stream having a capacity for the mentioned LWA flux is the key aspect in developing an efficient forecasting tool for blocking. A particularly useful technique could be to precisely quantify the threshold of the jet stream's capacity for the LWA flux and use that in forecasting.

Unfortunately, due to the time and workload needed to unilaterally determine the exact reasons for the occurrence of the events through the whole analysis discussed in this chapter and develop complete and appropriate tools and diagnostics for characterizing them, it was not possible to further investigate the impact of the events on the variables relevant for the Norwegian energy production. However, since the obtained results are quite promising, this remains a project worthy of further investigation. It has a potential to contribute to developing better methods and strategies to minimize the impacts of the extreme events on all areas affected. Based on the different plots of the precipitation rate, snowfall rate and surface temperature for the different events, which would be the parameters relevant for energy production, it is safe to assume that these events could have had quite a high impact on the production of energy. The production would have then benefited a lot from efficient forecasting and managing of the events.

Chapter 5

Conclusion

The results in this thesis have shown that it is a very difficult task to obtain a proper set of tools and techniques to predict extreme weather events and pinpoint their exact causes. While the analysis that was carried out here has proven to be conclusive and gave a lot of useful information and suggestions on steps going further, there are still some caveats that need to be addressed in further work.

The most important findings of the thesis are in the results related to the LWA and its budget equation components. The LWA has exactly shown which extreme weather events (Lærdal, Petra and Mykland) have definitely been related to certain persistence and blocking patterns in the atmosphere and which events haven't been related to these concepts (Odda and Finsland). The property of the zonal LWA flux being an indicator of blocking in the early stages has proven to be crucial in this regard. The jet stream having a capacity for the LWA flux and its analogy to a highway having a capacity for the number of vehicles on it was useful to compare the blocking to a relatable phenomenon such as the traffic jam. Also, the LWA technique has also proven useful in all seasons, unlike other methods of investigating extreme events such as Rossby wave amplification by resonance. The results related to the LWA budget equation components have helped pinpoint the exact dynamical aspects which were enhancing the persistence and blocking patterns. The biggest impact on the events came from the zonal LWA flux convergence, low-level meridional heat flux and the non-conservative processes (the diabatic sources and sinks of LWA). The flux convergence and the heat flux were enhancing the LWA, while the residual was dampening it. Therefore they offer a significant contribution to enlightening the so far poorly understood dynamical aspects of extreme weather events. This is important because the changes in the nature of the extreme events and their persistence and severity can't only be explained by thermodynamic arguments (Coumou and Rahmstorf, 2012; Schär et al., 2004; Petoukhov et al., 2013). These results can in the end offer a substantial argument that certain small-scale dynamic processes have caused or at least had a strong contribution to an extreme weather event.

One of the things that should be improved on in this kind of analysis is to make a more substantial effort on the usage of the exact regions that encompass the relevant large-scale circulation pattern as well as the time frame used in the calculation. In some cases it would be better to use wider, and in some smaller regions. The same goes for the time period where somewhere it was possibly better to use a smaller time period, and somewhere a larger one. The adjustments in setting up these parameters could prove to be crucial in obtaining better and more clear results on the aftermath of the events. The way to improve on this is to use techniques to mask out any circulation patterns that do not agree with the dominating pattern related to a selected extreme event. A thorough investigation of all the fields in the time steps before and after the central day of the event is needed in order to isolate all irrelevant factors which could hinder the analysis and its final results.

Another thing to consider, which is related to the problematic given in the previous paragraph, is a more thorough approach in the further statistical analysis of the data, such as in compositing. In these calculations it is also quite important to adjust them in the same way as mentioned in the previous paragraph, as they are supposed to give more conclusive and complete results than the methods used prior to them. It would also be useful to perform different statistical tests on the results, as in most studies of this kind, to check the statistical significance of the obtained results.

Improvements in the analysis could also come from a more thorough investigation of the events occurring just before the exact event of interest, as these events could also have possibly had somewhat of an influence on the event in question. Certain events could be part of a series of events with different impacts originating from the same circulation pattern, which extended further back in time and did not show significant changes throughout the whole time frame of all the events considered.

Furthermore, the actual impact of the events on the areas affected and its population and infrastructure needs to be more investigated. Proper techniques should be applied in order to obtain a sustainable and efficient product, which could be used on a regular basis for detecting these type of events in advance and minimizing their damaging impact. This remains a challenge yet to be pursued due to the extensive workload on defining and investigating the extreme events and is the logical next step in the further analysis of this topic. Since the results in this thesis have shown to be quite promising, it is definitely a worthy cause to keep doing research on this topic.

References

[1] Anaconda Inc. (2020). Anaconda software distribution.

[2] Arnesen, M. (2018). Etne varmest i landet. https://www.nrk.no/vestland/etne-varmest-i-landet-1.14062304.

[3] Audardottir Oldeide, A. (2014). Sjå oversikt over dei enorme øydeleggingane. https://www.nrk.no/vestland/sja-oversikt-over-dei-enorme-oydeleggingane-1.12018754.

[4] Berg, P., C. Moseley, and J. Haerter (2013, 03). Strong increase in convective precipitation in response to higher temperature. *Nature Geoscience 6*, 181–185.

[5] Berggren, R., B. Bolin, and C.-G. Rossby (1949). An aerological study of zonal motion, its perturbations and break-down. *Tellus 1*(2), 14–37.

[6] Branstator, G. (2002, 07). Circumglobal teleconnections, the jet stream waveguide, and the North Atlantic Oscillation. *J. Climate 15*.

[7] Breiteig, T. (2018). Ekstremværets år. https://www.ae.no/aktuelt/blogg/tarjei-breiteig/ekstremvarets-ar/.

[8] Charney, J. G. and P. G. Drazin (1961). Propagation of planetary-scale disturbances from the lower into the upper atmosphere. *Journal of Geophysical Research (1896-1977) 66*(1), 83–109.

[9] Charney, J. G. and A. Eliassen (1949). A numerical method for predicting the perturbations of the middle latitude westerlies. *Tellus 1*(2), 38–54.

[10] Coumou, D., J. Lehmann, and J. Beckmann (2015, 03). Climate change. the weakening summer circulation in the Northern Hemisphere mid-latitudes. *Science (New York, N.Y.) 348*.

[11] Coumou, D., V. Petoukhov, S. Rahmstorf, S. Petri, and H. J. Schellnhuber (2014). Quasi-resonant circulation regimes and hemispheric synchronization of extreme weather in boreal summer. *Proceedings of the National Academy of Sciences 111*(34), 12331–12336.

[12] Coumou, D. and S. Rahmstorf (2012, 03). A decade of weather extremes. *Nature Climate Change 2*.

[13] Coumou, D. and A. Robinson (2013, 08). Historic and future increase in the global land area affected by monthly heat extremes. *Environmental Research Letters 8*, 34018–6.

[14] Coumou, D., A. Robinson, and S. Rahmstorf (2013, 01). Global increase in record-breaking monthly-mean temperatures. *Climatic Change 118*.

[15] Francis, J., W. Chan, D. Leathers, J. Miller, and D. Veron (2009, 04). Winter Northern Hemisphere weather patterns remember summer Arctic sea-ice extent. *Geophys. Res. Lett 36*.

[16] Francis, J. and S. Vavrus (2012, 03). Evidence linking Arctic amplification to extreme weather in mid-latitudes. *Geophysical Research Letters 39*, L06801.

[17] Groisman, P., R. Knight, D. Easterling, T. Karl, G. Hegerl, and V. Razuvaev (2004, 01). Trends in precipitation intensity in the climate record. *J. Clim. 18*.

[18] Harris, C. R., K. J. Millman, S. J. van der Walt, R. Gommers, P. Virtanen, D. Cournapeau, E. Wieser, J. Taylor, S. Berg, N. J. Smith, R. Kern, M. Picus, S. Hoyer, M. H. van Kerkwijk, M. Brett, A. Haldane, J. F. del Río, M. Wiebe, P. Peterson, P. Gérard-Marchant, K. Sheppard, T. Reddy, W. Weckesser, H. Abbasi, C. Gohlke, and T. E. Oliphant (2020, September). Array programming with NumPy. *Nature 585*(7825), 357–362.

[19] Held, I. (2001, 01). Stationary and quasi-stationary eddies in the extratropical troposphere: theory.

[20] Held, I. M. and B. J. Hoskins (1985). Large-scale eddies and the general circulation of the troposphere. In B. Saltzman (Ed.), *Issues in Atmospheric and Oceanic Modeling*, Volume 28 of *Advances in Geophysics*, pp. 3–31. Elsevier.

[21] Hersbach, H., B. Bell, P. Berrisford, G. Biavati, A. Horányi, J. Muñoz Sabater, J. Nicolas, C. Peubey, R. Radu, I. Rozum, D. Schepers, A. Simmons, C. Soci, D. Dee, and J.-N. Thépaut (2018a). ERA5 hourly data on pressure levels from 1979 to present. Accessed on < 22-10-2020 >, < 08-03-2021>, < 29-04-2021 >.

[22] Hersbach, H., B. Bell, P. Berrisford, G. Biavati, A. Horányi, J. Muñoz Sabater, J. Nicolas, C. Peubey, R. Radu, I. Rozum, D. Schepers, A. Simmons, C. Soci, D. Dee, and J.-N. Thépaut (2018b). ERA5 hourly data on single levels from 1979 to present. Accessed on < 03-03-2021 >, < 22-04-2021>.

[23] Hocke, K., M. Lainer, and A. Schanz (2015, 06). Composite analysis of a major sudden stratospheric warming. *Annales Geophysicae 33*, 783–788.

[24] Horton, D., N. Johnson, D. Singh, D. Swain, B. Rajaratnam, and N. Diffenbaugh (2015, 06). Contribution of changes in atmospheric circulation patterns to extreme temperature trends. *Nature 522*, 465–9.

[25] Hoskins, B. and D. Karoly (1981, 06). The steady linear response of a spherical atmosphere to thermal and orographic forcing. *J. Atmos Sci. 38*, 1179–1196.

[26] Hoskins, B., M. Mcintyre, and A. Robertson (2007, 10). On the use and significance of isentropic potential vorticity maps. *Quarterly Journal of the Royal Meteorological Society 111*, 877 – 946.

[27] Hoskins, B. J., A. J. Simmons, and D. G. Andrews (1977). Energy dispersion in a barotropic atmosphere. *Quarterly Journal of the Royal Meteorological Society 103*(438), 553–567.

[28] Hoyer, S. and J. Hamman (2017). xarray: N-D labeled arrays and datasets in Python. *Journal of Open Research Software 5*(1).

[29] Huang, C. and N. Nakamura (2015, 09). Local finite-amplitude wave activity as a diagnostic of anomalous weather events. *Journal of the Atmospheric Sciences 73*, 150914120227005.

[30] Huang, C. and N. Nakamura (2017, 05). Local wave activity budgets of the Pacific and Atlantic storm tracks in the Northern Hemisphere winter. *Geophysical Research Letters 44*.

[31] Huang, C. S. Y. (2015a). Demo script for the analyses done in Nakamura and Huang (2018, Science). `https://github.com/csyhuang/hn2016_falwa/blob/master/examples/nh2018_science/demo_script_for_nh2018.ipynb`. Accessed on < 29-04-2021 >.

[32] Huang, C. S. Y. (2015b). Python Library: hn2016_falwa (v0.4.1). `https://github.com/csyhuang/hn2016_falwa`. Accessed on < 29-04-2021 >.

[33] Hunter, J. D. (2007). Matplotlib: A 2d graphics environment. *Computing in Science & Engineering 9*(3), 90–95.

[34] Huntingford, C., P. Jones, V. Livina, T. Lenton, and P. Cox (2013, 07). No increase in global temperature variability despite changing regional patterns. *Nature 500*.

[35] Ighoubah, F. and S. Solheim (2014). Slik var de første meldingene om Lærdalsbrannen. https://www.nrk.no/vestland/beboer-meldte-selv-om-boligbrann-1.11482695.

[36] Jaiser, R., K. Dethloff, D. Handorf, A. Rinke, and J. Cohen (2012, 01). Impact of sea ice cover changes on the Northern Hemisphere atmospheric winter circulation. *Tellus A 64*.

[37] Jones, E., T. Oliphant, P. Peterson, et al. (2001). SciPy: Open source scientific tools for Python.

[38] Kornhuber, K., V. Petoukhov, S. Petri, S. Rahmstorf, and D. Coumou (2017, 09). Evidence for wave resonance as a key mechanism for generating high-amplitude quasi-stationary waves in boreal summer. *Climate Dynamics 49*.

[39] Lagerquist, R., M. Flannigan, X. Wang, and G. Marshall (2017, 08). Automated prediction of extreme fire weather from synoptic patterns in northern Alberta, Canada. *Canadian Journal of Forest Research 47*, 1175–1183.

[40] Lau, W. and K.-M. Kim (2012, 02). The 2010 Pakistan flood and Russian heat wave: Teleconnection of hydrometeorological extremes. *Journal of Hydrometeorology 13*, 392–403.

[41] Lehmann, J. and D. Coumou (2015, 12). The influence of mid-latitude storm tracks on hot, cold, dry and wet extremes. *Scientific Reports 5*, 17491.

[42] Lehmann, J., D. Coumou, and K. Frieler (2015, 08). Increased record-breaking precipitation events under global warming. *Climatic Change 132*.

[43] Lenderink, G. and E. Meijgaard (2008, 07). Increase in hourly precipitation extremes beyond expectations from temperature. *Nature Geoscience - NAT GEOSCI 1*, 511–514.

[44] Lenderink, G. and E. Meijgaard (2009, 06). Unexpected rise in extreme precipitation caused by a shift in rain type? *Nature Geoscience 2*, 373–.

[45] Limpasuvan, V., D. Thompson, and D. Hartmann (2004, 07). The life cycle of the Northern Hemisphere sudden stratospheric warmings. *Journal of Climate - J CLIMATE 17*, 2584–2597.

[46] Liu, J., J. A. Curry, H. Wang, M. Song, and R. M. Horton (2012). Impact of declining Arctic sea ice on winter snowfall. *Proceedings of the National Academy of Sciences 109*(11), 4074–4079.

[47] Lubis, S., C. Huang, N. Nakamura, N.-E. Omrani, and M. Jucker (2018, 02). Role of finite-amplitude Rossby waves and nonconservative processes in downward migration of extratropical flow anomalies. *Journal of the Atmospheric Sciences 75*.

[48] Løset, O., E. Hildal, and G. B. Hjetland (2014). Ordføraren i Aurland til innbyggjarane i Flåm: – Evakuer til Fretheim hotell. https://www.nrk.no/vestland/ordforaren-i-aurland_-_-evakuer-til-fretheim-hotell-1.12011040.

[49] Mann, M., S. Rahmstorf, K. Kornhuber, B. Steinman, S. Miller, and D. Coumou (2017, 03). Influence of anthropogenic climate change on planetary wave resonance and extreme weather events. *Scientific Reports 7*, 45242.

[50] Meredith, E., V. Semenov, D. Maraun, W. Park, and A. Chernokulsky (2015, 07). Crucial role of Black Sea warming in amplifying the 2012 Krymsk precipitation extreme. *Nature Geoscience 8*, 615–619.

[51] Merriam-Webster.com Dictionary (2021). s.v. "percentile,". https://www.merriam-webster.com/dictionary/percentile. accessed July 28, 2021.

[52] Met Office (2010 - 2015). *Cartopy: a cartographic python library with a matplotlib interface.* Exeter, Devon.

[53] Min, S.-K., X. Zhang, F. Zwiers, and G. Hegerl (2011, 02). Human contribution to more-intense precipitation extremes. *Nature 470*, 378–81.

[54] Nakamura, N. and C. Huang (2018, 05). Atmospheric blocking as a traffic jam in the jet stream. *Science 361*, eaat0721.

[55] Nakamura, N. and A. Solomon (2010, 12). Finite-amplitude wave activity and mean flow adjustments in the atmospheric general circulation. part i: Quasigeostrophic theory and analysis. *Journal of The Atmospheric Sciences - J ATMOS SCI 67*, 3967–3983.

[56] National Center for Atmospheric Research Staff (Eds). (2020). The climate data guide: Overview: Climate indices. https://climatedataguide.ucar.edu/climate-data/overview-climate-indices. Last modified 18 Dec 2020.

[57] NRK (2015). Ekstremværet Petra. https://www.nrk.no/sorlandet/ekstremvaeret-_petra_-1.12555674.

[58] Ogawa, F., N. Keenlyside, Y. Gao, T. Koenigk, S. Yang, L. Suo, T. Wang, G. Gastineau, T. Nakamura, H. N. Cheung, N.-E. Omrani, J. Ukita, and V. Semenov (2018, 02). Evaluating impacts of recent Arctic sea ice loss on the Northern Hemisphere winter climate change. *Geophysical Research Letters 45*.

[59] Pedlosky, J. (2013). *Geophysical Fluid Dynamics.* Springer New York.

[60] Petoukhov, V., S. Petri, K. Kornhuber, K. Thonicke, D. Coumou, and H. Schellnhuber (2018, 08). Alberta wildfire 2016: Apt contribution from anomalous planetary wave dynamics. *Scientific Reports 8.*

[61] Petoukhov, V., S. Rahmstorf, S. Petri, and H. Schellnhuber (2013, 03). Quasiresonant amplification of planetary waves and recent Northern Hemisphere weather extremes. *Proceedings of the National Academy of Sciences of the United States of America 110.*

[62] Petoukhov, V. and V. Semenov (2009, 04). A link between reduced Barents-Kara sea ice and cold winter extremes over northern continents. *Journal of Geophysical Research Atmospheres 115.*

[63] Platzman, G. W. (1968). The Rossby wave. *Quarterly Journal of the Royal Meteorological Society 94*(401), 225–248.

[64] Rex, D. F. (1950). Blocking action in the middle troposphere and its effect upon regional climate. *Tellus 2*(3), 196–211.

[65] Rommetveit, A. (2014). Det som skjer er skummelt. `https://www.yr.no/artikkel/_-det-som-skjer-er-skummelt-1.12010959`.

[66] Rossby, C. G. (1939). Relation between variations in the intensity of the zonal circulation of the atmosphere and the displacements of the semipermanent centers of action. *JOURNAL OF MARINE RESEARCH 2*(1), 38–55.

[67] Schubert, S., H. Wang, and M. Suarez (2011, 09). Warm season subseasonal variability and climate extremes in the Northern Hemisphere: The role of stationary Rossby waves. *Journal of Climate - J CLIMATE 24*, 4773–4792.

[68] Schulzweida, U. (2019, October). Cdo user guide.

[69] Schär, C., P. Vidale, D. Lüthi, C. Frei, C. Häberli, M. Liniger, and C. Appenzeller (2004, 02). 2004: The role of increasing temperature variability in European summer heatwaves. *Nature 427*, 332–6.

[70] Seabold, S. and J. Perktold (2010). statsmodels: Econometric and statistical modeling with Python. In *9th Python in Science Conference.*

[71] Seneviratne, S., N. Nicholls, D. Easterling, C. Goodess, S. Kanae, J. Kossin, Y. Luo, J. Marengo, K. Mcinnes, M. Rahimi, M. Reichstein, A. Sorteberg, C. Vera, and X. Zhang (2012, 04). *Changes in climate extremes and their impacts on the natural physical environment.*

[72] Smith, T. (2021). Autocorrelation. https://www.investopedia.com/terms/a/autocorrelation.asp. accessed July 28, 2021.

[73] Støfring Skovro, T. L. (2014). Det skal framleis regne i bøtter og spann. https://www.nrk.no/vestland/regnveret-tek-ikkje-pause-heilt-enno-1.12010212.

[74] Tachibana, Y., T. Nakamura, H. Komiya, and M. Takahashi (2010). Abrupt evolution of the summer Northern Hemisphere annular mode and its association with blocking. *Journal of Geophysical Research: Atmospheres 115*(D12).

[75] Trenberth, K. and J. Fasullo (2012, 09). Climate extremes and climate change: The Russian heat wave and other climate extremes of 2010. *Journal of Geophysical Research (Atmospheres) 117*, 17103–.

[76] Trenberth, K., J. Fasullo, and T. Shepherd (2015, 07). Attribution of climate extreme events. *Nature Climate Change 5*, 725–730.

[77] Vallis, G. (2006, 01). *Atmospheric and Oceanic Fluid Dynamics*.

[78] Van Rossum, G. and F. L. Drake (2009). *Python 3 Reference Manual*. Scotts Valley, CA: CreateSpace.

[79] Westra, S., L. Alexander, and F. Zwiers (2013, 04). Global increasing trends in annual maximum daily precipitation. *Journal of Climate 26*, 7834–.

[80] Woollings, T., A. Hannachi, and B. Hoskins (2010). Variability of the North Atlantic eddy-driven jet stream. *Quarterly Journal of the Royal Meteorological Society 136*(649), 856–868.

[81] Yr (2013, December 2013). Lærdal precipitation and temperature data for December 2013. https://www.yr.no/nb/historikk/graf/5-54110/Norge/Vestland/L%C3%A6rdal/L%C3%A6rdal?q=2013-12.

[82] Zender, C. S. (2008). Analysis of Self-describing Gridded Geoscience Data with netCDF operators (NCO), Environ. Modell. Softw., 23(10), 1338-1342.

[83] Zhang, X., H. Wan, F. Zwiers, G. Hegerl, and S.-K. Min (2013, 10). Attributing intensification of precipitation extremes to human influences. *Geophysical Research Letters 40*.